Revista Română de Inginerie Civilă

Indexată în bazele de date internationale (BDI)

ProQuest, INSPEC, EBSCO

INDEX COPERNICUS, ULRICH'S şi JOURNALSEEK

Volumul 13 (2022), Numărul 3

MATRIX ROM
OP CHIAJNA CP 2
077040 – ILFOV
Tel. 021 4113617 Fax. 021 4114280
e-mail: office@matrixrom.ro
www.matrixrom.ro

Romanian Journal of Civil Engineering is founded, published and funded by publishing house MATRIX ROM
Executive Director: mat. Iancu ILIE

Online edition ISSN 2559-7485
Print edition ISSN 2068-3987; ISSN-L 2068-3987

Numerical Modeling for Engineering Analysis, Designing and Monitoring of Support Systems for Twin-Tube Tunnel

Modelare numerică pentru analiza inginerească, proiectarea și monitorizarea sistemelor de suport pentru tunelul cu două tuburi

Houssam KHELALFA [(1) (2)*], U.SAKALLI [(3)], E. B. AYGAR[(3)], O.ŞİMŞEK [(3)], B. AYKAN [(3)], H. BOULMAALI[(4)]

[1] Civil Engineering and Environment Laboratory (LGCE) of University of Jijel, Jijel, Algeria

[2] Faculty of Engineering and Technology, Selinus University of Science and Literature (SUSL), Bologna, Italy

[3] MAPA İNŞAAT AŞ, Ankara, Turkey

[4] CTTP, Kouba - Algiers, Algeria

* Corresponding author. Tel.: +213697601497
E-mail address: khelalfahoussam@gmail.com
ORCID: 0000-0002-8052-6947

DOI: 10.37789/rjce.2022.13.3.1

Abstract

In this research work, Rock Mass Rating (RMR) was used for the characterisation of rock mass along the tunnel alignment based on physical, geological and geotechnical data of the project area. The support systems were recommended for all geotechnical units using RMR and tunneling quality index (Q-system) support chart. Furthermore, Various design input parameters such as physical and geotechnical properties, in situ stresses, modulus of deformation of rock mass, support systems recommended by RMR were used as input parameters in Phase2 2D 8.0 software, in order to compare the calculation results with in-situ monitoring using Amberg Tunnel 2.0 software, to validate the numerical models and to check the deformations of the tunnel in the temporary support stage.

Keywords: Tunnel, Rock Mass Ckassification, Provisional Support, Deformations, Numerical Modelling.

1. Introduction:

The Texanna twin-tube tunnel with 1.80 -km long (figure 1), was built as a road tunnel using the New Austrian Method (NATM) assuming that the excavation technique used is drilling-blasting and / or mechanical excavation, in anticipation of

heavy traffic in the framework of the project 'Penetrating Highway connecting Djen Djen Port to the East-West Highway', in a project of 110 km. The tunnel is located in the project route between KP: 24 + 818.545 - KP: 26 + 648.352 for the right tube and between KP: 0 + 711.683 - KP: 2 + 593.879 for the left tube. The rock mass classification was carried out using rock mass rating (RMR) based on geology of project area, bore holes data and physical and strength properties of rock samples collected from site. In the present work, the rock mass rating (RMR) were used as empirical methods for characterization of rock mass based on real-time geological and site geotechnical data and physical and strength properties of rock samples collected from the alignment of tunnel. The rock mass along the tunnel axis was classified into Five geotechnical units (class III, III-A, IV, IV-A, IV-B). The support systems for each geotechnical unit were designed. The rock mass behavior in term of the in situ monitoring of total deformations and effects of provisional support on (arch, bolts and shotcrete) due to excavation of the tunnel profile were investigated and analyzed by comparing with simulated model (Phase2- 2D software).

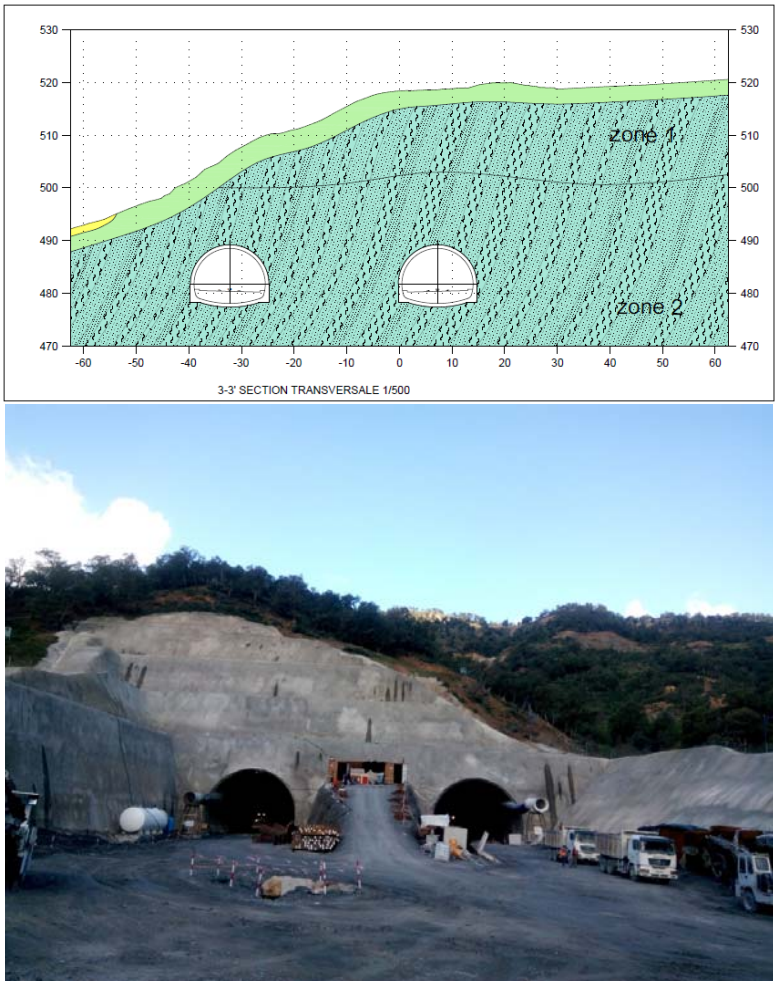

Fig. 1– Photography and Geological cross section and longitudinal profile of the south portal of the tunnel

The empirical and numerical design approaches are considered very important in the viable and efficient design of support systems, stability analysis for tunnel, and underground excavations [1]. During stages of excavation projects, the empirical methods like rock mass classification systems are considered to be used for solving engineering problems [2,3]. The empirical methods used defined input parameters in designing of any underground structures, recommendation of support systems, and determination of input parameters for numerical modeling [4]. The empirical methods classified the rock mass quantitatively into different classes having similar characteristics for easily understanding and construction of underground engineering structures [5]. Numerical modeling is gaining more attention in the field of civil and rock engineering for prediction of rock mass response to various excavation activities [6]. Modeling of rock mass is a very difficult job due to the presence of discontinuities, anisotropic, heterogeneous, and non-elastic nature of rock mass, using empirical and numerical methods [7]. The complex nature and different formation make the rock masses a difficult material for empirical and numerical modeling [8]. It is suggested that numerical and empirical methods be used together for the safe, stable and efficient design of tunnels, other underground structures in the rock mass environment and reliable support systems [9,10].

2. Geology of project area:

Between the mass of Babors, developed in the west and that of the Kabylian pedestal, which extends eastward over more than 100 PK (Petite Kabylie), there is a region of ridges and wooded hills, still well known, or dominate, under the neogene post-nappes, the Numidian series and the Mauritanian flysch of Guerrouch (formerly Texanna), to the south of the port of Jijel, on the northern edge of Tamesguida mapped by F. Ehrmann 1946. This author was noted in the valley of the DjenDjen wadi, the existence of "green rocks" presented as an ophiolitic complex with intercalations of cornea and glandular gneiss. In 1956, Mr. Durand Delga presents a precise cartography to the sector of Texenna. The metamorphosed "green rocks" are interpreted as a lacolith in the micaschists of the Kabylian pedestal, which is widely carried southward; conception that complete and corrected by Bouillin in 1971 [11]. It then defines the unit of " Sendouah-Tabellout" which stratigraphically comprises from bottom to top the following layers:

- Green rocks probably containing pillow lavas, which may represent an ophiolitic complex;
- Shales and limestones attributed to the Neocomian Jurassic;
- Cretaceous flysch, schisto-sandstone for the most part; this unit is overturned and metamorphosed, it is straddled by the Kabylian pedestal to the north, and faces, to the south, according to a very corrected contact, other series of flyschs carried on the Tellian domain.

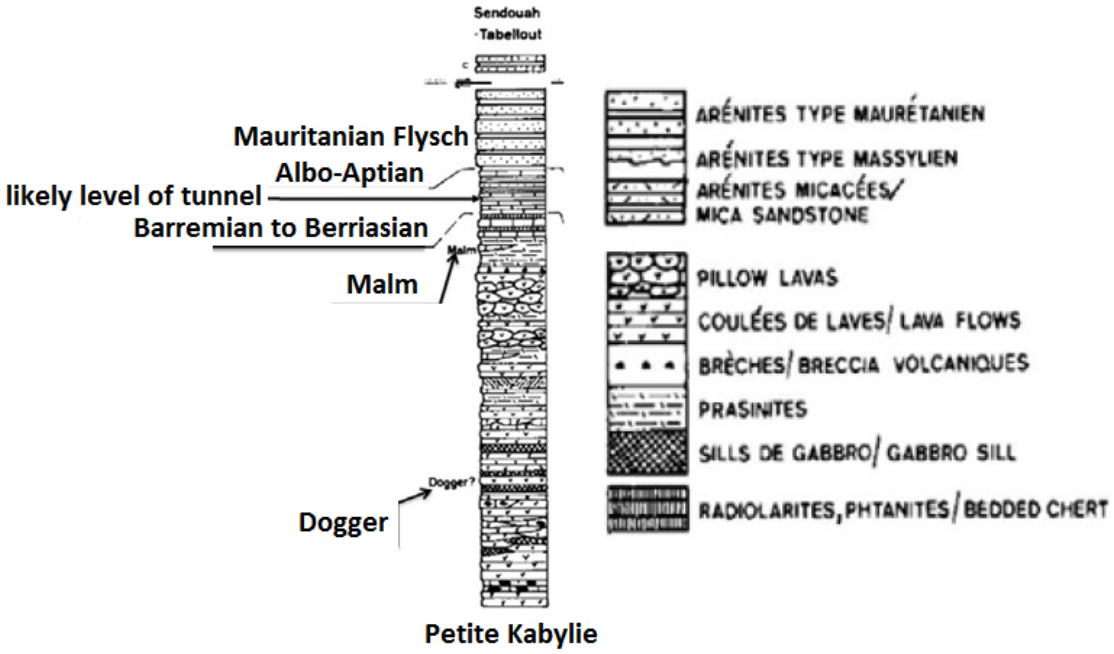

Fig. 2– Geological and structural maps of the western terminus of Kabylia (after H. Djellit, 1987) [11]

.

2.1 Geological conditions along the tunnel:

The alignment is not located in different lithological units as previously indicated but in an old Albo-Alpien Flysch composed entirely of the alternation of mudstone and sandstone. The flysch is composed of a mudstone with a folded, weakly-moderately decomposed, weakly-weak, and fine-grained sandstone character that has a medium-thick, poorly decomposed, moderately solid-solid rock nature. The first part of 10 m on the surface of the flysch unit is very or totally decomposed and has a very low-excessively low rock nature. However, this zone of decomposition does not reach the tunnel dimension and according to sounding studies, an alternation of mudstone and sandstone which includes a nature of weakly decomposed rock, partly weak, generally medium-solid will be observed at the tunnel level. The different geological conditions of rock mass along the alignment of tunnel are shown in Figures (3).

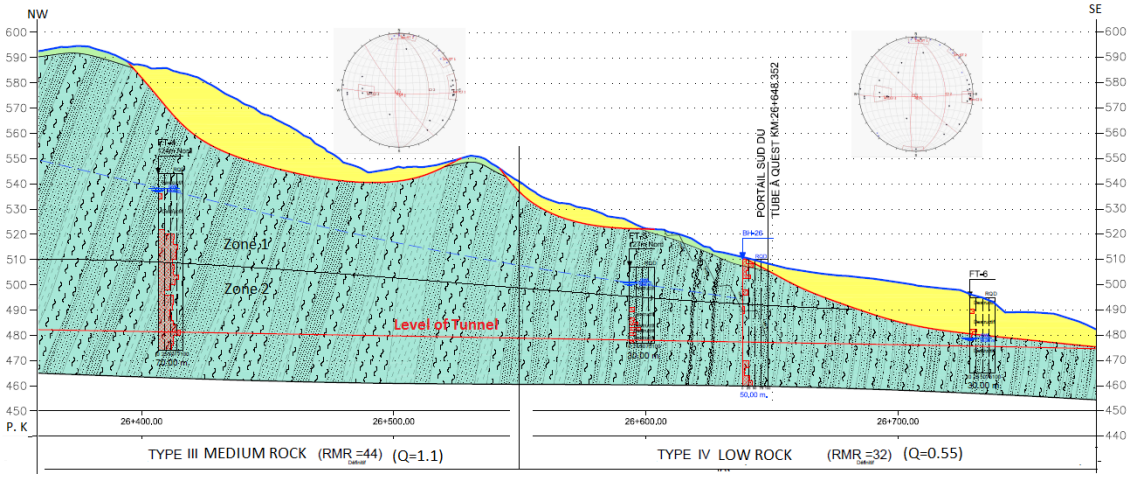

Fig. 3– Geology and cross-sectional view of tunnel alignment of this study

The geological conditions of the Texanna Tunnel site are composed by the Mauritanian Flysch, which consists essentially of shale-sandstone alternations with hard quartzite passages, resting on the surface of fractured and weathered shales. All of these formations cover the formation of hard argillite slightly weathered and fractured whose upper part, and in depth it is very hard and little fractured. This argillite is present almost all along the tunnel as shown in Figures (4).

Based on the foregoing considerations, it appears that the study area is located in an area characterized by average class II-a seismicity, according to the RPOA, 2008 (Algerian standard). In the case of well-built tunnels through a host rock of good quality, the seismicity effects are generally low. However, special attention should be given to areas with a host rock of poor quality, particularly at tunnel portal, where the coverage is lower and there is generally lower quality land. Under these conditions, special precautions must be taken in the design and construction phase to counter the seismic effects on the tunnel structure.

Fig. 4– Photography of tunnel alignment Geology of this study

3. Rock Mass Classification along the alignment of the tunnel:

3.1 RMR- system:

The empirical methods classify the rock masses into different categories having less or more similar geological and geotechnical properties on the basis of results obtained from rock mass characterization. The rock mass classification systems are considered very beneficial to use during the initial stages of the project when limited information about rock mass behavior, stresses and hydrological characteristics are available [12, 13]. The rock mass along the tunnel axis were classified into different categories based on Geo-mechanical classification system also called Rock mass rating (RMR- system) [4]. This system utilised the following six parameters for rock mass classification based on quality in to various groups of similar behaviours:

- Uni-axial Compressive strength (UCS);
- Rock Quality designation index (RQD);
- Spacing of discontinuities (DS);
- Condition of discontinuity (DC);
- Ground water condition (GWC);
- Orientation of discontinuities (DO).

Various physical and geotechnical properties of rock mass along the tunnel alignment were determined by testing the rock samples obtained along the tunnel alignment. The different physical and Mechanical properties of rock mass along the tunnel length are presented in Table (1).

#

3.2 Q- system:

The Rock mass classification systems are considered as an integral part of the designing of underground structure, support systems, stability analysis and in determination of input parameters for numerical modeling within the rock mass environment [14]. Various rock mass classification system has been developed based on civil and mining engineering case studies by different researchers. In this research, RMR and Q systems were used due to its flexibility in terms of input parameters and widespread range for selection of support systems. The Q-system is developed by Bortan in 1974 at Norwegian Geotechnical Institute (NGI) [15]. The Q-system has wide applications in underground excavations and „field mapping, and it depends on the underground opening and its geometry. The value of this system may be different for undisturbed and disturbed rock [16]. This system classifies the rock mass environment into different classes on the basis of:

- the rock quality designation (RQD),
- joint number (Jn),
- joint roughness number (Jr),
- joint alteration (Ja),
- joint water reduction factor (Jw),
- and stress reduction factor (SRF).

The values of this system indicate the quality of rock mass and give description about the stability of an excavation within the rock mass environment. The maximum value of Q-system indicates good quality of rock meaning good stability and the minimum value indicates poor quality of rock meaning poor stability [17, 18]. The RMR and Q classification systems were applied on bore hole data and physical and strength properties determined in laboratory of the collected rock samples along tunnel alignment. Based on the results obtained from RMR and Q system, the rock mass along the tunnel axis was divided into five geotechnical units. The results of RMR and Q classification system are presented in Table (1) and (2).

4. Provisional support system:

The fundamental principle of digging a tunnel with the new Austrian method is to transport the rock by itself (the ability to transform a mass of rock that surrounds the profile of a tunnel into a load-carrying element instead of an element that constitutes a load). Allowing the rock to deform slightly (provided that it remains within the permissible safety limits) considerably reduces the loads on the bearing system. The rock released under control transfers the load to the sides and thus uses its transport capacity to the maximum by forming a transport chain around the excavation. Instead of carrying all the load of the rock, the support systems are rather used to control the plastic deformations while preserving the integrity of the transport chain around the excavation and to avoid the excessive relaxations. So the flexibility of the system to

the point of adapting to the deformations of the rock is one of the most important criteria of the method. If the rock is too weak to carry its own load, the support used stabilizes the system by providing additional pressure still needed to reach equilibrium after approaching the rock carrying capacity. As a result, limited deformation is allowed before and after the application of the primary support system (provisional). The main feature of NATM is the application support at the exact moment. If the support is applied without allowing any deformation, the support system will be overloaded and will no longer be economical. And if not, deterioration of soil and excessive deformation will occur.

Table 1

Geotechnical Design Parameters and Rock mass classification for twin tube tunnel

Kilometric point (**P.K**)		between the exit gate part- KP: 26 + 550 of the right tube and exit gate - KP 2 + 490.970 of the left tube of the tunnel	between the KP part: 26 + 230 - KP: 26 + 550 of the right tube and KP: 2 + 191.682 - KP: 2 + 490.970 of the left tube of the tunnel
Rock class **type**		Low Rock (**IV**)	Middle Rock (**III**)
Geological determination		The level of the tunnel is located entirely in the flysch consisting of the alternation of mudstone and sandstone of the old albo-Alpien.	
Underground **water** condition		State of groundwater in the form of dripping and leaking	
UCS, Uniaxial compressive strength (MPa)		10,0	13,0
GSI, Geological strength Index		25	40
mi, Material Constant		10	10
D, Disturbance factor		0	0 – 0,8
Ei, Elasticity Modulus (GPa)		6,75	15,0
υ, Poisson's ratio		0.34	0.32
γ_n, Unit weight (kN/m3)		27	27
H, Effective Rock Height (m)		60	130
c, Cohesion (kPa)	D=0	139	345

	D=0.8			199
Ø, Internal friction angle (º)	D=0		32	33
	D=0.8			22
Em, Deformation modulus (GPa)	Nicholson & Bieniawski		0,49	2,2
	Hoek & Diederichs	D=0	0,4	2,4
		D=0.8		0,77
RMR, Rock Mass Rating			32	44
Q, Tunneling Quality Index			0,55	1,1

The elements of the provisional support system consist of the following systems and / or their various combinations depending on the class of rock or geological conditions encountered:

4.1 Shotcrete:

The use of shotcrete is essential as a supporting element that prevents the relaxation of the peripheral rock. Shotcrete is the element that provides the greatest support pressure among the support elements. A first-layer shotcrete will be applied in all support systems after excavation against the risk of failure and collapse of the layers. A second layer shotcrete will be applied in all support systems after the location of Steel lattice and steel Retaining.

Fig. 5– Photography of tunnel shotcrete stage

4.2 Steel lattice:

A steel lattice will be applied between the concrete layers to form the static and constructive reinforcement of the concrete coating. The use of steel lattice is intended to ensure adhesion between rock and shotcrete, stabilization, increase in shear strength and prevention of excessive cracks until the setting of concrete.

Fig. 6– Photography of tunnel Steel lattice stage

4.3 Steel retaining:

In principle, the steel support provides immediate support before the shotcrete freshly begins to wear and constitutes the reinforcement with the lattice after the concrete has acquired its strength. Steel support is also a support for drilled bolts and provides mental confidence for employees. HEB "180, 220" profiles are used in this project.

Fig. 7– Photography of tunnel Steel retaining stage

4.4 The pipes or pre-supporting iron bar:

The purpose of the piles support is to provide support by Umbrella effect around the forehead. For this purpose perforated pre- support will be used with Ø 5.0 "and 7.0" injection pipes depending on the rock classes. Their distance is between 20-40 cm depending on the class of rock. In addition, after attaching certain pipes to the hole, making them wait without an injection for a moment ensures the drainage of the groundwater that can come on the face. In the following by the injection these pipes will assume their own function.

Fig. 8– Photography of tunnel pre-supporting iron bar (Umbrella) stage

4.5 Rock bolts:

Rock bolts will be applied systematically as part of the support type system. Rock bolts are used in all support systems because they increase the quality and strength of the rock mass by increasing shear strength, reducing deformation in the tunnel and preventing rock breakage. The whole procedure will be performed by

injection given that it is not a design that aims to support the rock blocks or thin layers. The length of the rock bolts is chosen so that they extend at least ~ 2 m above the plastic zone formed around the tunnel. The diameter of the injection hole will be 1.5 of the diameter of the bolt. The bolts will be installed in radial position on the walls of the tunnel. Bolts of type SN and IBO will be used.

Fig. 9– Photography of tunnel Rock bolts stage

5. Numerical modeling and Analyzes performed with the Phase 2 2D software:

The numerical analyzes were performed with the Phase 2 2D program (Version 8.0). Is a finite element program developed by the University of Toronto which models the masses of rock and the sustained behaviors of these masses. The program is progressively modeling the underground excavation, providing support with bolts, steel retaining, steel lattice and shotcrete. In addition, the load split between the excavation phases and the material softening can be applied to the model. The designation of support systems based on practice and experience, numerical analyzes were considered as a guide for practical decisions. The support system will have to be revised according to the actual field situation and the geological mapping and the footage results.

5.1 Soil and provisional support modeling:

The calculation sections are taken on the part represented by the rock formation between the determined KP (kelometric point). The calculations for these sections are valid for the part represented by the section. The parameters of the rock mass are estimated with these calculation sections according to the recommendations and approaches of the literature. Excavation coordinates are given in the X-Y system that accepts the center of the tunnel in the zero coordinate (O1). These units are given in meters in the program.

Table 2

Provisional Support Systems Offered in Twin-tube Tunnel under the Massif Rocky Classification System and recommendation

Rock class type			Low Rock (**IV**)		Middle Rock (**III**)	
R, Tunnel radius (m)			7.5		7.5	
P_0, In-situ pressure (MPa)			1.62		3.51	
ESR, Excavation Support Ratio			0.9 - 1.1		0.9 - 1.1	
Sfr+B, Support class (Grimstad and Barton 1993, Barton 1995 & 2002)			6		6	
k=0.25+7Eh(0.001+1/z)			0.30		0.39	
Excavation / Provisional support	Advancement of the upper half / lower half.	Calotte	advance of the upper half by 20 to 25 m maximum		advance of the upper half by 35 to 50 m maximum	
		Strauss	advancement of the lower half of 2.0 m maximum		advancement of the lower half of 3.0 m maximum	
Steel retaining	Steel S275JR	Dimension (mm)	HEB 220		HEB 180	
		Distance between them (m)	0.75		1.25 - 1.50	
Shotcrete	RN-30/40	Dimension (cm)	35		25	
Steel lattice	Steel FeE400	Dimension (mm)	(2x Q589/443) (150x150x6.5)		(2x Q221/221) (150x150x6.5)	
Anchor plate	Steel FeE26	Dimension (mm)	200/200/15		200/200/15	
Drain pipes	if necessary	Dimension (m)	3x 12		/	
Injection Pre-supporting iron bar	ST37	t=3mm, a=30cm	45x (Ø 7.0, L= 8m)		45x (Ø 5.0, L= 6m)	
Rock bolt	Steel FeE400 (PG PULT = 250 KN in St III steel)	SN, Ø 32 mm	Lenght	/	Lenght	L=6m
			Mumber	/	Mumber	19 - 23
		IBO, Ø 32 mm	Lenght	L=8m	Lenght	/
			Mumber	29 -33	Mumber	/
Deformation measurements (mm)			Will be performed every 10 meters along the tunnel			

Relevant soil modeling is very difficult in soil excavations given the many uncertainties and complexity. The numerical analyzes are performed according to the elastic-plastic solution. Thus the detailed modeling which includes all the conditions is neither possible nor this modeling is useful. The relaxation of material used in the weak rock masses as indicated above is applied at 0.65 (65%) in the excavation of the upper half and 0.35 (35%) is reflected in the model with the installation of the supports of the upper half and when excavating the lower half. The purpose of this distribution is to determine the rate of load to be carried by the rock and the rate of load to bear by the supports. The linear composite is applied in 3 layers on the model in the excavations of the upper part, the lower part and the slab. In the excavation levels, the first layer of shotcrete lining and the steel retaining (HEB) and the second layer of shotcrete liner and steel lattice are entered into the model. The analyzes are carried out in two stages namely, for earthquake and without earthquake. Simplification of the model may be possible under the following conditions:

- Reduction of three-dimensional conditions to two dimensions,
- Acceptance of the symmetry of the section with the axis,
- Simplification of the soil with simple descriptions,
- Simple and comprehensive description of the progress conditions of the tunnel and the excavation,
- Soil is considered homogeneous and isotropic.

5.2.1 Evaluation of the deformations of the middle rock class (III) of the part between KP: 26 + 230 - KP: 26 + 550 of the right tube and KP: 2 + 191 - KP: 2 + 490 of the left tube of the tunnel:

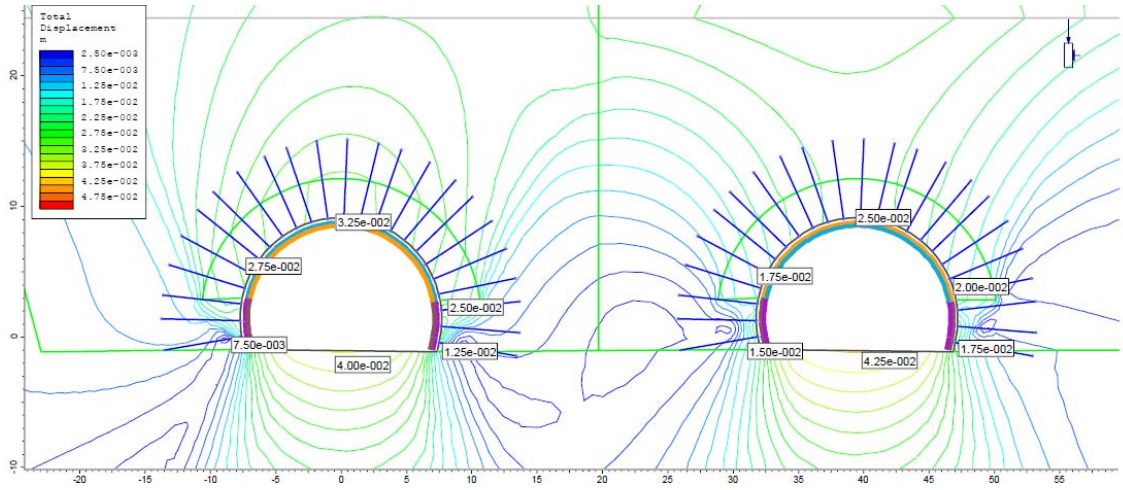

Fig. 10– (a) Total displacement in Situation without earthquake in class III.

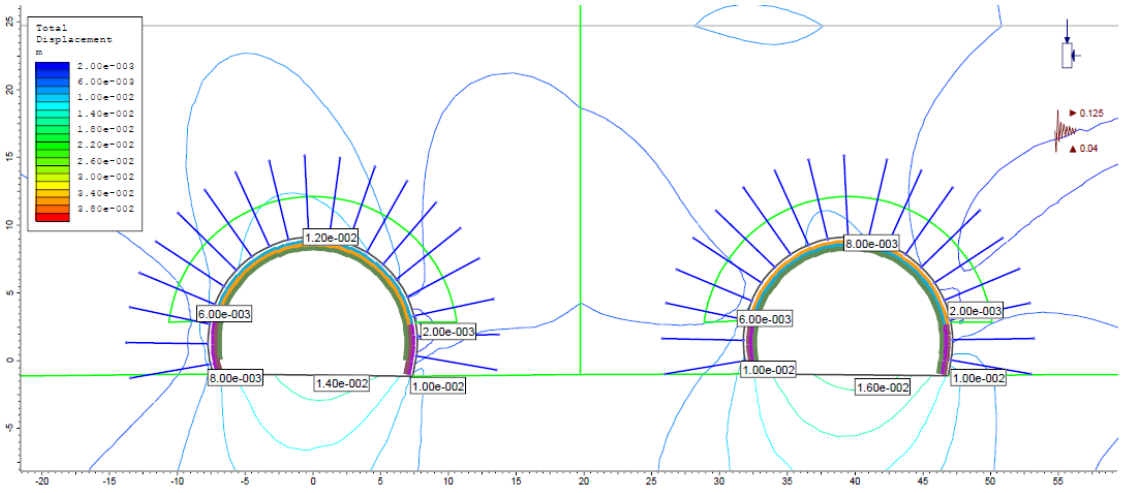

Fig. 10– (b) Total displacement in Situation after earthquake in class III.

Examination of displacement formed around the tunnel (figure 10, a) indicates a displacement of 3.25 cm in the ceiling (summit), 2.75 cm and 2.50 cm in the left and right wings of the tunnel, 0.75 cm and 1.25 cm in the lower left and right parts of the tunnel and 4 cm in the bottom of left tunnel tube. In the right tunnel tube, is observed a displacement of 2.5 cm in the tunnel ceiling, 1.75 cm and 2.0 cm in the left and right wings, 1.50 cm and 1.75 cm in the left and right lower halves and 4.25 on the bottom. When the earthquake was applied the examination of the deformations around the tunnel (Figure 10, b) shows in the left tunnel tube, a displacement of 1.2 cm in the tunnel ceiling, 0.6 cm and 0.2 cm in the left and right wings, 0.8 cm and 1.0 cm in the left and right lower halves and 1.4 on the bottom. In the right tunnel tube, a displacement of 0.8 cm in the ceiling of the tunnel, 0.6 cm and 0.2 cm in the left and right wings, 1.0 cm in the left and right lower halves and 1.6 on the bottom. According to the results, it appears that the provisional support system consisting of steel lattice, steel retaining, bolts and shotcrete is able to carry the loads from the tunnel.

5.2.2 Evaluation of the deformations of the low rock class (IV) of the part between KP: 26 + 550 and the exit of the right tube & KP: 2 + 490.970 and the exit of the left tube of the tunnel:

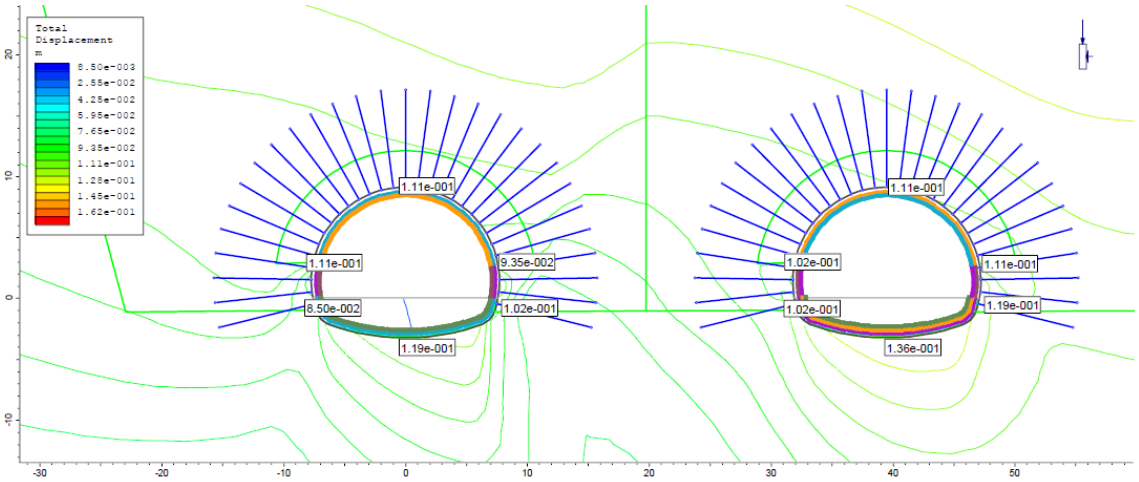

Fig. 11– (a) Total displacement in Situation without earthquake in class IV.

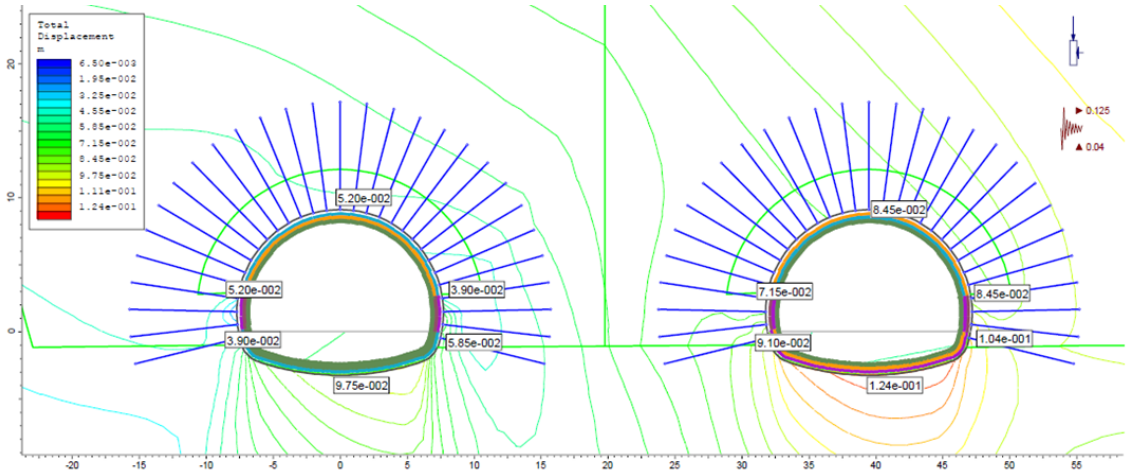

Fig. 11– (b) Total displacement in Situation without earthquake in class IV.

The examination of the deformations around the tunnel (figure 11, a) indicates a displacement of 11.1 cm in the ceiling, of 11.1 cm and 9.35 cm in the left and right wings of the tunnel, of 8.50 cm and 10.2 cm in the lower left and right parts of the tunnel and of 11.9 cm in the bottom of the left tunnel tube. In the right tunnel tube, there is a displacement of 11.1 cm in the ceiling of the tunnel, of 10.2 cm and 11.1 cm in the left and right wings, of 10.2 cm and 11.9 cm in the left and right lower halves and of 13.6 cm on the bottom. When the earthquake was applied the examination of the deformations around the tunnel (Figure 11, b) shows in the left tunnel tube, there is

a displacement of 5.2 cm in the tunnel ceiling, 5.2 cm and 3.9 cm in the left and right wings, 3.9 cm and 5.85 cm in the left and right lower halves and 9.75 on the bottom. In the right tunnel tube, there is a displacement of 8.45 cm in the tunnel ceiling, 7.15 cm and 8.45 cm in the left and right wings, 9.1 cm and 10.4 cm in the left and right lower halves and 12.4 on the bottom. According to the results, it appears that the provisional support system consisting of steel lattice, steel retaining, bolts and shotcrete is able to carry the loads from the tunnel.

6. Monitoring of the underground deformation:

Tunnel ground deformation monitoring is the main means for selecting the appropriate methods of excavation and retaining from among those provided in the design to ensure the safety of the tunnel construction (including the safety of personnel in the tunnel and the safety of structures on the ground surface). The construction of the system is planned for the continuation of the stop of the deformations and movements of the ground likely to occur after the construction of the elements of primary support in this system. In this case, it is accepted that there will be no load transfer on the coating concrete as the pressure from the ground is supported by the provisional support system. As a result, a separate analysis was not performed for the coating concrete. The monitoring program includes the specification of the measurement procedure, the location of the monitoring devices and the monitoring schedule. Attention is given to the fact that monitoring results are often affected by instrumentation, installation and environmental effects. The type of instrumentation chosen must ensure the following:

- A feasible installation procedure,
- Sustainability during the monitoring period,
- Protection against damage during construction,
- Simple processing of measurements (acquisition and transmission of data),
- Precision is required.

In general, close readings of excavation activities are taken daily; the frequency is reduced with the distance to the forehead and the decrease of the displacement rates. Shorter monitoring intervals may be required due to the specific project requirements. Monitoring sections in tunnels and shafts are usually located at distances of 5 to 20 m depending on the conditions and requirements limits. A possible concept showing minimum reading frequencies and ranges for surface and underground monitoring for a summit-wings-bottom sequence as shown in figure (12).

Fig. 12– Photography of the tunnel underground monitoring

In general, there are types of failure that cannot be detected in time by deformations monitoring, it is recommended to use additional monitoring of absolute displacements, but in a small extent. Thus the presence of an emergency surveillance system in case of adverse field conditions is ensured. In the case of block rock mass tunnels, the characteristic hazards are the detachments caused by the discontinuity of the blocks, therefore the observations must concentrate on the soil structure, the location and the orientation of the discontinuity with respect to the alignment of the tunnel. In the case of tunnels with moderate to high overload in the bedrock or foliar mass, the characteristic risks are; the orientation of the stratification or foliation, the displacement of the pavement, the displacements of the soil and the structure of the soil. consequently the Observation focused on; visual inspections, laboratory tests, absolute displacement monitoring.

6.1 Monitoring methods and requirements:

Measurements are performed using a total station and objectives. Precise prism lenses as well as bi-reflex lenses (reflectors) are used and their spatial position in the global coordinate system or project is determined. Discrete three-dimensional displacement measurements are performed by repeated measurements (usually on a daily basis). Since full monitoring cannot usually be performed from one position, an interconnected observation pattern is required, which is established using identical reference points. Stable reference points are differentiated from points that always move. Points with a defined maximum displacement rate (usually <1mm / month) can be used as reference points.

The principle of "free parking determined" is used to obtain the position of the instrument. The absolute position of all coordinate components of the marked measuring points shall be determined with an accuracy of +/- 1 mm (standard deviation) with respect to adjacent measuring sections over the entire observation period. The following sources of error should be avoided:

- Observations near the tunnel wall (minimum wall distance of 0.5 m to 1 m),
- Measurement errors due to refraction (for example. observation through or near heat sources),
- Position of the instrument near the side walls,
- Observations in asymmetrical connection,
- Measurements in a very dusty environment or when there is a lot of vibration (i.e. Caused by machines).

The surveyor must record and submit the following items after each measurement action:

- Measurement sequence system (relative to the measurement section or along the tunnel),
- Unmeasured points and reason indication (destroyed, not visible, etc.),
- Significant displacements (measurement error, rapid increase in displacements),
- Readings to zero,
- Monitoring conditions (air quality, vibration, limited visibility, sources of heat, etc.).

The geometric definition of the sections is shown on the drawings. The purpose of these sections is to measure convergences in the tunnel during construction. In general, the convergence sections will be composed by 5 points distributed as shown above, one in the summit, two in the forward section (calotte), in the gables at a height of 1.50m from the base excavation and the other two, at the stross section, at a height of 1.50m from the tunnel bottom, also in the gables.

6.2 Deformations diagrams from monitoring results:

A lateral and longitudinal displacement of 40-55 mm / month has been observed in some sections of the middle rock (Class III) left tube calotte (Figure 13). Also in the right tube calotte, lateral and longitudinal movements of 30-40 mm / 2 months (Figures 14) and lateral displacements of 90 mm / 2 months (Figures 14a, c), which forces us to reinforce immediately by bolts IBO / L = 8m (3 top, 2 wall right side, 2 wall left side), on the other hand, the remains sections are stable. Consequently; deformations were stopped and class III-A was created. In along the low rock tunnel (Class IV) (Figures 15, 16); in the left tube; a maximum settlement of 80 to 120 mm / 4 months was observed (Figure 15 a, b, c), lateral and longitudinal displacements of 40- 100 mm / year (Figures 15). In the right tube; maximum deformations of 20 to 40 mm / 2 months have been observed (figure 16 a), deformations up to 70 mm / 2 months (Figure 16 b), maximum settlements of 60 to 80 mm / year (Figure 16c, d),

deformations of 60-150 mm / 10 months (Figures 16 e, f, g), which forces us to reinforce immediately by bolts IBO / L = 16m (6 top) and sometimes bolts IBO / L = 12m (2 lateral right, 2 lateral left), on the other hand, the remains sections are stable. Consequently; deformations were stopped and classes IV-A, IV-B were created.

Real deformations are more than numerical modeling when we compare the monitoring results with numerical modeling results, we can say that it is logical, because the software cannot really simulate at one hundred percent construction tunneling phenomenon without making uncertainties between real and digital data. In conclusion, maximum attention must be given to deformations when the implementation of tunnel digging and the setting up of provisional support.

6.2.1 Middle rock (Class III):

Left tube:

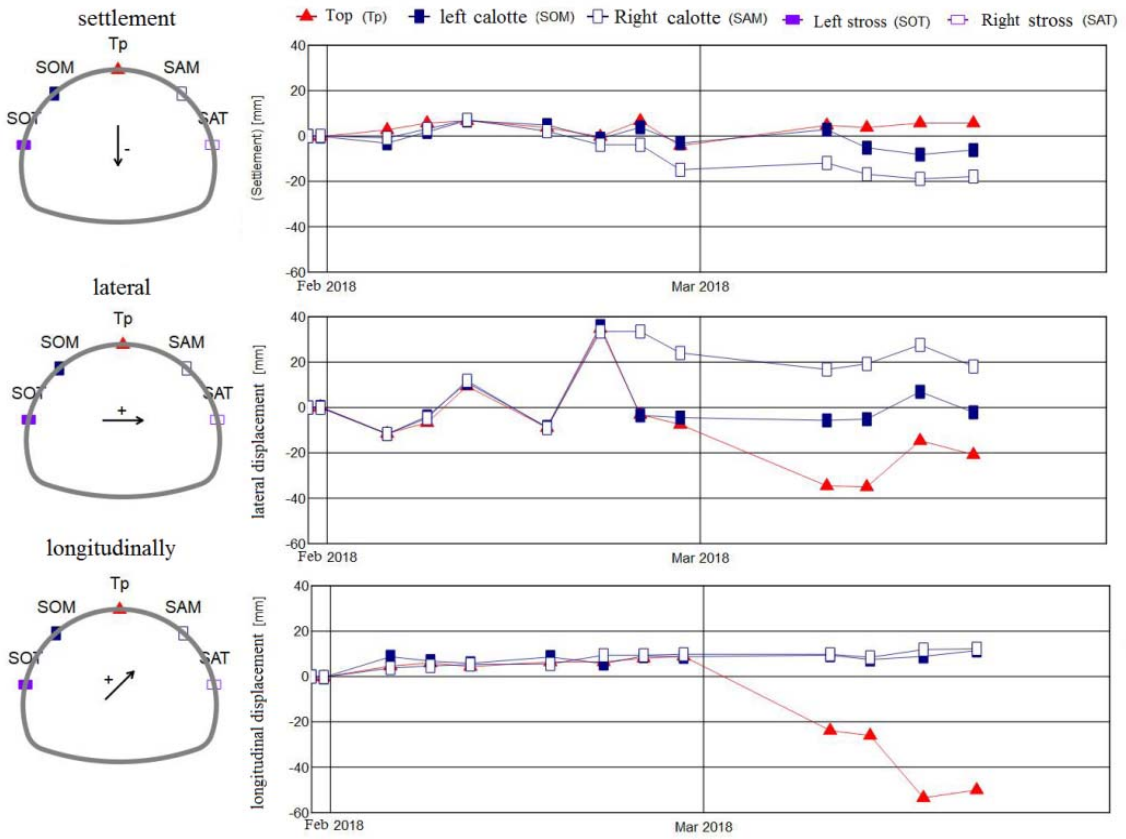

Fig. 13– Left tube Tunnel Cross section KP - 2,485.000 / First measure: 30.01.2018, Last measure: 21.03.2018

Right tube:

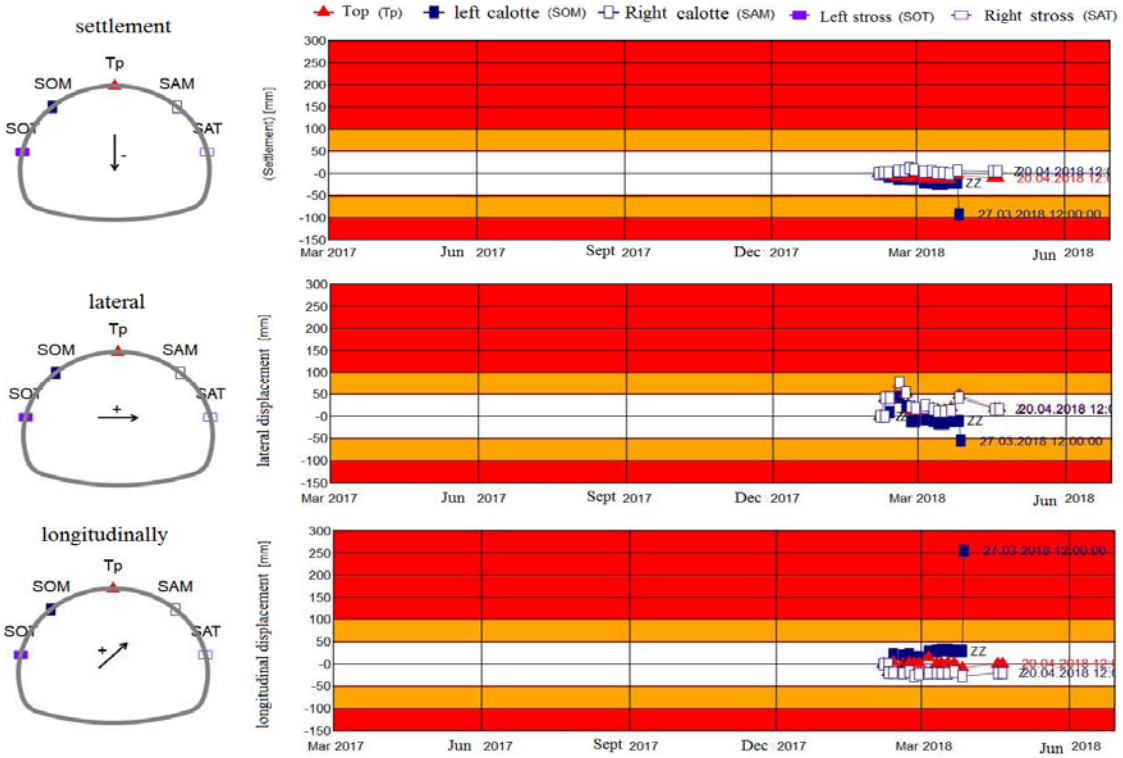

Fig. 14– (a) Right tube Tunnel Cross section KP 26,512.000/ First measure: 5.02.2018, Last measure: 20.04.2018.

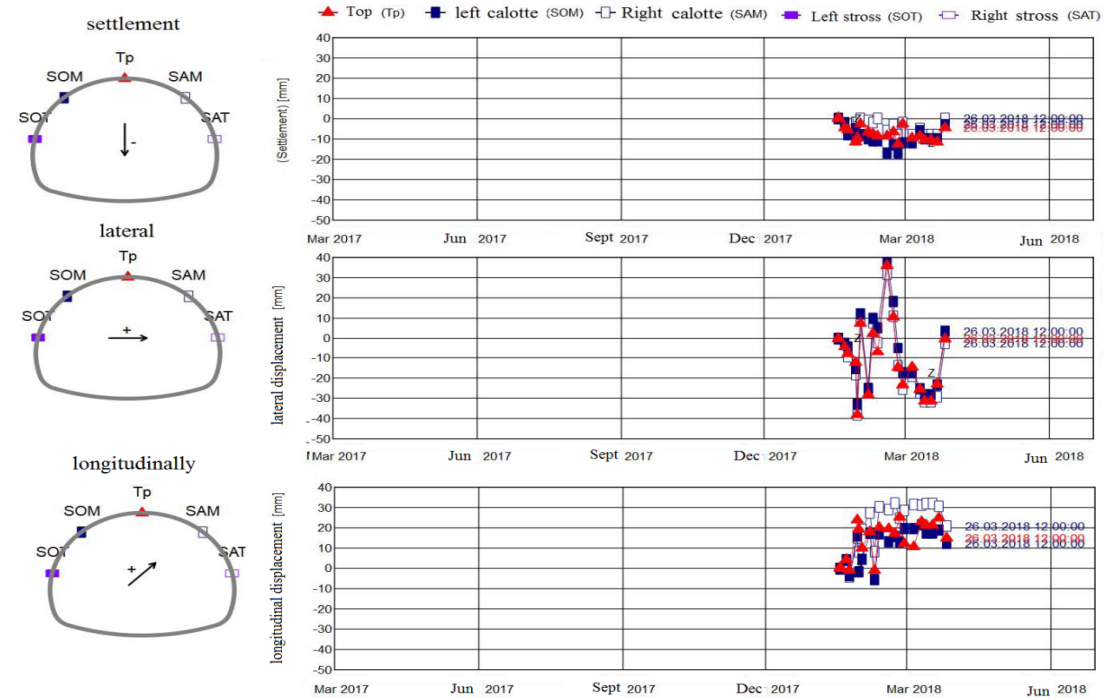

Fig. 14– (b) Right tube Tunnel Cross section KP 26,527.000/ First measure: 17.01.2018, Last measure: 26.03.2018

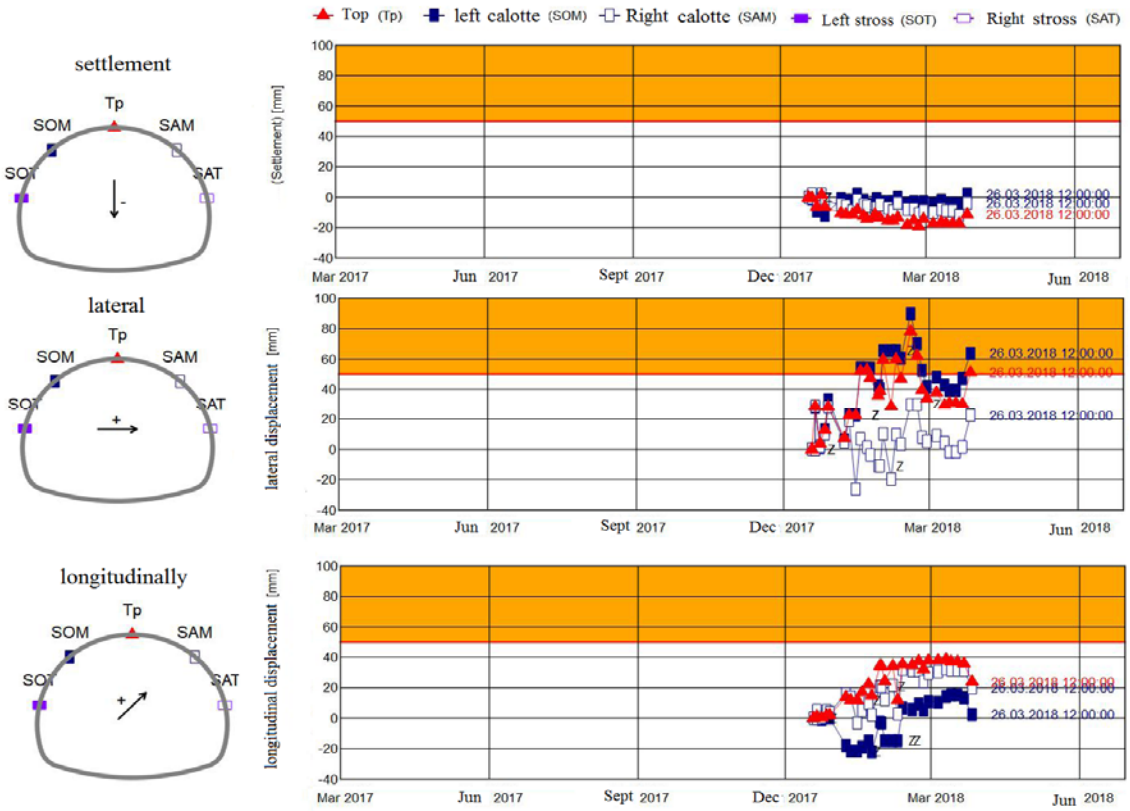

Fig. 14– (c) Right tube Tunnel Cross section KP 26,543.000 / First measure: 18.12.2017, Last measure 3.04.2018

6.2.2 Low rock (Class IV):
Left tube:

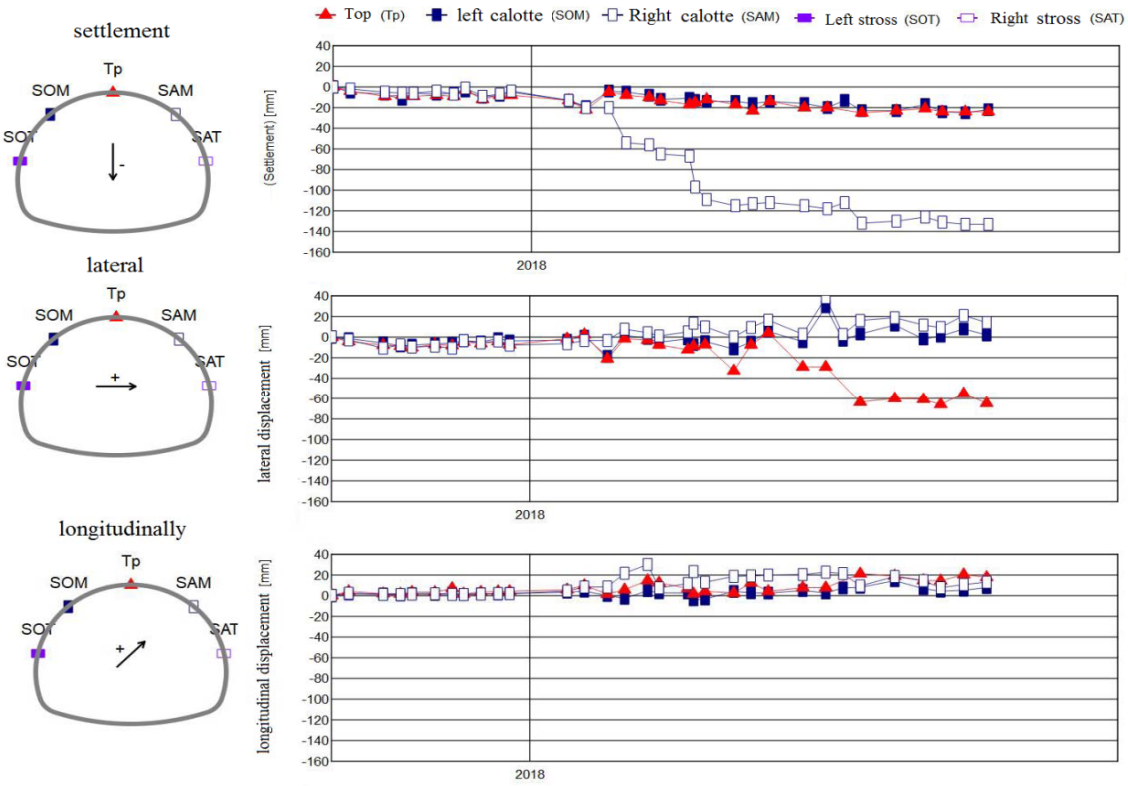

Fig. 15– (a) Left tube Tunnel Cross section KP 2,501.000/ First measure: 15.05.-2017, Last measure: 7.04.2018

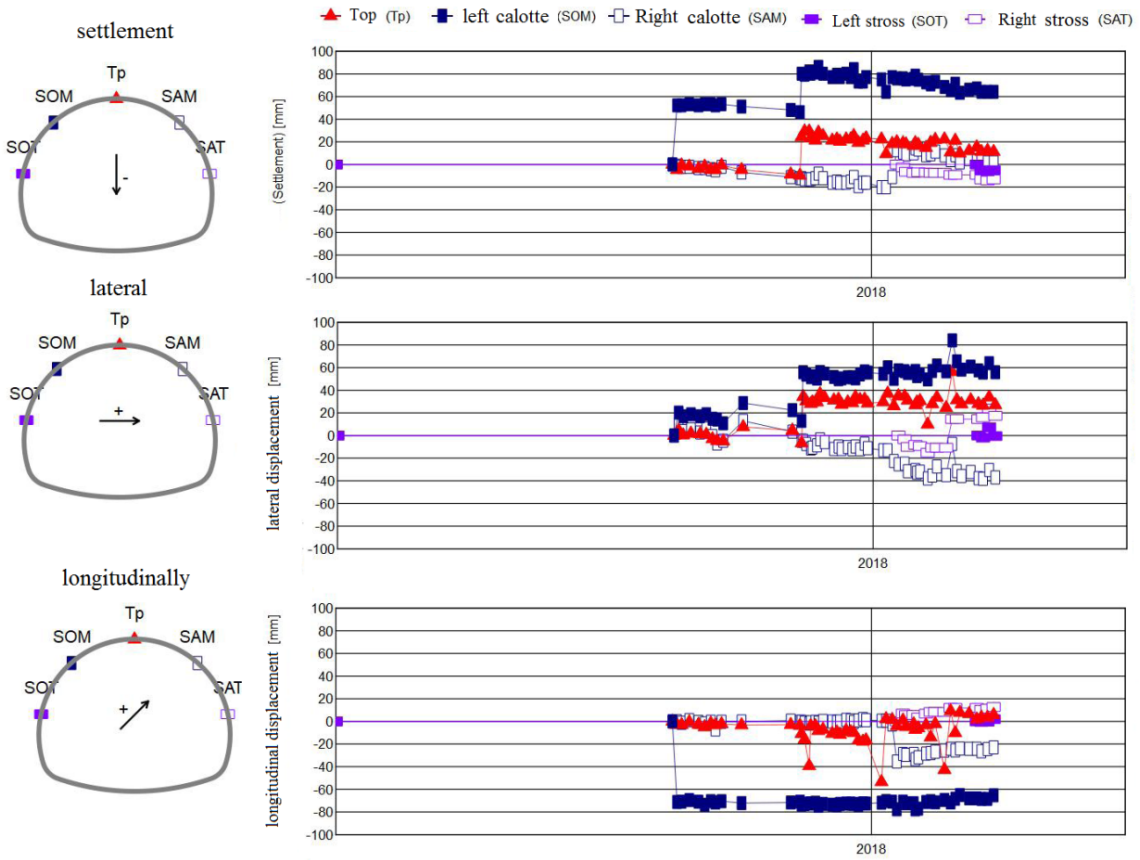

Fig. 15– (b) Left tube Tunnel Cross section KP 2,516.000/ First measure: 17.01.2017, Last measure: 21.03.2018

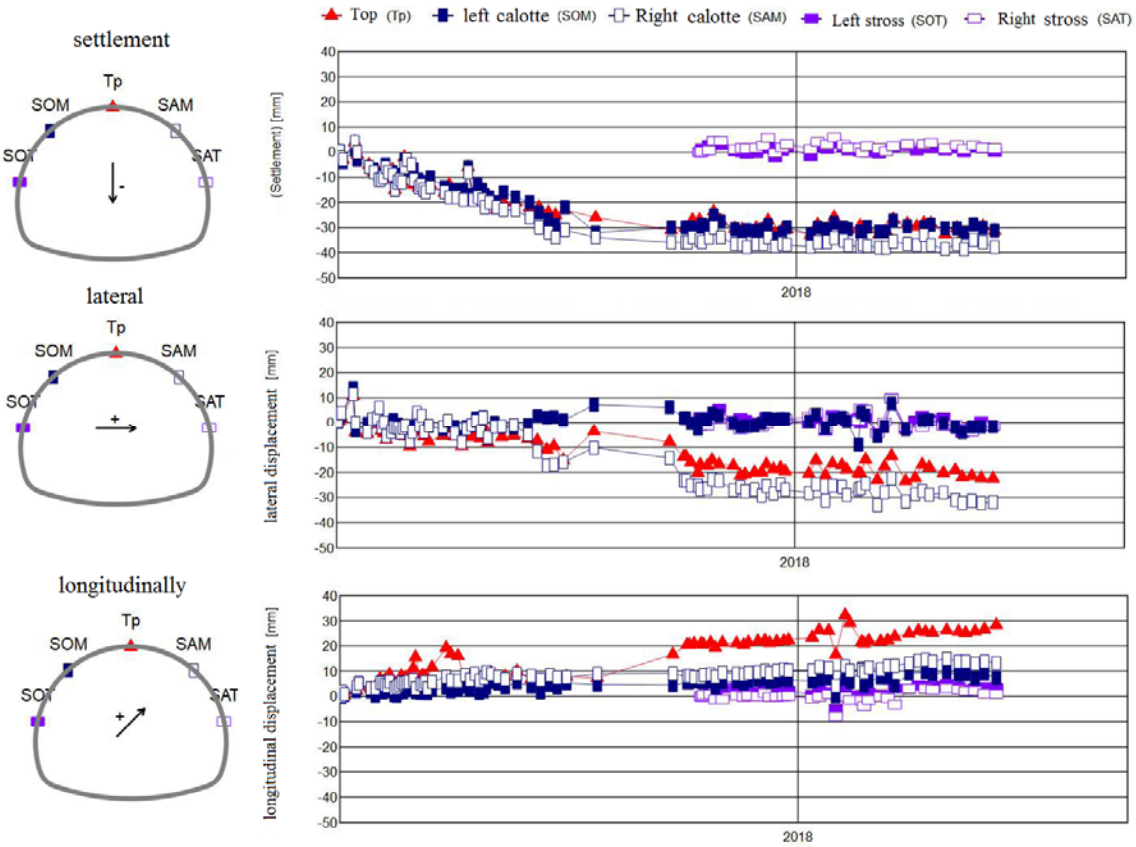

Fig. 15– (c) Left tube Tunnel Cross section KP 2,541.000/ First measure: 21.06.2017, Last measure: 26.03.2018

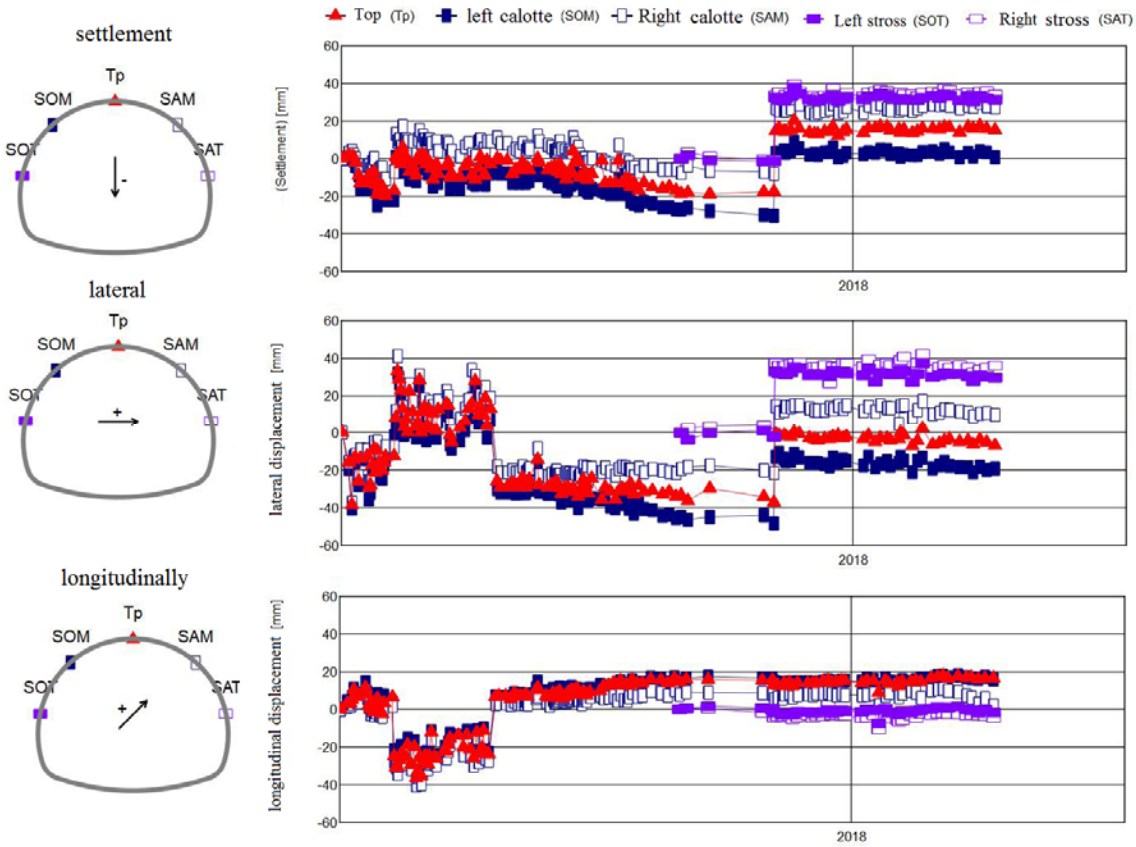

Fig. 15– (d) Left tube Tunnel Cross section KP 2,555.000/ First measure: 4.03.2017, Last measure: 26.03.2018

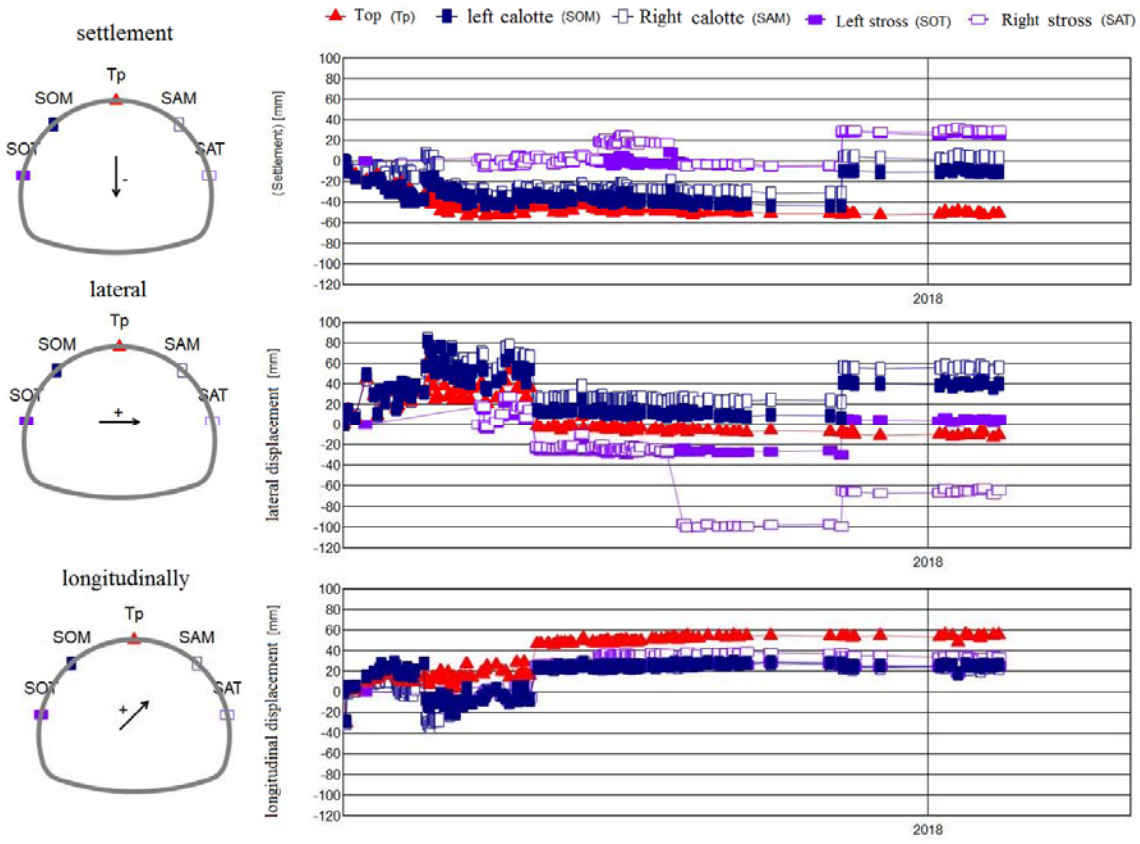

Fig. 15– (e) Left tube Tunnel Cross section KP 2,566.000/ First measure: 19.02.2017, Last measure: 8.02.2018

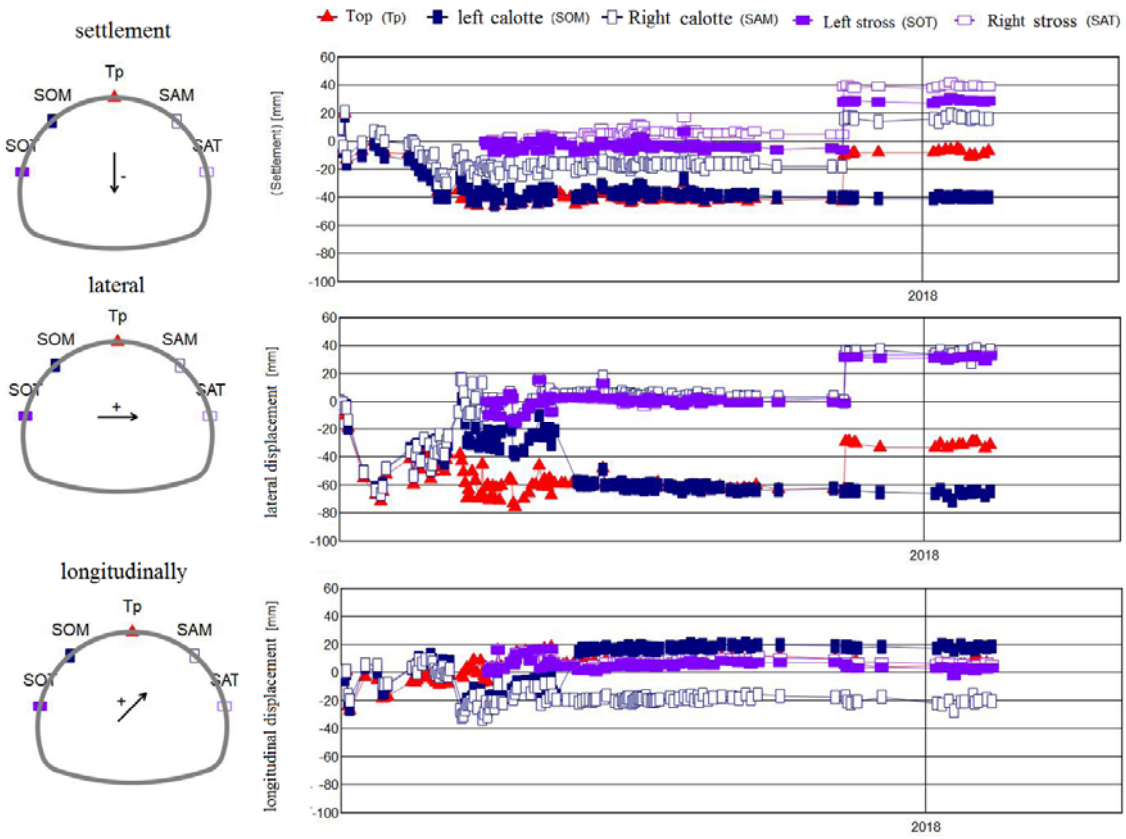

Fig. 15– (f) Left tube Tunnel Cross section KP 2,577.000/ First measure: 26.01.2017, Last measure: 8.02.2018

Right tube:

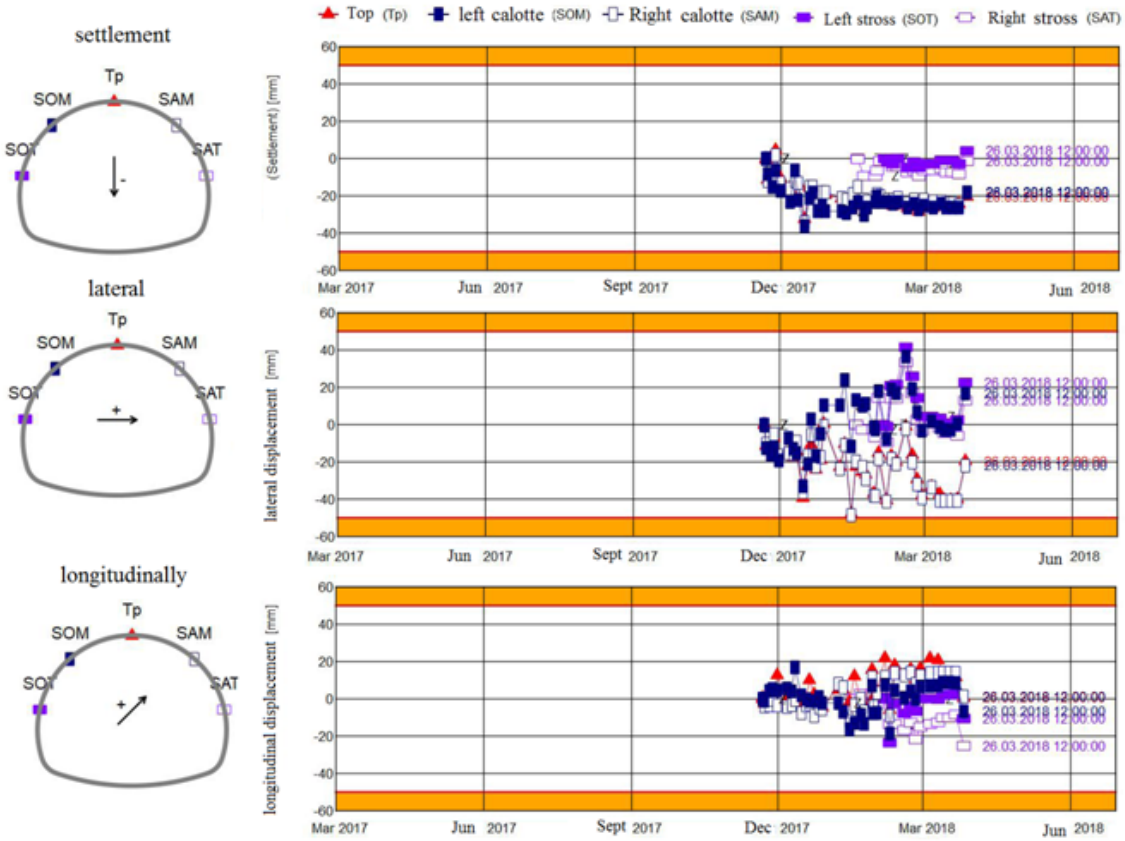

Fig. 16– (a) Right tube Tunnel Cross section KP 26,562.000/ First measure: 21.11.2017, Last measure: 26.03.2018

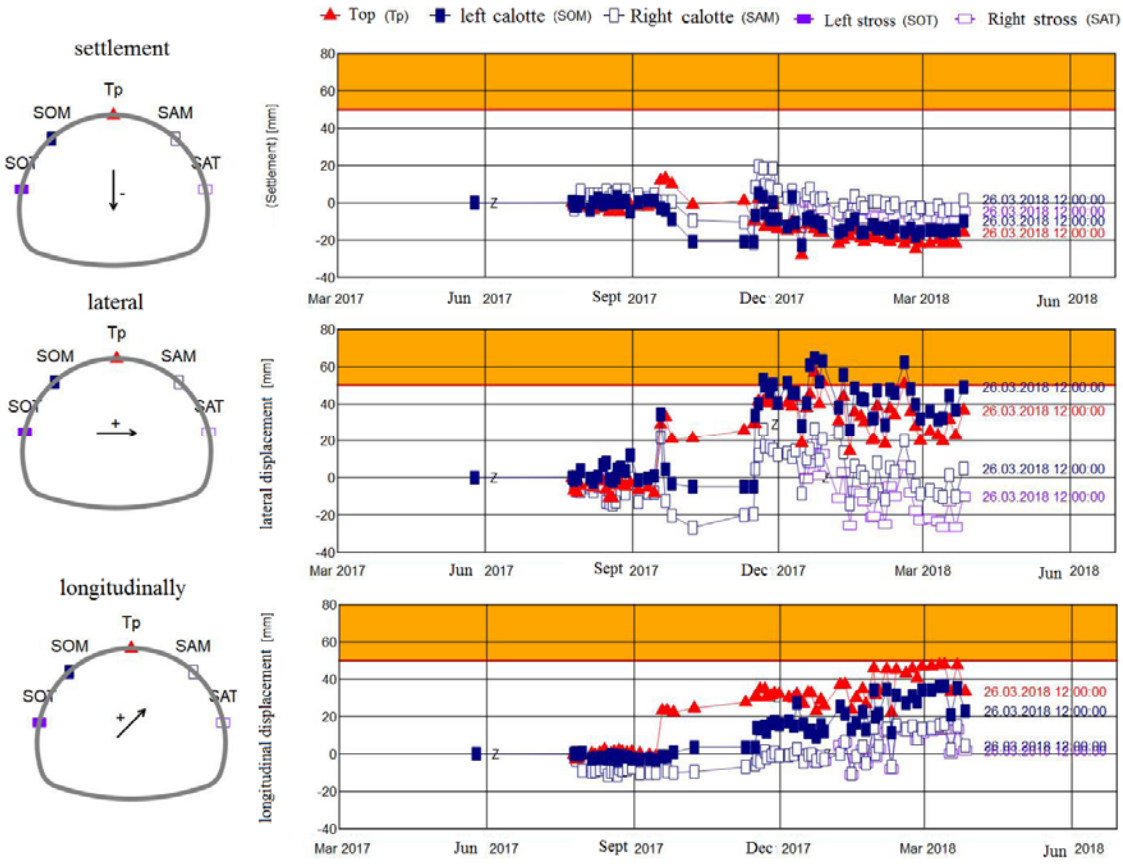

Fig. 16– (b) Right tube Tunnel Cross section KP 26,576.000/ First measure: 15.05.-2017, Last measure: 26.03.2018

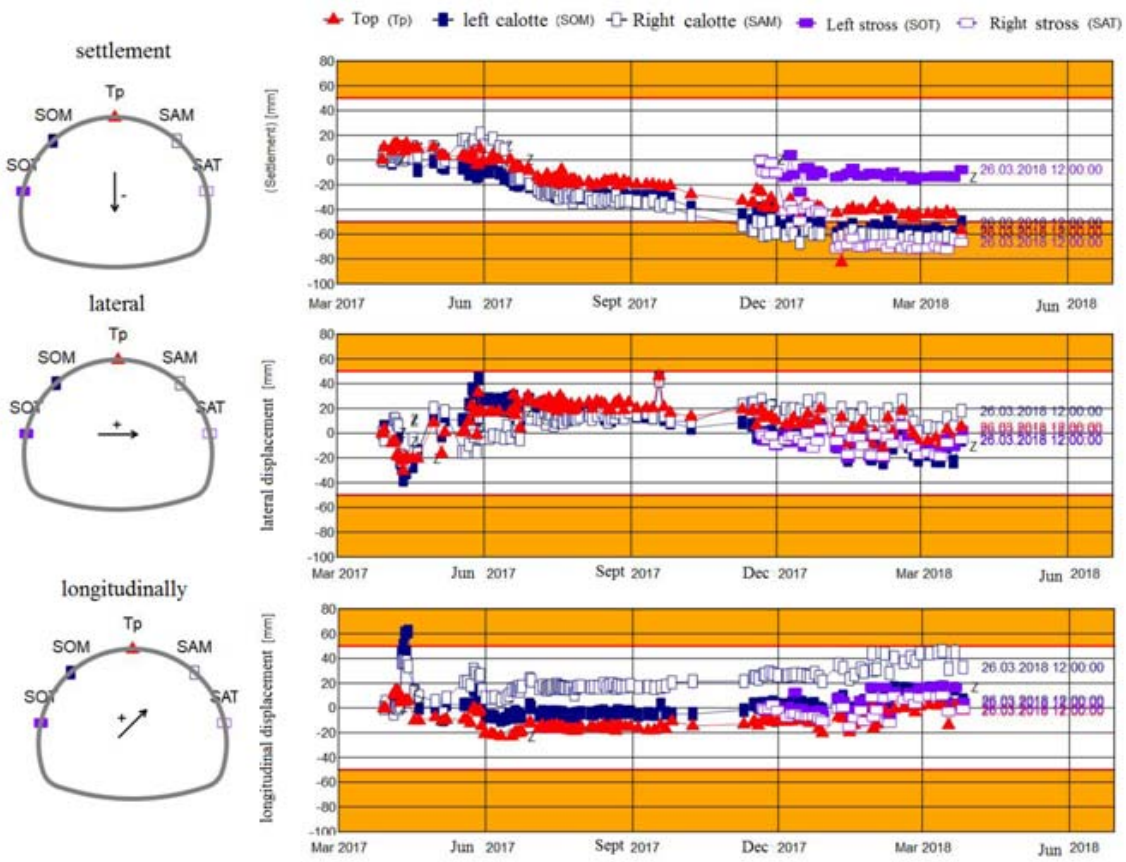

Fig. 16– (c) Right tube Tunnel Cross section KP 26,588.000/ First measure: 15.05.-2017, Last measure: 26.03.2018

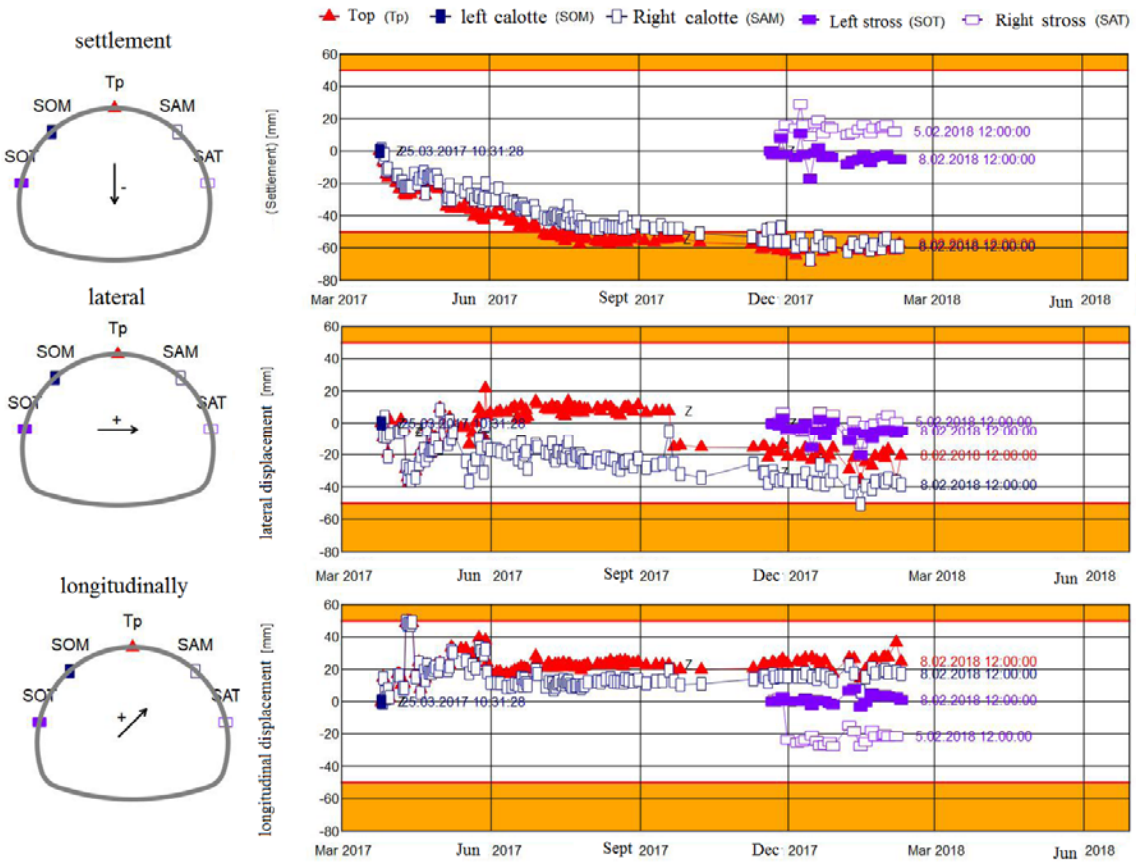

Fig. 16– (d) Right tube Tunnel Cross section KP 26,603.000/ First measure: 15.05.-2017, Last measure: 8.02.2018

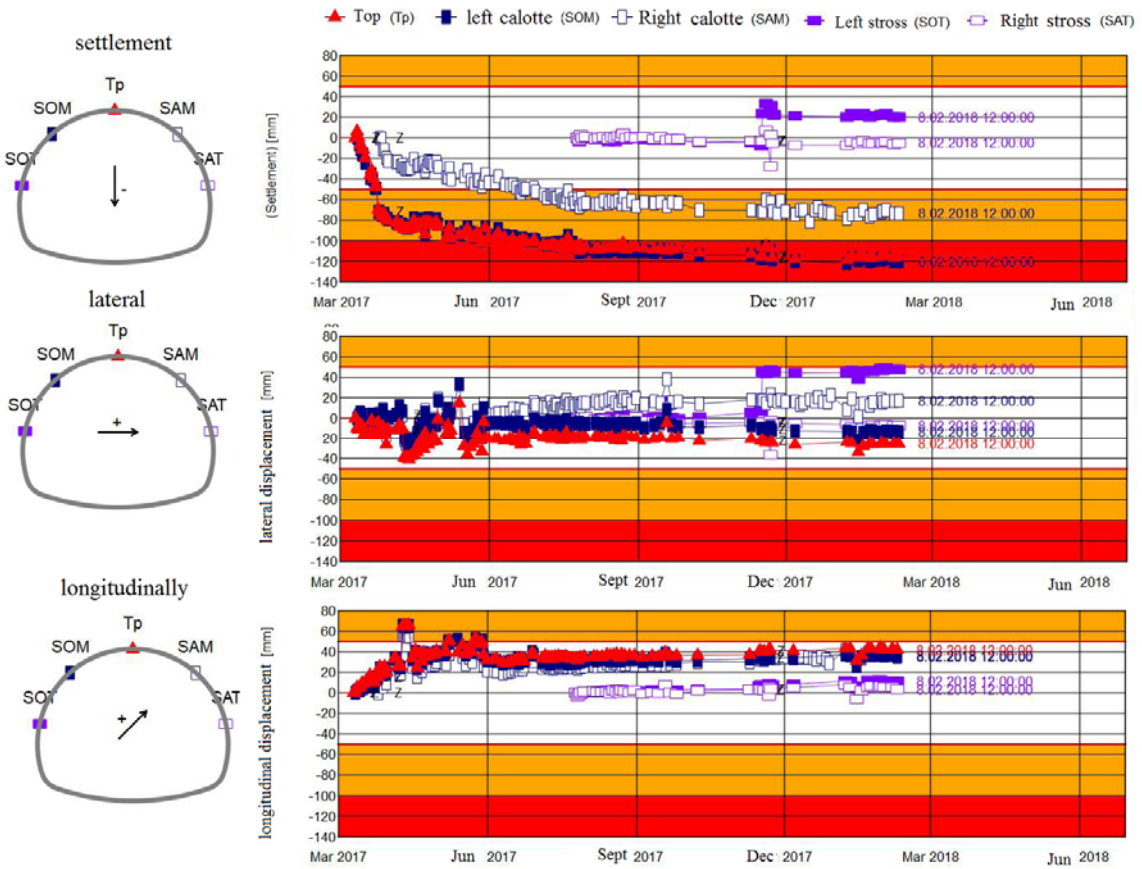

Fig. 16– (e) Right tube Tunnel Cross section KP 26,616.000/ First measure: 15.05.2017, Last measure: 8.02.2018

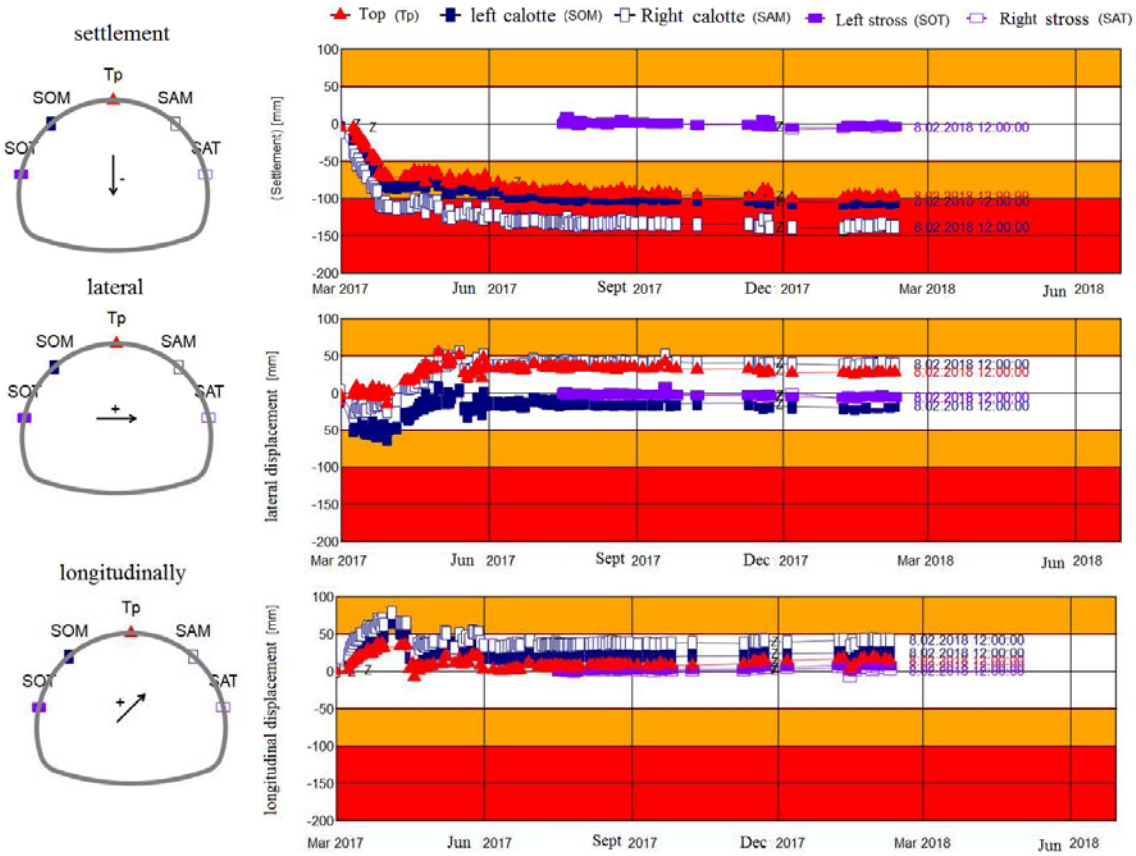

Fig. 16– (f) Right tube Tunnel Cross section KP 26,626.000/ First measure: 15.05.2017, Last measure: 8.02.2018

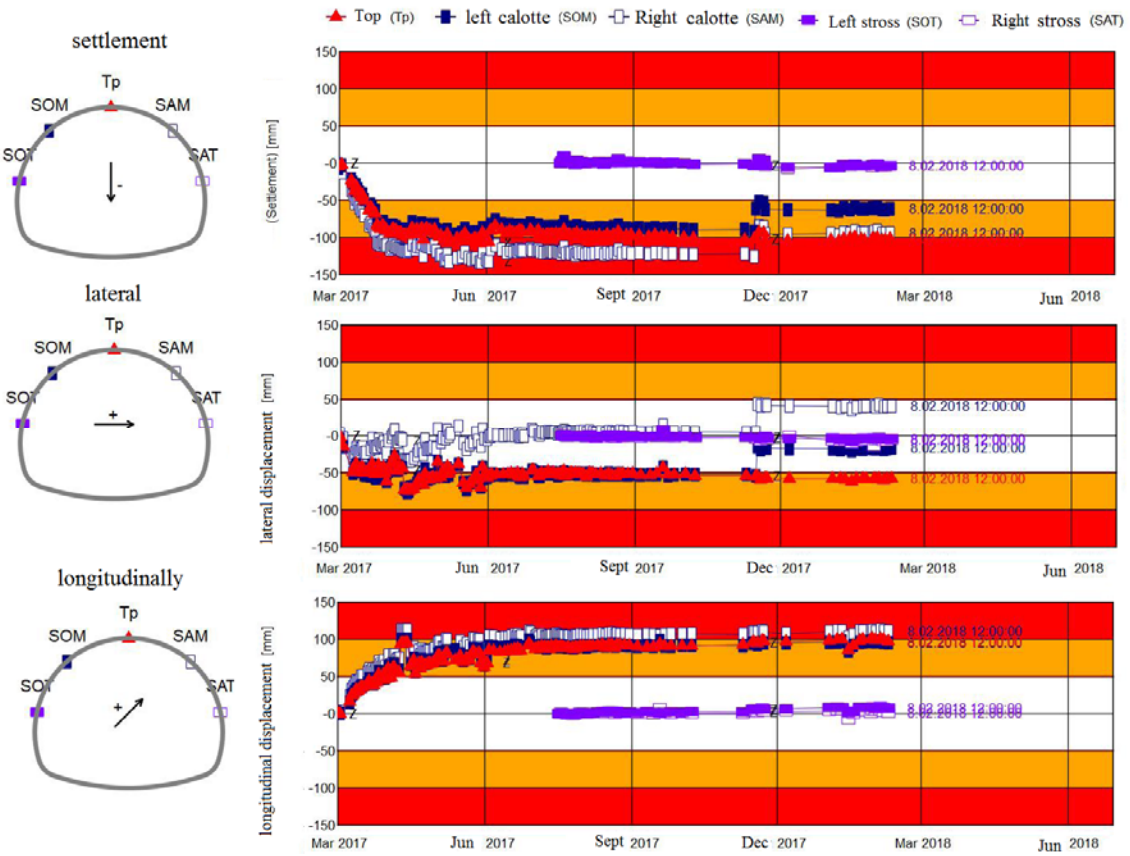

Fig. 16– (g) Right tube Tunnel Cross section KP 26,635.000/ First measure: 15.05.2017, Last measure: 8.02.2018

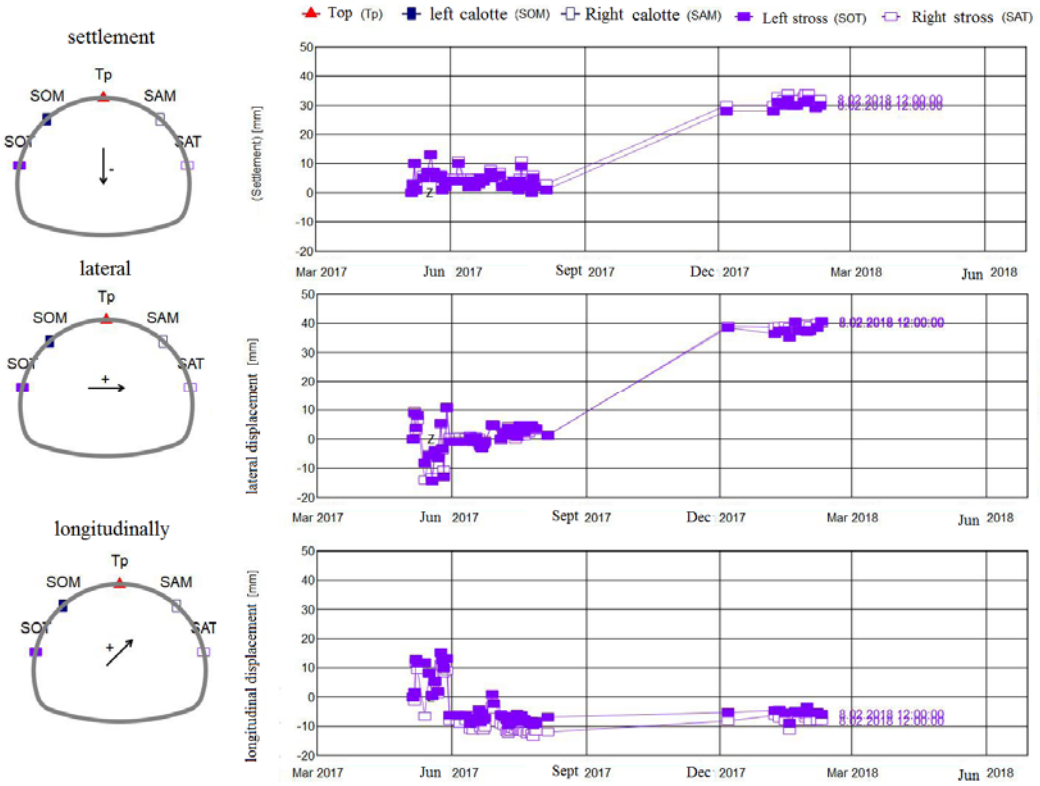

Fig. 16– (h) Right tube Tunnel Cross section KP 26,641.000/ First measure: 15.05.2017, Last measure: 8.02.2018

7. Conclusion:

The characterization of the rock mass and the site is very essential for tunnel design. Effective characterization provides reliable design input parameters for classification systems. The construction of any engineering structure in the rock mass causes the redistribution of stresses in situ which is not evaluated by empirical methods, it evaluates only the quality of the rock mass. Therefore, it is very necessary to evaluate/predict the quality of rock mass and in turn the "RMR- Q - systems" value with more precision. Moreover, the empirical methods do not analyze either the performance of the support systems, the distribution of the constraints around the opening and the deformation around the tunnel while it is used for the determination of the input parameters for numerical methods. for this purpose; The artificial intelligence used to deal with such nonlinear relations problems of engineering and it can also be used to confirm and improve the design solutions in any engineering projects. Numerical modeling in rock and civil engineering is used as a tool that facilitates the site engineers to evaluate the rock mass behavior and its effects on engineering structures and support systems. This Method resolved complex engineering problem utilising Plane Strain Two Dimension (2D) Analysis, Axisymmetric 2D Analysis and Three Dimension (3D) Analysis.

It is necessary to create a coating system (shotcrete, steel lattice, HEB and anchor bolts) with able to operate with the environment and able to provide bearing capacity immediately after excavation in order to meet the requirements, measure and evaluate continuously the deformations and surface movements inside the tunnel during excavation activities. On the other hand, deformations formed and possible structural damage must be measured and monitored. Measurements made are evaluated with the geomechanical conditions and necessary modifications after the geotechnical measurements required in the tunnel must be made and evaluated during construction to perform some revisions in the support systems (thickness of shotcrete, coating interval, bolt density etc.) and production parameters by the following recommendations:

- Benefit the most of the natural resistance of the rock mass, to this end insert support systems at the most opportune moment,
- Use flexible support systems that can accommodate rock deformations and support to ensure full contact between the support system and the excavation surface,
- Quickly avoid excessive relaxation of deformities using provisional support,
- Control excavation and support systems with permanent deformation footage, carry out a progressive excavation or move to other classes of support if necessary,
- Ensure the total functioning of the support system, particularly in low rocks,
- Provide flexibility for rock classes and support systems specified based on observations and measurements made during excavation.

Acknowledgements:

This work is under the auspices of the General Directorate of Scientific Research and Technological Development of the Algerian Ministry of Higher Education and Scientific Research.

Appendix A.

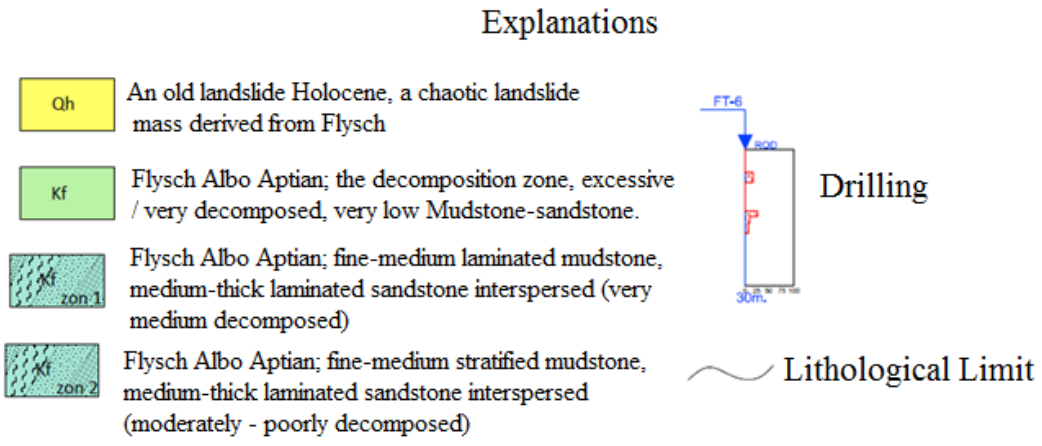

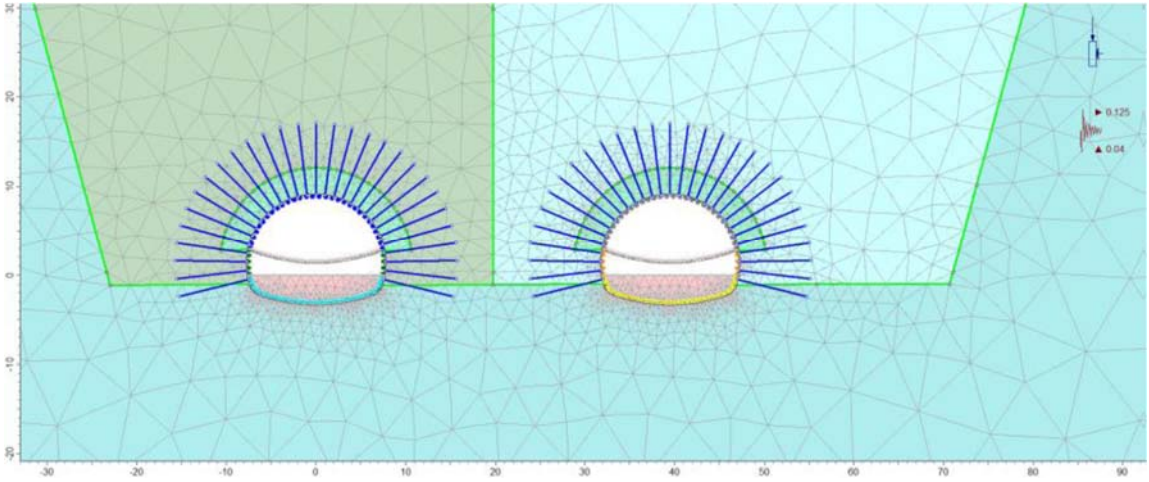

Fig. 17– (a) The model created with the program Phase2 2D between KP: 26 + 230 and KP: 26 + 550 of the right tube and KP: 2 + 191.682 and KP: 2 + 490.970 of the left tube, (Middle Rock III)

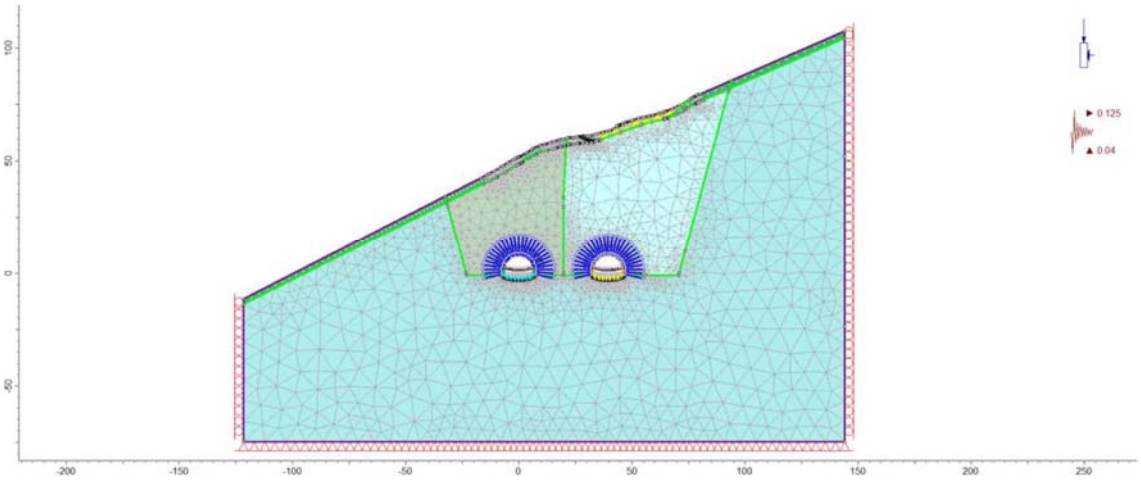

Fig. 17– (b) The model created with the program Phase2 2D between KP: 26 + 550 and the output of the right tube & KP: 2 + 490.970 and the output of the left tube (Low Rock IV)

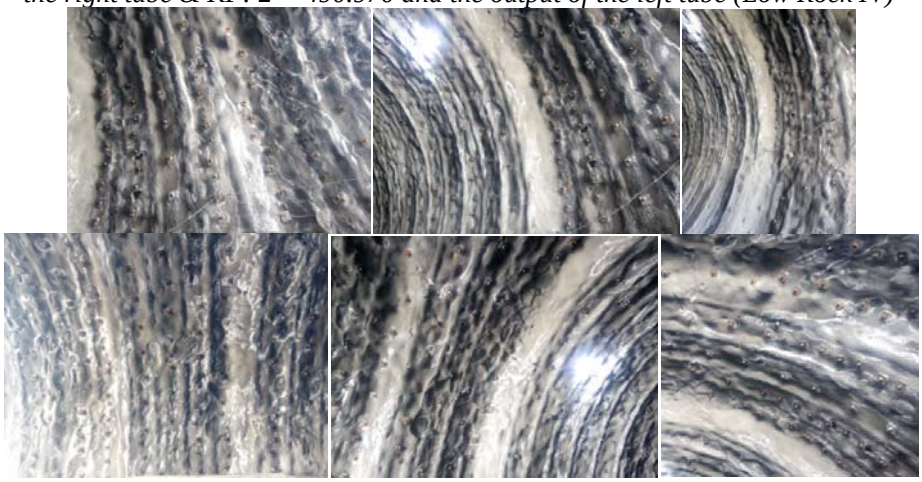

Fig. 17– Photography's of reinforced zone in the low rock zone IV

REFERENCES

[1]- Rasouli, M. 2009. "Engineering Geological Studies of the Diversion Tunnel, Focusing on Stabilization Analysis and Support Design, Iran." Engineering Geology 108: 208–224.
[2]- Ali, W. Rock Mass Characterization for Diversion Tunnels at Diamer Basha Dam, Pakistan – a design perspective. International Journal of Scientific Engineering and Technology; 2014; 1292–1296.
[3]- Genis, M., H. Basarir, A. Ozarslan, E. Bilir, and E. Balaban. 2007. "Engineering Geological Appraisal of the Rock Masses and Preliminary Support Design, Dorukhan Tunnel, Zonguldak, Turkey." Engineering Geology 92: 14–26.
[4]- Z. T. Biniawski, "Classification of Rock Masses for Engineering: The RMR System and Future Trends," in Rock Testing and Site Characterization, Pergamon, Oxford, UK, 1989.
[5]- G. F. Andriani and M. Parise, "Applying rock mass classifications to carbonate rocks for engineering purposes with
a new approach using the rock engineering system," Journal of Rock Mechanics and Geotechnical Engineering, vol. 9, no. 2, pp. 364–369, 2017.
[6]- A. Vakili, "An improved unified constitutive model for rock material and guidelines for its application in numerical modelling," Computers and Geotechnics, vol. 80, pp. 261–285, 2016.
[7]- L. Jing, "A review of techniques, advances and outstanding issues in numerical modelling for rock mechanics and rock engineering," International Journal of Rock Mechanics and Mining Sciences, vol. 40, no. 3, pp. 283–353, 2003.
[8]- J. A. Harrison and J. P. Hudson, Engineering Rock Mechanics. Part 2: Illustrative Workable Examples, Pergamon, Oxford, UK, 2000.
[9]- Gurocak, Z., P. Solanki, and M. M. Zaman. 2007. "Empirical and Numerical Analyses of Support Requirements for a Diversion Tunnel at the Boztepe Dam Site, Eastern Turkey." Engineering Geology 91: 194–208.
[10]- Bobet, A. 2010. "Numerical Methods in Geomechanice." The Arabian Journal for Science and Engineering 35, Number 1B.
[11]- Hamou Djellit, Évolution tectono-métamorphique du socle Kabyle et polarité de mise en place des nappes de flysch en petite Kabylie occidentale (Algérie), Supported in 1987 at Paris 11 university, in partnership with University of Paris-Sud. Faculty of Sciences of Orsay (Essonne).
[12]- Hoek, E., Kaiser, P.K., and Bawden, W. F. (1993): Support of Underground Excavations in Hard Rock, 47-50.
[13]- Hoek, E., and Brown, E.T. (1997): Practical estimation of rock mass strenght. International Journal of Rock Mechanics and Mining Science, 34: 1165-1186.
[14] Evrim Sopac, and Haluk Akgun (2008): Engineering geologi cal investigations and the preliminary support design for the proposed Ordu Peripheral Highway Tunnel, Ordu, Turkey. Engineering Geology, 96: 43-61.
[15]- Bortan, Using the Q-System, Sweden and Norway, Norwegion Geotechnical Institute, Oslo, Norway, 2013.
[16]- Miranda, Gomes, T.A., Correia and Nogueira (2015): academia.edu. (P. Cortez, Producer) Retrieved march monday, From http://www.academia.edu/3114361/ Alternative models for the calculation of the RMR and Q indexes for granite rock masses.
[17]- El-Naqa, A. Application of RMR and Q geomechanical classification systems along the proposed Mujib Tunnel route, central Jordan .Bull Eng Geol Environ (2001) 60: 257. https://doi.org/10.1007/s100640100112.
[18]- S.Y Choi and H.D Park, Comparison among different criteria of RMR and Q-system for rock mass classification for tunnelling in Korea, Volume 17, Issue 4, October 2002, Pages 391-401. doi.org/10.1016/S0886-7798(02)00063-9.

Experimental and Numerical investigation on the effect of CFRP straps with different orientation angles on the strength of the beam

Investigație experimentală și numerică asupra efectului benzilor CFRP cu unghiuri de orientare diferite asupra rezistenței fasciculului

Gandla Nanabala Sreekanth[1], S.Balamurugan [2]

Research scholar[1], Centre for Disaster Management and Mitigation[1], VIT University[1], Vellore[1], Tamilnadu,[1] India
Nanabala.sreekanth2016@vitstudent.ac.in[1]

Assistant Professor Sr[2], Department of Structural and Geotechnical Engineering[2], School of Civil and Chemical Engineering[2], VIT University[2], Vellore[2], Tamilnadu[2], India
balamurugan.s@vit.ac.in[2]

DOI: 10.37789/rjce.2022.13.3.2

Abstract –
Now a days all the civil engineering structures are designed earthquake resistant to withstand the high intensity earthquakes that are occurring more frequently. But there is a need to strengthen the already existing structures to withstand for earthquakes. Usage of CFRP sheets is a technique to strengthen a structural member of a structure to withstand for natural occurring calamities.
This study presents the experimental and numerical investigation on the effect of CFRP sheets with varying angles of straps on the strength of the beam. The objective of this work is to explore the behaviour of RC beam strengthened with CFRP sheet and straps. Numerical analysis was carried out using software to represent the ultimate load vs deflection and ultimate load carrying capacity of the beam.
Comparison of experimental with numerical results exhibited, that beam strengthened with angled straps showed more effective in enhancing the deflections, failure modes and ultimate strength of the RC beam. The strength of CFRP straps with different orientations were analyzed and compared.

Key Words – *Unidirectional carbon fiber, epoxy, load versus, deflection graph, ultimate load carrying capacity.*

1. Introduction

Deterioration of old structure and replacing it with a new structure may lead to various disadvantages like financial, material, and labour cost, etc. Instead of deteriorating, strengthening of structure is the best solution. Retrofitting is required in many cases like poor construction, inferior material, unexpected loads, earthquakes, etc. Flexural and shear strengthening arrangement remains the best method in increasing the stiffness, ultimate strength and cracking behaviour of the RC beam [1]. Many researches have been conducted on the RC beams retrofitted with flexural and shear strengthening by CFRP sheets through experimental and numerical analysis. The

analysis has showed that flexural and shear strengthening of beam would avoid the debonding failure, which provides good strength and ductility[2]. New techniques have emerged in recent times for increasing the flexural and shear strength of beams, Instead of bonding of CFRP externally they have made holes along the web of the beam and inserting the FRP material into the holes and filling the holes with grout to increasing the shear strength of the beam[3],Near surface mounted CFRP bars to enhance the overall load carrying capacity ,moment redistribution and ductility of the beam[4], Another anchoraging technique *i.e*, CFRP stitching along U-wrap is used for shear deficient beams it is new method for shear strengthening of beam[5], Another method for increasing the shear strength of the beam stands by using the shear deficient beam and using two schemes one is the externally bonded near surface mounted carbon fiber polymer u wrap strips and welded wire mesh and second strengthening scheme is CFRP u-wraps and horizontal CFRP strips of externally bonded to the beam[6]. Externally bonded reinforcement in groove (EBRIG) technique is used to enhance the shear capacity of the beam in this regard, as the spacing of stirrups increases the effective strains in the carbonfibre also increases ductility with increases in stirrups[7]. Experimental and numerical analysis has done to investigate the precracked and repaired beams and strengthened by CFRP sheets results indicated that improved load vs deflection curve and as the number of CFRP layers increases shear stresses rises[8]. A new improved anchorage technique by using steel pins,steel clamps and the initial compression induced by the clamps were investigated and found that steel clamps provide high strength[9]. The grade of steel plays a major role in the debonding of the fibre as the grade of steel increases the bond efficiency of CFRP laminates increased[10]. Combination of GFRP bars and CFRP sheets are used to increase the flexural performance of the beam. The test results revealed that central deflection and crack sizes are reduced considerably by increasing the number of CFRP layers and GFRP reinforcement ratio[21]. Debonding of CFRP is one of the problem but end self locking a technique to prevent the debonding of the CFRP from the beam, due to this intermediate crack debonding is subsequently reduced and an increase in the ultimate load and ductility is observed that ensuring failure of CFRP rupture or concrete crushing regardless of debonding[22]. Researchers have done on the flexural retrofitting of CFRP sheets bonded on the sofit of the beam. The main influence is bonding of CFRP to the sofit of the beam. Bonding plays a major role in the strengthening of structures. Bonding of cfrp sheets to the surface can be increased using different methodslike by improving the surface of the structure, by grooving method, by externally bonded reinforcement and externally bonded reinforcement on grooves or by anchored cfrp strips. Increasing the bonding delays the debonding and increases the ductility of the beam and also increases the ultimate load carrying capacity.[21,29,31,37]. A few studies also conducted on the length and thickness[19], concrete cover thickness[34] and effect of end anchorages[24] on the debonding failure and flexural strength of the beam. Externally bonded reinforcement is a basic strengthening technique applied for a existing damaged structure. The reason behind is high strength to weight ratio, stiffness and load carrying capacity.

Various parameters of this strengthening method have been investigated in the past years. The parameters include the effects of strengthened precracked beam[20], effect of strengthened shear failed beams[23] and also damaged concrete cover[34]. Special attention has been paid on the determination of type of resins they are rubber modified resin, cement based resin, bio based resin for bonding the CFRP to sofit of the beam[22,25,42].

From the above works it is clear that externally bonded carbon fiber sheets are currently being studied for strengthening of structural components. In this study carbon fiber is externally bonded to increase the flexural and shear strength of the beam. The effects of inclined straps on the load carrying capacity, crack patterns of the RC members loaded in four point bending test were specifically evaluated.

In earthquake prone area buildings get easily damaged due to high impact p,s,l waves, so retrofitting becomes a major factor for strengthening the structure. In the present work G+5 building is designed with different types of loadings i.e, dead load, live load, earthquake loads and building were analyzed for a critical section. The below figure shows the building plan of a G+5 and critical section.

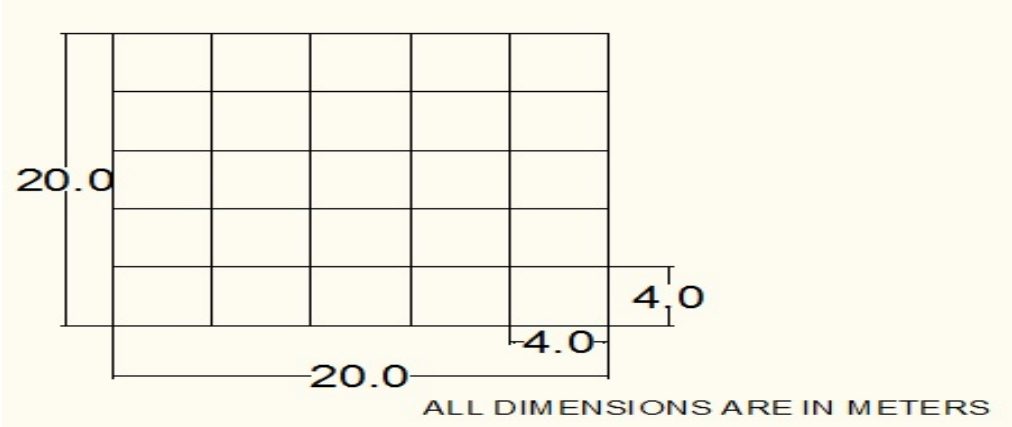

Fig:-1 Plan of building

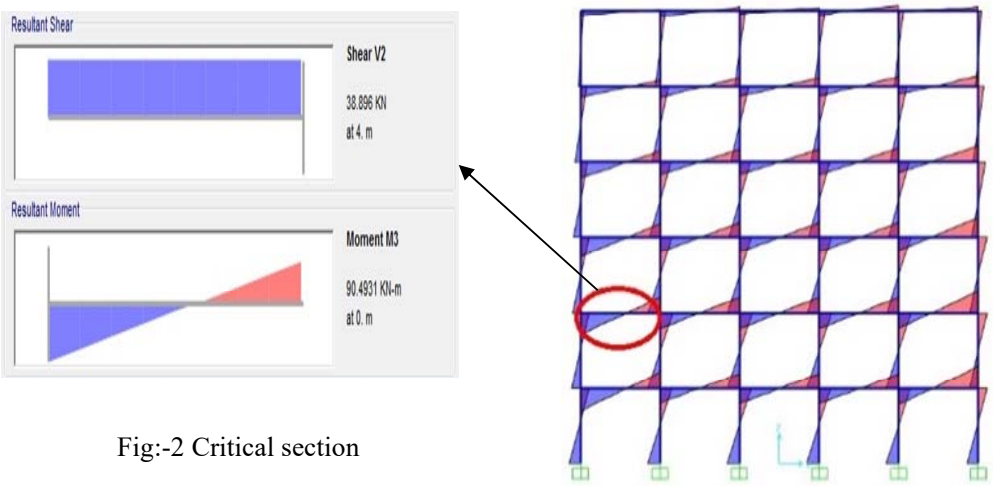

Fig:-2 Critical section

From the critical section, beam is derived and it is consized to suit the lab conditions. After consizing, the beam is as shown in the figure below.

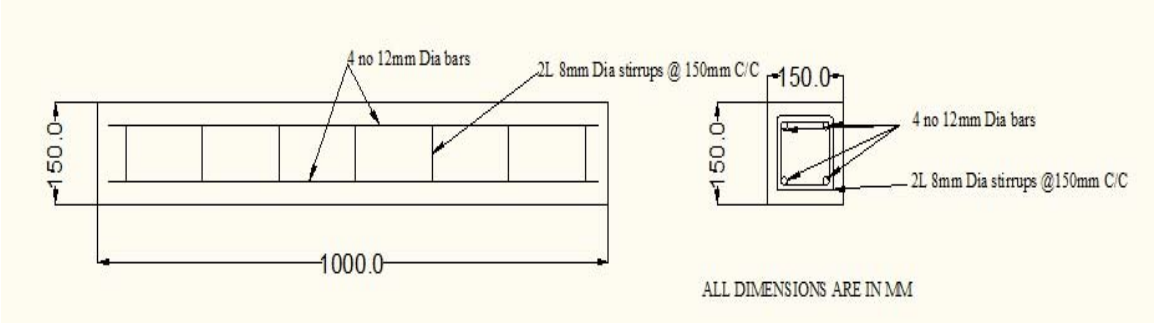

Fig:-3 Geometric dimensions of beam

2. Material Properties

A. Concrete

OPC grade53 cement confirming to IS 12269-1987 was used in the study. Fine aggregate locally available and crushed angular coarse aggregate passing 20mm sieve have been used. Tests are conducted on the materials as per IS standards. The mix proportions have been calculated according to the design mix as per IS 10262-2009 in order to achieve the 25N/mm^2. Calculated mix proportions are with a W/C ratio of 0.5 with a slump of 100mm. Six cubes were casted using the mix proportions and the results are tabulated below.

Table:1

Test results of concrete cube

Compressive strength of concrete cube (MPa)	Sample 1		Sample 2		Sample 3	
Days	7	28	7	28	7	28
M25 mix(N/mm^2)	18.6	32.8	20.3	34.5	19.6	33.2

B. Reinforcement

Fe500 HYSD 12mm &8mm dia bars having characteristic strength of 500 MPa were used and three samples have been tested in universal testing machine. 12mm dia bars used as longitudinal reinforcement and 8mm dia bars as stirrups.

C. CFRP and Epoxy

Different types of fiber reinforced polymer are available in market and carbon fiber reinforced polymer is one of them. Carbon fiber of 230 GSM have been used in the project and it is used as externally bonded reinforcement. Epoxy is used to bond the cfrp to the surface of the concrete. Epoxy named Araldite has been used in this

work. The properties of carbon fiber and araldite epoxy are supplied by the manufacturer are summarized in Table 2&3.

Fig:-4 uni-directional carbon fiber sheet

Table:-2

Properties of carbon fiber

Thickness (mm)	Tensile strength (MPa)	Elastic modulus (GPa)	Cracking ductility(%)	Weight of carbon fiber (g/m^2)
0.112	4900	230	1.5%	230

Table:-3

Properties of epoxy

Tensile strength (MPa)	Tensile modulus (MPa)	Cracking ductility(%)	Elastic modulus (MPa)	Specific gravity (g/cm^3)
64	3700	3.4	3200	1.17

D. Specimen details

The dimensions of the beam were 150mm wide by 150 mm deep by 1000mm long. The reinforcement consist of 12mm at top and bottom, shear reinforcement of 8mm bars as stirrups shown in fig.3. Table 3 shows the 5 RC beams strengthened with the coupled shear and flexure in the form of sheets and straps. One beam CS was kept without retrofitting for comparison. The rest of the beams were divided into four categories A,B,C,D. In A series the beam was retrofitted with CFRP sheets and the straps are inclined at 30^0. In series B t4e beams are retrofitted with CFRP sheets and straps are inclined at 45^0, In series C straps are inclined at 60^0, and In series D straps are perpendicular to the longitudinal direction.

Table - 4

Series	FRP provided	Orientation of strap(^{0})	Number of layers
A1,A2,A3	Sheet+Strap	30	1,2,3
B1, B2, B3	Sheet+Strap	45	1,2,3
C1, C2, C3	Sheet+Strap	60	1,2,3
D, D2, D3	Sheet+Strap	90	1,2,3

E. Sample preparation and test setup

The surface of the beam was cleaned and the epoxy spread on the bottom surface of the beam and then the CFRP sheet was placed on the epoxy and it was pressed with roller for uniformity and excess epoxy removed, next the epoxy is applied on where the straps to be laid and the CFRP straps are spread on the epoxy applied surface and the process is continued for the remaining layers. All the beams were simply supported over a span of 1000mm and tested under four-point loading. The load was applied using a hydraulic servo of 600Kn capacity with a loading of 5kN/min.

F. Testing of beams

Five beams were casted and cured for 28 days. Out of five beams, one beam kept as control specimen and rest of the four specimens were strengthened with unidirectional carbon fiber having thickness of 0.112mm. Universal testing machine (UTM) is used for testing of beams. The strengthened beams are showed in the figures 5,6,7 with four point bending test which consist of beam supported on the two steel roller bearing 150 mm from the end of the beam remaining portion is divided into equal parts and test is conducted. The deflections of the beam were recorded.

3. Experimental Procedure

- Analysing the G+5 structure using software to find the critical section.
- Finding the physical properties of materials like aggregate, cement etc.,
- Calculation of Mix Design for Concrete.
- Casting the beam.
- Applying CFRP Straps in different angles with 1,2,3 Layers.
- Testing the beams using Universal Testing Machine with 3 point loading to find the deflections.
- By using Finite element analysis software the beam is analysed with and without FRP straps.
- Results are compared with analytical and numerical approaches.

4. Results of Tested Beams

A. Orientation of angle at 30^o:-

Fig:-5 1 layer

Fig:-6 2 layer

Fig:-7 3 layer

Specimen A_1 :-

The beam strengthened with one layer CFRP sheet with 30º angles during testing showed combination of shear cracks and delamination of strap. For this beam an ultimate load of 168.45kN and corresponding mid span deflection of 6.13mm was achieved. It achieved strength of 90.3% greater than the control specimen.

Specimen A_2 :-

The beam strengthened with 2 layers CFRP sheets with 30º angle exhibited concrete crushing at top of the beam. For this beam an ultimate load of 209.64kN and a corresponding mid span deflection of 7.19mm. The strength achieved was 121.14% more than the control specimen.

Specimen A_3 :-

The beam strengthened with 3 layers CFRP sheets with 30º angle exhibited concrete crushing at top of the beam. For this beam an ultimate load of 219.69kN with a corresponding mid span deflection of 9.04mm. The strength achieved was 148.24% more than the control specimen.

B. Orientation of angle at 45º:-

Fig:-8 1 layer

Fig:-9 2 layer

Fig:-10 3 layer

Specimen B_1 :-

The beam strengthened with one layer CFRP sheet with 45º angles during testing showed combination of shear cracks and delamination of strap. For this beam

an ultimate load of 181.11kN and corresponding mid span deflection of 6.7mm was achieved. It achieved a strength of 104.64% more than the control specimen.

Specimen B_2 :-

The beam strengthened with 2 layers CFRP sheets with 45^o angle exhibited shear cracks and concrete crushing at top of the beam. For this beam an ultimate load of 199.4kN and a corresponding mid span deflection of 8.76mm was recorded and the strength achieved 125.31% more than the control specimen.

Specimen B_3 :-

The beam strengthened with 3 layers CFRP sheets with 45^o angle exhibited concrete crushing at top of the beam. For this beam an ultimate load of 214.11kN with a corresponding mid span deflection of 9.3mm. The strength achieved was 141.93% more than the control specimen.

C. Orientation of angle at 60^o:-

Fig:-11 1 layer

Fig:-12 2 layer

Fig:-13 3 layer

Specimen C_1 :-

The beam strengthened with one layer CFRP sheet with 60^o angles showed combination of shear cracks and delamination of strap. For this beam an ultimate load of 190.68kN and corresponding mid span deflection of 6.78mm was achieved. It recorded a strength of 115.46% more than the control specimen.

Specimen C_2:-

The beam strengthened with 2 layers CFRP sheets with 60^o angle exhibited shear cracks and concrete crushing at top of the beam. For this beam an ultimate load of 200.1kN and a corresponding mid span deflection of 7.98mm. The strength achieved was 126.1% mare than the control specimen.

Specimen C_3:-

The beam strengthened with 3 layers CFRP sheets with 60^o angle exhibited concrete crushing at top of the beam. For this beam an ultimate load of 224.58kN with a corresponding mid span deflection of 9.08mm. the strength achieved was 153.76% more than the control specimen.

D. Orientation of angle at 90^o:-

Table No:-5

Results of the Specimens

Specimen	Load at first crack(kN)	Ultimate load(kN)	Ultimate deflection(mm)	Ductility index	Shear strength(kN)	Contribution of CFRP(kN)
CS	31.2	88.5	4.83	1.16	44.25	0
A_1	45.34	168.45	6.14	1.27	84.23	79.95
A_2	56.54	209.64	7.19	1.48	104.82	121.14
A_3	63.46	219.69	9.04	1.87	109.845	131.19
B_1	47.76	181.11	6.7	1.38	90.5	92.61
B_2	52.1	199.4	8.76	1.81	99.7	110.9
B_3	68.91	214.11	9.3	1.92	107.05	125.61
C_1	49.47	190.68	6.78	1.40	95.35	102.18
C_2	53.81	200.1	7.98	1.65	100.05	111.6
C_3	71.2	224.58	9.08	1.87	112.3	136.08
D_1	43.07	172.37	7.87	1.62	86.185	83.87
D_2	47.53	179.82	7.17	1.48	89.91	91.32
D_3	49.16	187.37	6.65	1.37	93.68	98.87

Fig:-14 1 layer

Fig:-15 2 layer

Fig:-16 3 layer

Specimen D_1:- The beam strengthened with one layer CFRP sheet with 90^o angles showed combination of delamination of straps, shear cracks and concrete crushing. For this beam an ultimate load of 172.37kN and corresponding mid span deflection of 7.87mm was achieved. It recorded a strength of 90.64% more than the control specimen.

Specimen D_2:- The beam strengthened with 2 layers CFRP sheets with 90^o angle exhibited delamination of straps, shear cracks and concrete crushing at top of the beam. For this beam an ultimate load of 179.82kN and a corresponding mid span deflection of 7.17mm. The strength achieved was 103.19% mare than the control specimen.

Specimen D_3:- The beam strengthened with 3 layers CFRP sheets with 90^o angle exhibited concrete crushing at top of the beam. For this beam an ultimate load of 187.34kN with a corresponding mid span deflection of 6.65mm. the strength achieved was 111.68% more than the control specimen.

5. Finite Element Modelling

In the finite element analysis a tool named Ansys17.0 is used for nonlinear model to analyse the retrofitted beam. The element, Solid 65 used for concrete model as it has capable of cracking in tension, crushing in compression, plastic deformation and creep. The important property of this solid65 element is it can handle nonlinear material properties. Element, Link8 used for steel model in reinforced concrete. The purpose of using this element is as it has the capability of handling plastic deformation. Solid45 was used for 3-D modeling of adhesive. This element had features of plasticity, creep, swelling, stress stiffening, large deflections and large strain capabilities. Solid46, the element used for reinforced fiber polymer sheets with number of layers. CONTA174 and TARGE170 are used for bonding of CFRP to concrete. CONTA174 is generally used for rigid-flexible and flexible-flexible contact analysis.

Properties of materials in modelling:-

A. Concrete and steel reinforcement

Linear stress strain analysis is used to model the concrete and steel reinforcement. The properties of the materials are shown in the Table:-6. The properties of steel much easier than the properties of concrete.

Table :-6

Properties of concrete and steel

Material	Material property	value
Concrete	Compressive strength @28days (MPa)	31.25
	Tensile strength(MPa)	2.1
	Modulus of elasticity (GPa)	25
	Poissons ratio	0.2
	Shear coefficient for open crack	0.2
	Shear coefficient for closed crack	0.8
Steel reinforcement	Modulus of elasticity (GPa)	210
	Poissons ratio	0.3
	Ultimate stress (MPa)	500

B. CFRP sheets and Epoxy:-

The properties of these materials are given by the manufacturer and same properties are used in the analysis. The properties are mentioned below in Table no:-7.

Table:-7

Properties of CC and Epoxy

Material	Material property	Value
CFRP	Elastic modulus (GPa)	230
	Poissons ratio	0.3
	Layer thickness(mm)	0.112
	Layer number	1,2,3
Epoxy	Elastic modulus (MPa)	3200
	Poissons ratio	0.3
	Tensile strength(MPa)	30
	Layer thickness	1
	Layer number	1,2,3

Beam modelling:-

Figure 17 shows the finite element model of RC beam element where solid 65 is the property defined for RC beam in Ansys software with support and loading conditions. Longitudinal reinforcement and stirrups are shown in fig18. Discrete method, element link180 is used in the modelling. The interface between the concrete-epoxy-CFRP is assumed to be perfect bonding as shown in the fig.19.

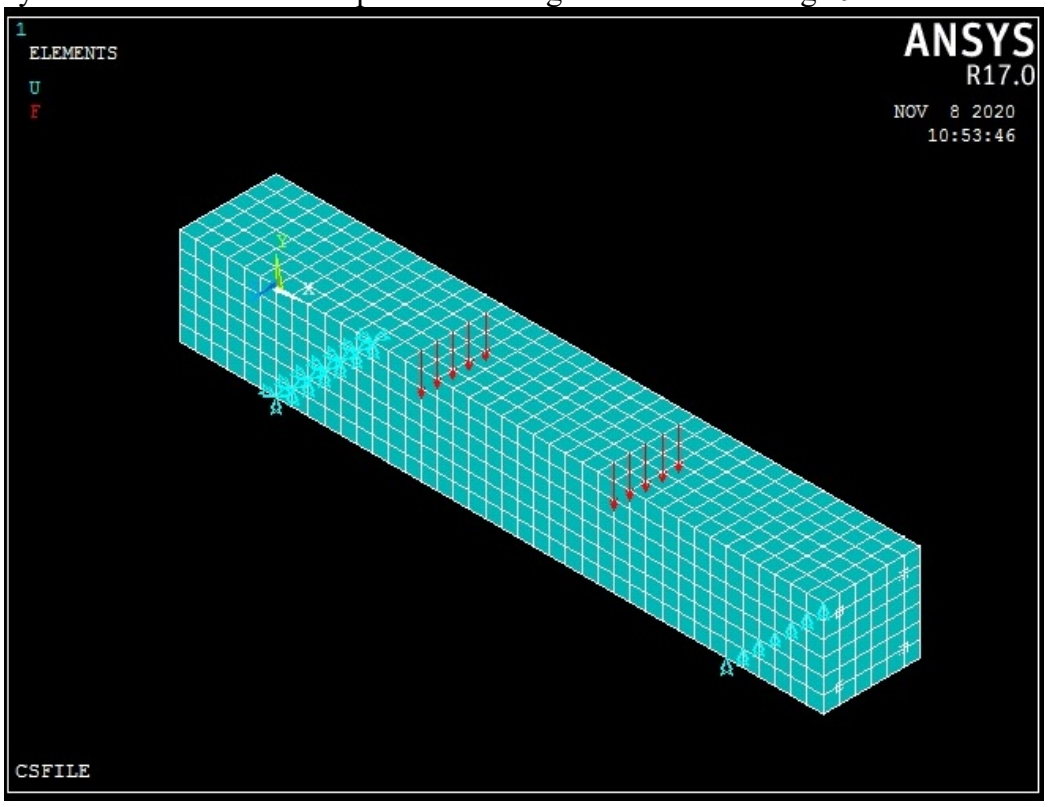

Fig:-17 Full beam model with boundary and loading conditions

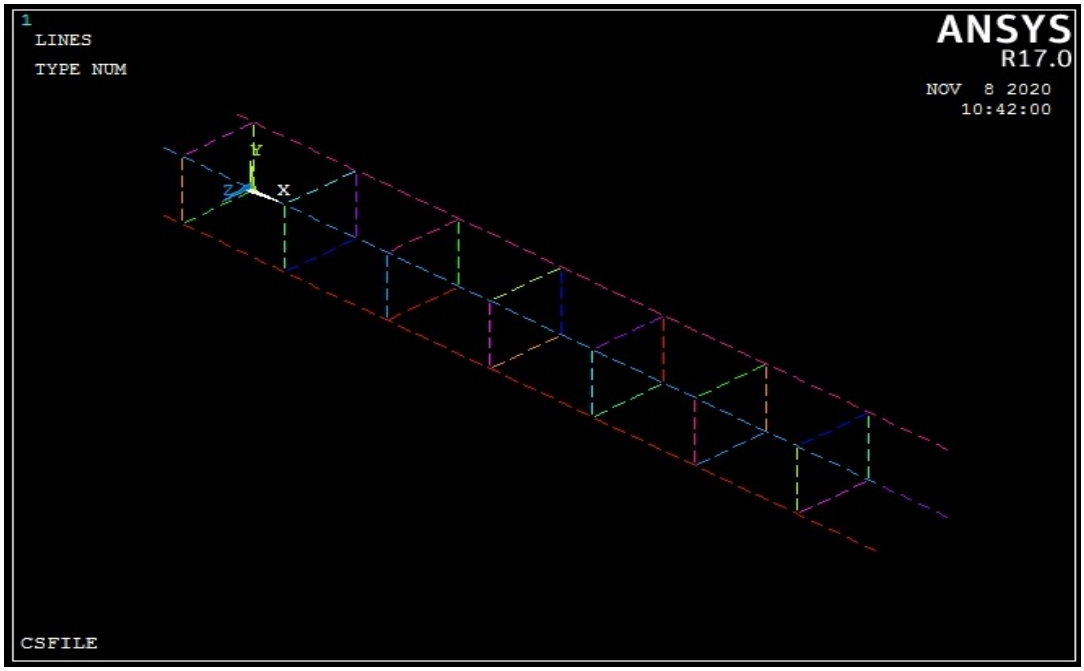

Fig:-18 Longitudinal reinforcement and stirrups in FE model

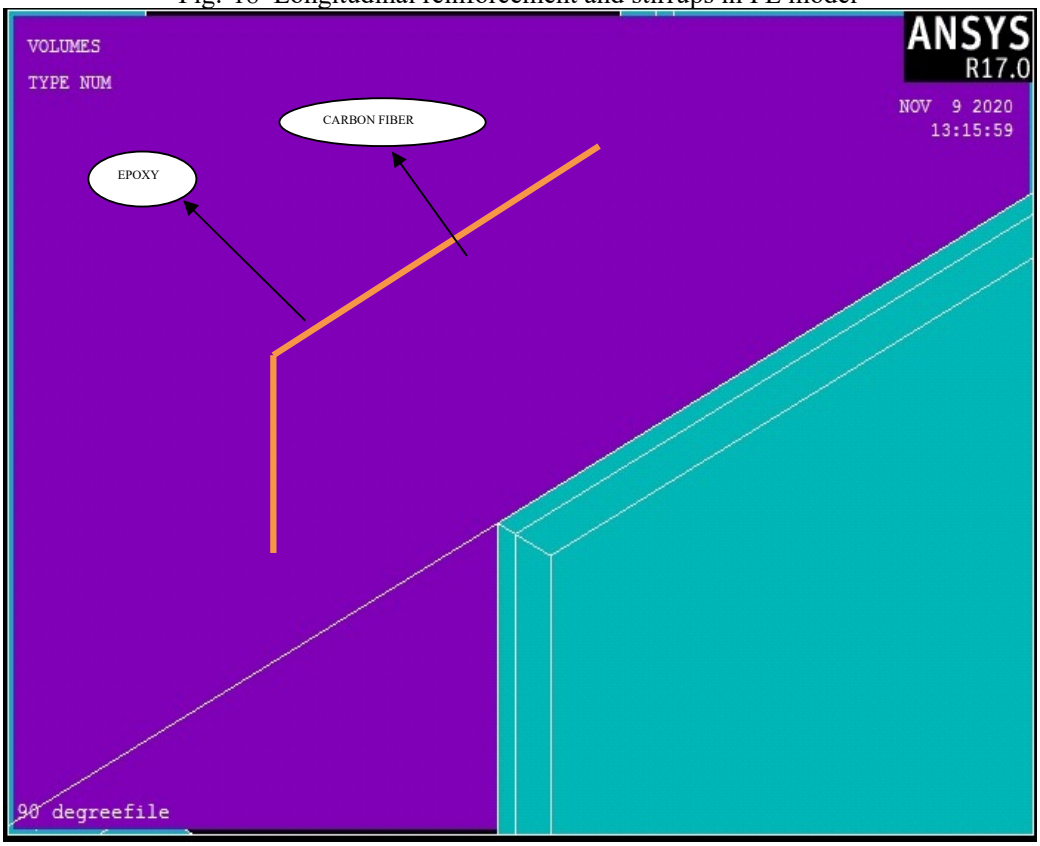

Fig:- 19 Modelling of single layered CFRP sheet and epoxy

6. Results

The comparison of experimental and numerical results of load vs deflection of control specimen and 12 strengthened beams are showed in fig 20-25. A noticeable agreement between experimental and numerical analysis is observed. The FE beams are considered to be strong and slightly stiffer than real one. Because a perfect bond is considered between the concrete and reinforcement in the FE analysis.

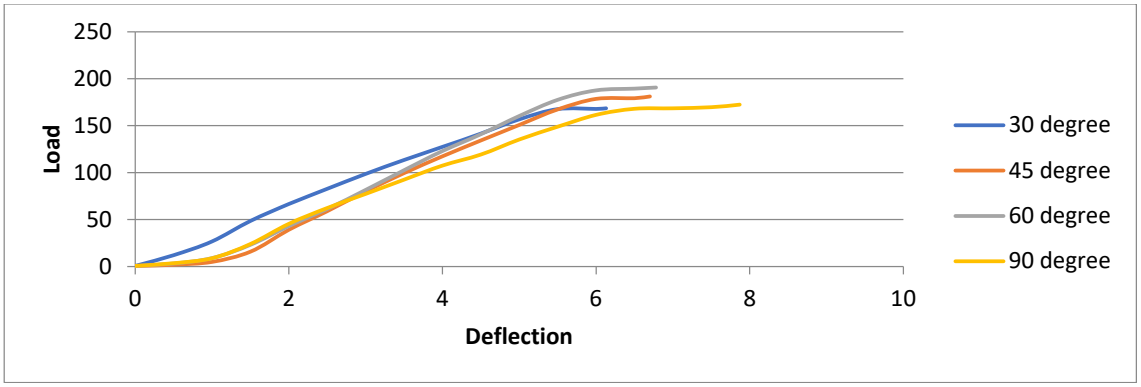

Fig:-20 Experimental Load vs Deflection graph for 1 layer CFRP

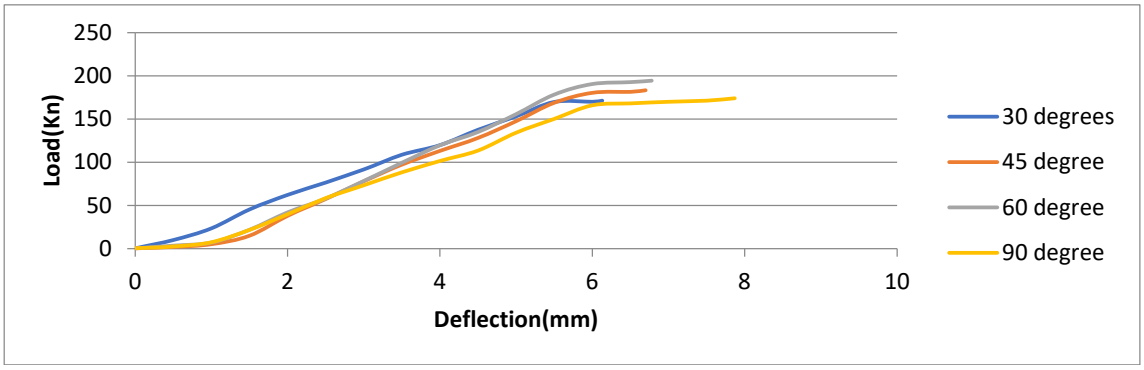

Fig:- 21 Numerical Load vs Deflection graph for 1 layer CFRP

Fig 20 and 21 resemblance the experimental and numerical values of specimens A1,B1,C1,D1 out of which specimen C1 obtaied the highest load 194.42kN with a deflection of 6.88mm

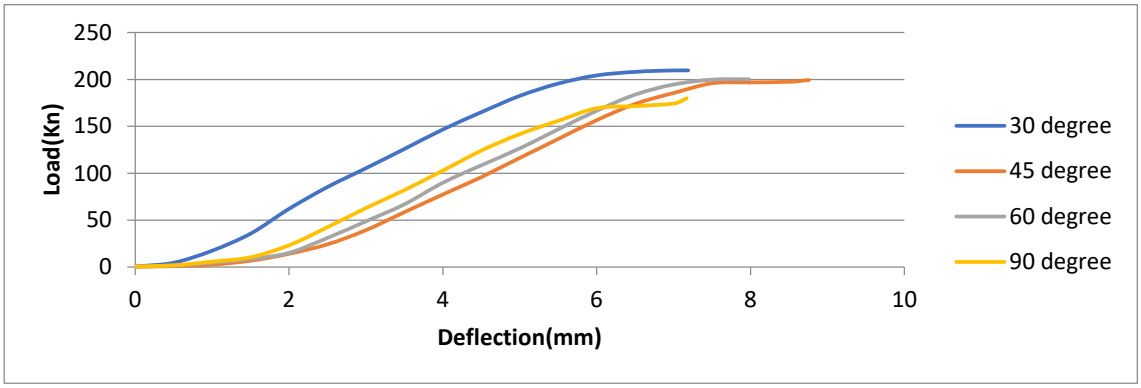

Fig:-22 Experimental Load vs Deflection graph for 2 layer CFRP

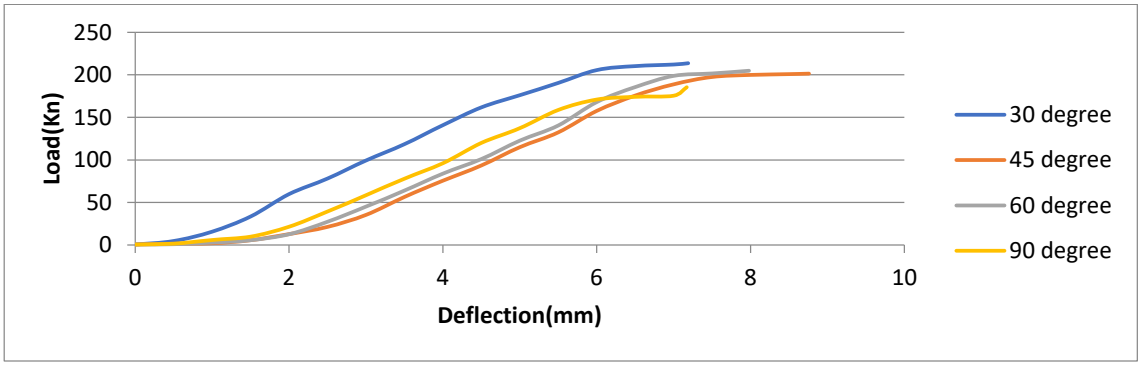

Fig:-23 Numerical Load vs Deflection graph for 2 layer CFRP

Fig 22 and 23 resemblance the experimental and numerical values of specimens A2,B2,C2,D2 out of which specimen A2 obtaied the highest load 213.58kN with a deflection of 7.19mm which is similar to the experimental values.

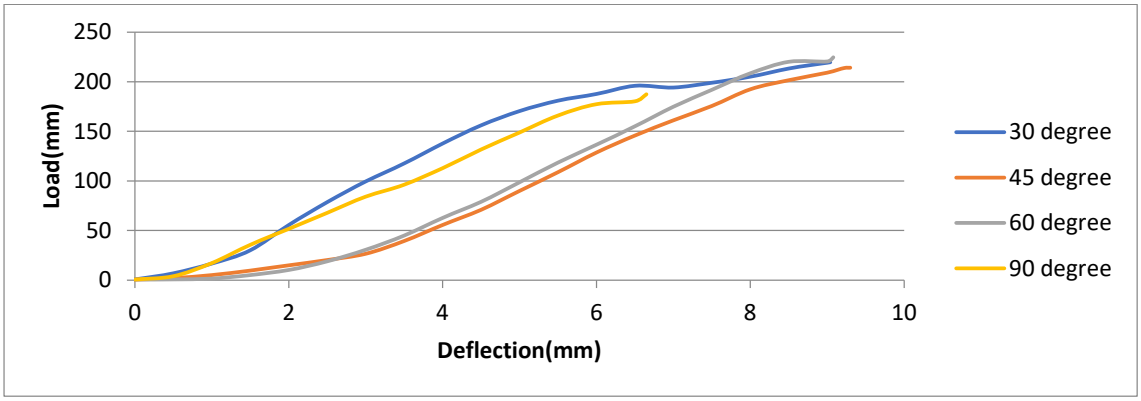

Fig:-24 Experimental Load vs Deflection graph for 3 layer CFRP

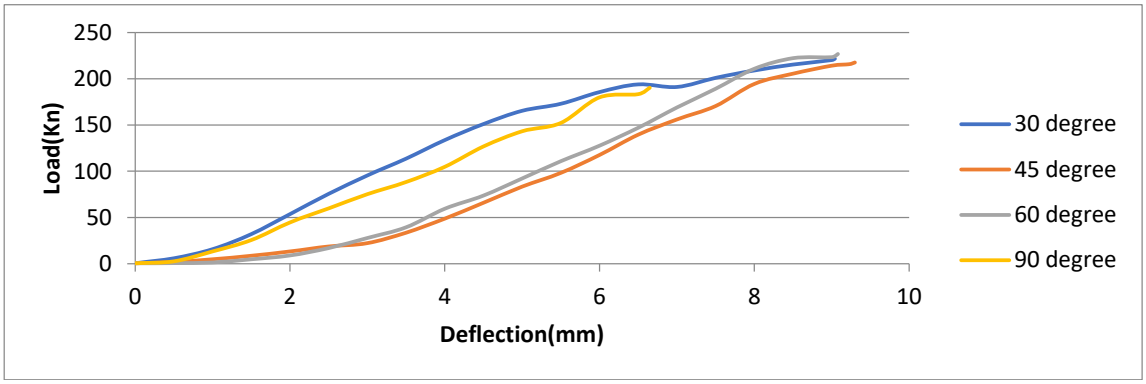

Fig:-25 Numerical Load vs Deflection graph for 3 layer CFRP

Fig 24 and 25 resemblance the experimental and numerical values of specimens A3,B3,C3,D3 out of which specimen C3 obtaied the highest load 226.74kN with a deflection of 9.08mm

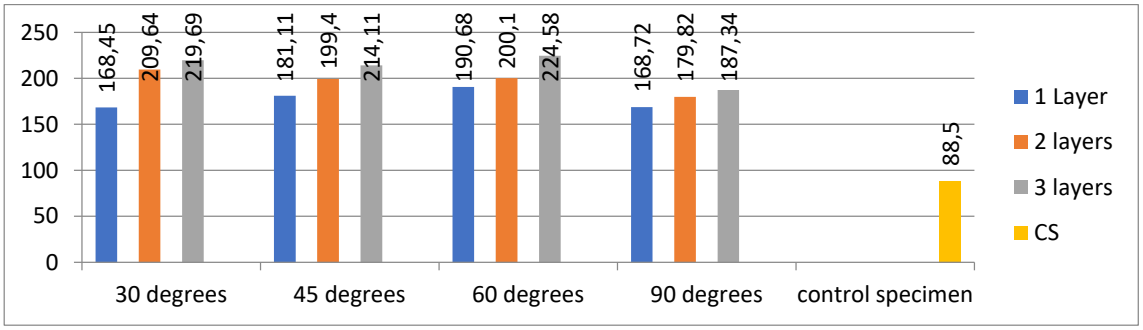

Fig:-26 comparison of ultimate load capacity

Retrofitting method will enhance the strength of the beam. By observing the ultimate load carrying capacity of the control specimen and strengthened beams it is clear that strengthened beams has more ultimate load carrying capacity, retrofitted beam *ie,* strap orientation 60^{O} with three layers beam had a strength of 224.58 kN. The ultimate load carrying capacity of the beam increased by 153.76% when compared to control specimen. It registered the highest load carrying capacity than the other strengthened beams.

All the retrofitted specimen have gained a strength of more than 100% than control specimen, except strap orientation of 30^{O} and 90^{O} with 1 layer showed less than 100% strength than control specimen . Among the four sets of strap orientations i.e, 30^{O},45^{O},60^{O},90^{O} of retrofitted beams, the beam retrofitted with strap orientation of 30^{O} with 1 layer beam exhibited the least load carrying capacity with the value of 168.45 KN, which is 90.3% greater than the ultimate load carrying capacity of control specimen.

7.Conclusions

The experimental and numerical results of the control specimen and four strengthened beams in flexure and shear by CFRP sheets and straps are presented below.

From the results of the strengthened beams the following conclusions are drawn

- The beam strengthened with flexural sheet with orientation angle of 30^{o} with 3 layers of CFRPshowed the highest load carrying capacity than other strengthened beams .
- From the experimental and numerical comparison,it clearly indicated that the specimen C_3 is better than the other strengthened beams
- To avoid the debonding failure of flexural sheet, utilization of straps act as anchorages to the flexural sheet and it acts as a working technique to keep intact the CFRP sheet to the beam.
- When compared with the control specimen the strengthened beams attains 90.3% to 153.76% of ultimate load carrying capacity respectively.
- The longitudinal sheet provided at the sofit of the beam had increased the flexural strength of the beam due to that flexural cracks are minimised.
- The presence of CFRP inclined straps also minimised the shear cracks while increasing the thickness.
- It was observed that the inclination of the straps upto 60^{O} are opposite to the shear crack formation so the holding capacity of the beam to minimise shear cracks also increased due to the ultimate load carrying capacity of the beam had increased.
- As the straps are perpendicular the beam withstands more displacement than the other beams but the ultimate load carrying capacity was slightly less than the other retrofitted beams.
- It was found that wrapping of CFRP straps around the three sides of the beam registered more effective in improving ultimate load carrying capacity, flexural strength and deflections of the beam.
- The beams retrofitted with single layer was failed with shear cracks and delamination of straps.
- The beams retrofitted with 3 layers had failed in concrete crushing at top of the beam.

8.References

[1] Jiangfeng Dong, Qingyuan Wang, Zhongwei Guan,“Structural behaviour of rc beams with external flexure and flexure-shear strengthening by frp sheets”. Composites: Part B 44 (2013) 604–612.

[2] Riyadh Al-Amery, Riadh Al-Mahaidi, “Coupled flexure-shear retrofoitting of rc beams using cfrp straps”. Composite Structures 75 (2006) 457–464.

[3] E.Moradi, H. Naderpour, A. Kheyroddin "An experimental approach for shear strengthening of RC beams using a proposed technique by embedded through-section FRP sheets". Composite Structures 238(2020) 111988.

[4] Mohammad Abdallah, Firas Al Mahmoud, Abdelouahab Khelil, julien Mercier, " Assessment of the flexural behaviour of Countinuous RC beams strengthened with NSM-FRP bars, experimental and analytical study". Composite Structures 242(2020) 112127.

[5] Riyadh Al-Amery , Riadh Al-Mahaidi , "Numerical analysis of multi-layered CFRP retrofitted RC beams with partial interaction". Composite Structures 75 (2006) 479-488.

[6] Abolfazl Eslamia, Alireza Moghavema, Hamid R. Shayegh, Hamid R. Ronagh, " Effect of FRP stitching anchors on ductile performance of shear deficient RC beams retrofitted using FRP U-wraps" Structures 23 (2020) 407-414.

[7] Abdulrahman Albidah, Aref Abadel, Husain Abbas, Tarek Almusallam, Yousef Al-Salloum, " Experimental and analytical study of strengthening scemes for shear deficient RC beams". Construction and building materials 216 (2019) 673-686.

[8] Amir Shomali, Davood Mostofinejad , Mohammad Reza Esfahani, " Experimental and Numerical investigation of shear performance of RC beams strengthened with FRP using grooving method". Journal of Building Engineering 31 (2020) 101409.

[9] Mostefa Hamrat , Farid Bouziadi , Bensaid Boulekbache , Tahar Hassaine Daouadji, Selma Chergui, Abderahim Labed, Sofiane Amziane, " Experimental and numerical investigation on the deflection behaviour of pre-cracked and repaired reinforced concrete beams with fiber reinforced polymer". Construction and Building Materials 249(2020) 118745.

[10] Tomas Skuturna, Juozas Valivonis, "Experimental study on the effect of anchorage system on RC beams strengthened using FRP". Composites Part B 91 (2016) 283-290.

[11] Przemysław Bodzak, "Flexural behaviour of concrete beams reinforced with different grade steel and strengthened by CFRP strips". Composites Part B 167 (2019) 411–421.

[12] Hassan Falah Hassan, Mu'taz Kadhim Medhlom, Abdullah Sinan Ahmed, Mohammed Husein Al-Dahlaki, " Flexural behaviour of concrete beams reinforced by GFRP bars and strengthened by CFRP sheets". Case Studies in Construction Materials 13 (2020) e00417.

[13] . A.H. Al-Saidy, A.S. Al-Harthy , K.S. Al-Jabri , M. Abdul-Halim , N.M.Al-Shidi. "Structural performance of corroded rc beam repaired with cfrp sheets". Composite Structures 92 (2010) 1931–1938.

[14] Anumol Raju, Liji Anna Mathew, " Retrofitting of RC beam using frp". International Journal of Engineering Research & Technology (IJERT) , ISSN 2278-0181 VOL 2 ISSUE 1,JAN 2013.

[15] Mansoor Ahmad Bhat, Er. Gurpreet Singh, "Retrofitting of reinforced concrete beams by using carbon fiber reinforced polymer sheets". International Journal of Civil Engineering and Technology (IJCIET), Volume 9, Issue 9, September 2018, pp. 1782–1790.

[16] M.A.Shahawy, M.Arockiasamy, T.Beitelman and Sowrirajan, "Reinforced concrete rectangular beams strengthened with cfrp laminates". Composites part-B 27B (1996) 225-223.

[17] L.J. Li, Y.C. Guo, F. Liu, J.H. Bungey , " An experimental and numerical study of the effect of the thickness and length of cfrp on performance of repaired reinforced concrete beam". Construction and building materials 20 (2006) 901-909.

[18] By Marco Arduini and Antonio Nanni, " Behaviour of prepacked Rc beams strengthened with carbon FRP sheet". J. Compos. Constr. 1997.1:63-70.

[19] Ivano Iovinella , Andrea Prota , Claudio Mazzotti , " Influence of surface roughness on the bond of FRP laminates to concrete". Construction and building materials 40 (2013) 533-542.

[20] Bo Gao, Jang-Kyo Kim, Christopher K.Y. Leung, " Experimental study on Rc beams with frp strips bonded with rubber modified resins". Composites Science and Technology 64 (2004) 2557–2564.

[21] M.N.S. Hadi, " Retrofitting of shear failed reinforced concrete beams" Composite Structures 62 (2003) 1–6.

[22] Franklin F.R Frederick, U.K. Sharma, V.K. Gupta, " Effect of end anchorage in external CFRP confinement on shear damaged RC beams". Procedia Engineering 125 (2015) 953 – 958.

[23] S. Hashemi, R. Al-Mahaidi, " Flexural performance of CFRP textile-retrofitted Rc beams using cement-based adhesive at high temperature". Construction and Building Materials 28 (2012) 791–797.

[24] Huy Pham, Riadh Al-Mahaidi, "Experimental investigation into flexural retrofitting of reinforced concrete bridge beams using FRP composites". Composite Structure 66 (2004) 617-625.

[25] Hai Yan Zhang, Jia Yan, Venkatesh Kodur, Liang Cao, "Mechanical behaviour of concrete beams shear strengthened with textile reinforced geopolymer motar". Engineering Structures 196 (2019) 109348.

[26] Aqeel Ahmed. Venkatesh Kodur, "The experimental beaviour of RFP-strengtened RC beams subjected to design fire exposure". Engineering Structures 33(2011)2201-2211.

[27] Davood Mostofinejad, Kamyar Khozaei, "Effect of GM patterns on the durability and debonding control of FRP sheets in RC strengthened beams". Construction and Building Materials 93 (2015) 110-120.

[28] Amira Adel Abdel Hamed, Khaled Farouk Omar El-kashif, Hamed Mohamed Salem, "Flexural strengthening of preloaded reinforced concrete continuous beams: An experimental investigation". Alexandria Engineering Journal.

[29] Davood Mostofinejad, Amirreaz Moghaddas, "Bond efficiency of EBR and EBROG methods in different flexural failure mechanisms of FRP strengthened RC beams". Construction and Building Materials 54 (2014) 605-614.

[30] T.Liu and Y.Xiao, F.ASCE, "Impact behaviour of CFRP-Strip-Wrapped RC Beam without Strrups". J.Compos. Constr., 2017, 21(5): 04017035.

[31] Moatasem M. Fayyadh, Hashim Abdul Razak, "Assessment of effectiveness of CFRP repaired RC beams under different damage levels based on flexural stiffness". Construction and Building Materials 37 (2012) 125-134.

[32] A.H. Al-saidy, K.S. Al-jabri, "Effect of damaged concrete cover on the behaviour of corroded concrete beams repaired with CFRP sheets".Composite Structures 93 (2011) 1775-1786.

[33] Omrane Benjeddou, Mongi Ben Ouezdou, Aouicha Bedday, "Damaged RC beams repaired by bonding of CFRP laminates". Construction and Building Materials 21 (2007) 1301-1310.

[34] M.R. Esfahani, M.R. Kianoush, A.R. Tajari, "Flexural behaviour of reinforced concrete beams strengthened by CFRP sheets". Engineering Structures 29 (2007) 2428-2444.

[35] Celebi Mertoglu, Ozgur Anil, Cengizhan Duruncan, "Bond behaviour of anchored CFRP strips on the concrete surfaces". Construction and Building Materials 123 (2016) 553-564.

[36] A.R. Khan and T. Ayub, "Role of u-shaped anchorages on the performance of rc beams strengthened by cfrp plates". The Second Official International Conference of International Institute for FRP in Construction for Asia-Pacific Region.

[37] Narayan Tiadi, B.S. Tyagi, Siddgarth Jain, "Retrofitting of rc continuous beam with glass FRP sheet". International Researc Journal of Engineering and Technology(IRJET).

[38] M.C. Sundarraja, S. Rajamohan, "Strengthening of RC beams in shear using GFRP inclined strips – An experimental study". Construction and Building Materials 23 (2009) 856-864.

[39] A.N. Nayak, A. Kumari, R.B. Swain, "Strengthening of RC Beams Using Externally Bonded Fibre Reinforced Polymer Composites". Structures 14 (2018) 137-152.

[40] Ciaran McSwiggan, Amir Fam, "Bio-based resins for flexural strengthening of reinforced concrete beams with FRP sheets". Construction and Building Materials 131 (2017) 618-629.

[41] Hee Sun Kim, Yeong Soo Shin, "Flexural behaviour of reinforced concrete (RC) beams retrofitted with hybrid fiber reinforced polymers (FRPs) under sustaining loads". Composite Structures 93 (2011) 802-811.

[42] Lawrence C. Bank, Dushyant Arora, "Analysis of RC beams strengthened with mechanically fastened FRP (MF-FRP) strips". Composite Structure 79 (2007) 180-191.

[43] Togay Ozbakkaloglu, Ph.D and Murat Saatcioglu, Ph.D, "Tensile behaviour of FRP Anchors in Concrete". J.Compos. Constr. 2009.13:82-92.

[44] Tara Sen, H.N. Jagannatha Reddy, "Strengthening of RC beams in flexure using natural jute fibre textile reinforced composite system and its comparative study with CFRP and GFRP strengthening systems". International Journal of Sustainable Built Enviranment (2013) 2, 41-55.

[45] Giulio Alfano, Fiorenzo De Cicco, Ph.D and Andrea Prota, "Intermediate Debonding Failure of RC Beams Retrofitted in Flexure with FRP: Experimental Results versus Prediction of Codes of Practice". J. Compos. Constr. 2012.16:185-195.

[46] Baris Yalim, Ahmet Serhat Kalayci, and Amir Mirmiran, "Performance of FRP-Strengthened RC Beams with different Concrete Surface Profile". J. Compos. Constr. 2008.12:626-634.

[47] Jinlong Pan, Christopher K.Y. Leung, Min LUuo, "Effect of multiple secondary cracks on FRP debonding from the substrate of reinforced concrete beams". Construction and Building Materials 24 (2010) 2507-2516.

[48] Sahar S. Choobbor, Rami A. Hawileh, Adi Abu-Obeidh, Jamal A. Abdalla, "Performance of hybrid carbon and basalt FRP sheets in strengthening concrete beams in flexure". Composite Structures 227 (2019) 111337.

Porous thermal insulation building material made of recycled glass waste by microwave heating

Material de construcție poros termoizolant fabricat din deșeu de sticlă reciclată prin încălzire cu microunde

Lucian Păunescu[1], Sorin Mircea Axinte[2,3], Bogdan Valentin Păunescu[4], Felicia Cosmulescu[5]

[1]Cosfel Actual SRL
95-97 Calea Grivitei street, M4 room, sector 1, Bucharest 010705, Romania
E-mail: lucianpaunescu16@gmail.com

[2]Daily Sourcing & Research SRL
95-97 Calea Grivitei street, sector 1, Bucharest 010705, Romania
E-mail: sorinaxinte@yahoo.com

[3]Department of Applied Chemistry and Materials Science, University „Politehnica" of Bucharest
1-7 Gh. Polizu street, sector 1, Bucharest 011061, Romania
E-mail: sorinaxinte@yahoo.com

[4]Consitrans SA
56 Polona street, sector 1, Bucharest 010504, Romania
E-mail: pnscbogdan@yahoo.com

[5]Cosfel Actual SRL
95-97 Calea Grivitei street, M4 room, sector 1, Bucharest 010705, Romania
E-mail: feliss2014@gmail.com

DOI: 10.37789/rjce.2022.13.3.3

Rezumat. *Lucrarea prezintă rezultate experimentale obținute în procesul fabricării sticlei celulare utilizând încălzirea indirectă cu microunde. Intensificarea absorbției microundelor a fost realizată utilizând un creuzet din carbură de siliciu având peretele acoperit cu un film din oxid de ytriu. Încălzirea cu microunde și folosirea oxidului de ytriu reprezintă originalitatea lucrării. Rețeta conținând deșeu de sticlă, cenușă și carbură de siliciu a permis producerea sticlei celulare la 960-970 ºC cu consumuri economice de energie (sub 0,86 kWh/kg). Produsele au caracteristicile specifice sticlei celulare cu densitatea intre 0,27-0,33 g/cm^3, conductivitatea termică între 0,064-0,073 W/m·K și rezistența la compresiune între 1,35-1,45 MPa.*

Cuvinte cheie: sticlă celulară, încălzire cu microunde, deșeu de sticlă, cenușă de cărbune, carbură de siliciu, oxid de ytriu.

Abstract. *The paper presents experimental results obtained in manufacturing process of cellular glass using the indirect microwave heating. The microwave absorption intensification was achieved using a silicon carbide crucible having the wall coated with a yttrium oxide film. The microwave heating and the use of yttrium oxide are the paper originality. The recipe containing glass waste, ash and silicon carbide allowed cellular glass production at 960-970 ºC with economical energy consumption (below 0.86 kWh/kg). The products have specific characteristics of cellular glass with density between 0.27-0.33 g/cm^3, thermal conductivity between 0.064-0.073 W/m·K, and compressive strength between 1.35-1.45 MPa.*

Key words: cellular glass, microwave heating, glass waste, coal ash, silicon carbide, yttrium oxide.

1. Introduction

In the last 3-4 decades, most countries in the world have been concerned about recycling waste which is generated intensively and its storage in landfills is no longer an acceptable solution for the health of the environment and people. The glass industry, a major consumer of primary energy, has adopted the solution of reusing glass waste as a raw material in the production of new glass even before the initiation of the current global waste recovery measures. According to the literature [1], 1 kg of cullet replaces 1.2 kg of traditional raw materials (sand, sodium carbonate, and limestone) and the energy consumed in the glass manufacturing process decreases by about 3 % for every 10 % of cullet added to the starting material mixture. Also, the emission of greenhouse gases (mainly carbon dioxide) decreases by 5 % for every 10 % used cullet. However, the glass industry prefers its own glass waste resulting from the technological manufacturing process and avoids recycling the wastes predominantly accumulated from the post-consumer drinking bottle and the demolition and modernization of buildings due to the need of their selection by color (default, quality), which is an expensive operation.

If in several European countries, primarily Switzerland and Germany, there are very high recycling rates (90 %), in the United States recycling the residual glass is low (only 33 %), the raison being the diversity of glass quality requirement of the manufacturers as well as the long distances between the location of the collection and sorting centers and that of the industrial producer, which significantly increases the cost of the supply operation [1].

Under these conditions, a wide field of recycled glass application to other users has opened up. The use of glass as an alternative material for the construction sector is the main direction of valorization. Unlike other waste types, glass is completely recyclable and its properties remain unchanged even at the end of the product's life cycle [1].

According to [2], from a structural point of view, the glass can be classified into three categories: soda-lime glass (Na_2O-CaO-SiO_2) which is a combination of sodium silicate and calcium silicate, that dissolves at low temperature and can be efficiently

expanded or welded, potash-lime glass (K_2O-CaO-SiO_2) which is a mix of potassium silicate and calcium silicate, that dissolves at high temperature, being also called „hard glass", and potash-lead glass (K_2O-PbO-SiO_2) which is a mixture of potassium silicate and lead silicate, with excellent refractive power. Obviously, the soda-lime glass is the most widely used commercial glass found in the main glass products. This is the reason why this residual glass type is predominantly recycled and is preferred for various manufacturing techniques of expanded glass usable in construction.

The usual method of making the cellular glass is to incorporate into the finely ground glass-based raw material a solid or liquid expanding agent (carbonaceous products, carbides, or carbonates are preferred), which release a gas at high temperature as a result of a chemical reaction. The temperature range in which the reaction takes place must include the softening point of the glass, so that the medium in which the gas is distributed to have an adequate viscosity for its blockage and the formation of bubbles [3].

Since the 1980s, several industrial manufacturers have developed cellular glass manufacturing activities in Europe, the United States, and China using recycled glass waste, the products having as main characteristics light weight, high porosity, low thermal conductivity, and at least acceptable compressive strength (above 1 MPa), to which resistance to fire, water and steam, frost, corrosion, aggression of external agents, very high durability, chemical and physical stability, lack of toxicity, etc. are added [3, 4]. A diversification of features, especially mechanical and geometric exists, taking into account the requirements of the field of application of expanded products. Thus, manufacturers supply cellular glass in the form of blocks and boards for thermal insulation of building masonry (with apparent density of 0.165 g/cm^3, thermal conductivity of 0.05 W/m·K, and compressive strength of 1.6 MPa [5]), or as a filler for load bearing thermal insulation under foundation slabs, underground thermal insulation of energy fluid pipes and storage tanks, industrial floor tiles, road and railway construction components, bridge abutments, airport runway, drainage, sports fields, roof gardens, swimming pools, etc. (with bulk density between 0.11-0.17 g/cm^3, lump density between 0.22-0.38 g/cm^3, thermal conductivity between 0.05-0.08 W/m·K, and compressive strength up to 6 MPa [6-8]).

Industrially, the manufacture of cellular glass takes place in conveyor belt furnaces heated by conventional methods (electricity or thermal energy). In the case of thermal insulation blocks or boards production, raw material is loaded into metal molds, which are moved along the entire length of the furnace passing through the intense heating area, then through the tempering area and are discharged as cellular glass at the cold end. The porous gravel or aggregate manufacture involves placing the raw material on the conveyor belt in the form of a compact layer, moved on the all conveyor length and discharged at the cold end in the form of lumps with size up to 70-80 mm.

Testing the application of the unconventional technique of raw material microwave heating to obtain cellular glass adequate for their use as thermal insulation materials in construction were small-scale performed in the last years on adapted microwave oven in the Romanian company Daily Sourcing & Research. Except the

manufacturing recipes and the conventional heating techniques constantly used by the industrial producers, other attempts for technological improving were not reported in the literature. Changing the heating technique adopted by the Romanian company is singular in this area in the world and the result previously obtained showed an excellent energy efficiency compared to the conventional techniques. In terms of quality, the physical, thermal, mechanical, and microstructural features of expanded materials are comparable to those industrially achieved.

Numerous experiments in the manufacture of cellular glass in microwave field have been performed using soda-lime glass waste as the main raw material and various expanding agent types. The heating technique adopted by authors has been the predominantly direct microwave heating by placing a SiC and Si_3N_4 ceramic tube or crucible with thickness wall between 2.5-3.5 mm between the material and the wave emission source. Using this technique and calcium carbonate as an expanding agent, very light weight cellular glass (apparent density between 0.16-0.19 g/cm^3), with good thermal insulation properties (thermal conductivity between 0.034-0.040 W/m·K and porosity between 91.4-92.7 %), the compressive strength having acceptable values (1.12-1.22 MPa) have been produced. The specific energy consumption has been values below 1 kWh/kg [9, 10]. Other experiments have led to obtaining (by heating at 900-905 ºC) dense cellular glasses with high compressive strength (14.1 MPa), apparent density between 0.77-0.82 g/cm^3 and thermal conductivity in the range 0.124-0.135 W/m·K [11], using colored glass waste, blast furnace slag (31-39.25 %), borax (7.8-8.1 %), titanium oxide (5 %), sodium phosphate (3 %) and sodium carbonate ($CaCO_3$) (5-6.5 %). Also, the specific energy consumption has been low (0.90-0.95 kWh/kg). Using a raw material mixture predominantly composed of clay (70.5-83.4 %) together with glass waste (2.6-15.5 %), coal fly ash (9 %), and silicon carbide (SiC) (5 %), the direct (100 %) microwave heating at 1055-1150 ºC without affecting the microstructural homogeneity has been possible [12]. The specific energy consumption has been very low, reaching the lowest value of 0.58 kWh/kg. The compressive strength has been between 7.8-8 MPa, apparent density between 0.60-0.69 g/cm^3, and thermal conductivity in the range 0.100-0.116 W/m·K. Manufacturing the cellular glass gravel by microwave irradiation technique has been also achieved, being used the main industrial manufacturing recipes successively including SiC, $CaCO_3$, glycerol as expanding agents, borax and sodium silicale as additives, the products being almost similar to those industrially manufactered [13].

Significant intensification of microwave absorption ability through the wall of an irradiated SiC crucible with a wave field can be obtained by coating the outer surface of crucible with thin layer of yttrium oxide (Y_2O_3) achieved by spraying. The dielectric properties of Y_2O_3 (tangent loss and dielectric constant) increase at high coating film temperature, enhancing the microwave absorption [14]. The method of Y_2O_3 nanoparticle using is known in the last years being applied in several domains, according to AzoNano, the leading online publication for the nanotechnology community [15], (television, microwave filters, inorganic synthesis of compounds, making fluorescent lamps, etc.). The method was not applied in manufacturing process

of cellular glass, its use in the present paper having original character. Previous tests of the authors in expansion process of glass waste using an existing Y_2O_3 coated crucible [16] showed enhancing the microwave absorbtion capacity and consequently, increasing the heat flux transferred to the material through indirect heating.

The work aims at manufacturing the cellular glass using the Y_2O_3 coated crucible containing a mixture of glass waste, coal fly ash, and SiC as an expanding agent, one of the common preparing recipes, to highlight the high energy efficiency of this process.

2. Method and materials

SiC is one of the most efficient expanding agents used in the manufacturing process of cellular glass from glass waste. In the industrial processes, its weight proportion is about 2 % [6, 13]. The soda-lime glas waste is the only raw material that makes up the finely ground starting mixture, coal fly ash being excluded because it raises the temperature limit required for sintering and expanding the material. According to [6], the Norwegian company Glasopor does not use commercial SiC, but waste SiC from the silicon industry for economic reasons. However, in other processes, coal fly ash is added together with glass and SiC due to its contribution to obtaining a homogeneous microstructure of the foamed product [17].

SiC using as an expanding agent involves the oxidizing atmosphere of the furnace, which must supply the oxygen necessary for the release of the foaming gas (CO_2 or CO) and a solid compound (SiO_2 or SiO) that enters into the molten glass composition.

The basic chemical reaction is (1), which is initiated at above 900 ºC.

$$SiC + 2O_2 = SiO_2 + CO_2 \quad (1)$$

If the oxygen concentration in the furnace atnosphere is insufficient for the reaction (1), the following reaction (2) takes place.

$$SiC + O_2 = SiO + CO \quad (2)$$

According to [3], the temperature range in which the two chemical reaction occur is 950-1150 ºC.

As stated above, the experiment described in the paper was based on the unconventional microwave heating of raw material placed into a SiC crucible whose outer side wall is coated with a yttrium oxide (Y_2O_3) film. The slightly truncate crucible with the outer diameter of the opening of 117 mm, the botton diameter of 95 mm, the height of 90 mm, and the wall thickness of 8 mm was purchased from China including also the Y_2O_3 film. The mixture was previously prepared by grinding and mixing the three compounds (glass waste, coal fly ash and SiC), water addition as a binder, loading into a metal mold, axially pressing and removing from the mold as a

compact cylindrical material (with density between 1.6-1.8 g/cm^3) having the diameter of about 7 cm and the height of about 6 cm.

The microwave heating equipment was an oven with installed power of 800 W of the type commonly used in household, constructivelly adapted for operation at temperatures up to 1200 ºC (Fig. 1 a). The heating of microwave susceptible materials (the SiC crucible with Y_2O_3 film) is initiated in their core, unlike the conventional heating in which the walls, hearth and vault of the oven are initially heated. Therefore, very efficient thermal protection with ceramic fiber mattresses (Fig. 1 b) was made around the crucible (and above the corresponding lid), so that the unprotected metal walls of the microwave oven were kept below 65 ºC. The thermal process control was based on the correlation between the heating time and the heated material temperature, previously experimentally determined.

a b

Fig. 1. Images of the experimental equipment
a – adapted 800 W-microwave oven; b – ceramic fiber thermal insulation of the Y_2O_3 coated crucible.

The recycled glass waste from post-consumer colored drinking bottle was the main raw material of this experiment. Approximately equal weight proportions of drinking bottles differing by color (colorless, green and amber) were used. In terms of quality, the three glass waste types are soda-lime glasses, whose oxide composition varies within restricted limits according to Table 1. The analyses were performed by X-ray fluorescent spectrometry at the Metallurgical Research Institute of Bucharest.

Table 1

Oxide composition of glass waste types

Glass type	Oxide composition (wt. %)								
	SiO_2	Al_2O_3	CaO	Fe_2O_3	MgO	Na_2O	K_2O	Cr_2O_3	SO_3
Colorless	71.5	1.9	12.0	0.1	1.0	13.3	0.1	0.1	0.2
Green	71.2	1.8	10.2	0.4	2.2	13.0	0.5	0.2	0.3
Amber	71.4	1.9	10.3	0.3	2.3	13.2	0.6	0.1	0.3

The glass waste processing operations (washing, color selection, breaking, grinding and sieving) were performed in Bilmetal Industries SRL Popesti-Leordeni, Ilfov. The grain size of the waste after these operations was allowed below 100 μm.

Coal fly ash as an industrial by-product of the Romanian thermal power plant of Paroseni was purchased at a granulation below 250 μm, being reduced below 100 μm after grinding and sieving operations.

SiC as an expanding agent was purchased from the market at a fine grain size below 10 μm and was used in the experiment without further mechanical processing.

Four experimental variants based on the manufacturing recipe containing glass waste, coal fly ash, SiC, and water addition were adopted by the authors (Table 2). Given the value ranges of these components used in various previous experiments, coal fly ash was used between 9-11 % and SiC between 2.8-3.1 %. The recycled glass waste has resulted with values between 85.9-88.2 %, while the water addition was kept constant at 15 %.

Table 2

Adopted experimental variants

Variant	Recycled glass waste (wt. %)	Coal fly ash (wt. %)	SiC (wt. %)	Water addition (wt. %)
1	88.2	9.0	2.8	15.0
2	87.1	10.0	2.9	15.0
3	87.0	10.0	3.0	15.0
4	85.9	11.0	3.1	15.0

3. Results and discussion

The main parameters of the experimental manufacturing process of cellular glass by microwave irradiation of the crucible coated with Y_2O_3 film containing the material subjected to heating are shown in Table 3.

Table 3

Parameters of the manufacturing process

Parameter	Variant			
	1	2	3	4
Dry raw material/cellular glass amount (g)	365/355	365/357	365/356	365/356
Sintering/foaming temperature (ºC)	960	965	967	970
Heating time (min)	32.5	33	33.5	34.25
Average heating rate (ºC/min)	29.5	28.6	28.3	27.7
Average cooling rate (ºC/min)	5.8	5.6	5.7	5.7

Index of volume growth	1.80	1.90	1.95	2.10
Specific energy consumption (kWh/kg)	0.81	0.82	0.84	0.86

The dry raw material amount was adopted and kept in all experimental variants at the value of 365 g. As mentioned above, the experimental methodology was used to determine the temperature of the materials subjected to heating based on the correlation between heating time and temperature, experimentally identified by previous measurements, the thickness and quality of the thermal insulation layer being kept constant. Thus, the variation of the heating duration between 32.5-34.25 min led to increasing the final temperature of the expanded material from 960 to 970 ºC. The average heating rate had very high values (27.7-29.5 ºC/min), significantly above the usual level of this functional parameter, indicating the remarkable effect of microwave absorption in the wall of the crucible coated with Y_2O_3 film. The increase in volume of the expanded material was determined to be a doubling of the initial volume, i.e. a common increase in the use of SiC (around 3 %) and coal fly ash (around 10 %). The specific energy consumption recorded very low values (less than 0.86 kWh/kg), confirming the energy efficiency of the innovative tested heating process.

Significant images of the cross section with homogeneous porosity of the cellular glass samples manufactured in the four variants are shown in Fig. 2.

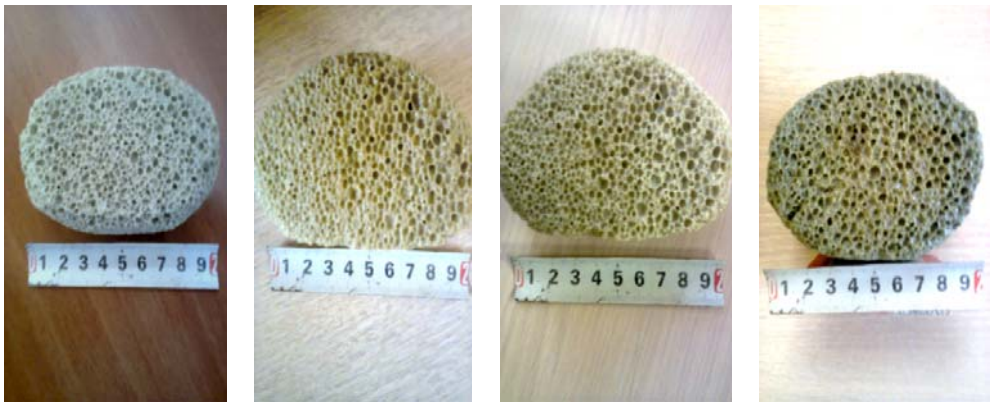

a b c d

Fig. 2. Appearance of the cellular glass products
a – variant 1; b – variant 2; c – variant 3; d – variant 4

Common methods of analysis were used to characterize cellular glass samples from a physical, mechanical, thermal, and morphological point of view. The apparent density was measured by the gravimetric method [19]. The porosity was calculated by the comparison method of the “true” and apparent density of the material, experimentally measured [20]. The compressive strength was determined with a TA.XTplus Texture analyzer. Using the guarded-comparative-longitudinal heat flow method (ASTM E1225-04) the thermal conductivity was measured. The water absorption for 24 hours was determined by the water immersion method (ASTM

D570). The microstructural appearance of the four products was investigated with ASONA 100X Zoom Smartphone Digital Microscope. The results of the features determination of cellular glass samples are presented in Table 4.

Table 4

Features of cellular glass samples

Variant	Apparent density (g/cm^3)	Porosity (%)	Thermal conductivity (W/m·K)	Compressive strength (MPa)	Water absorption (vol. %)	Pore size (mm)
1	0.33	84.3	0.073	1.45	1.5	0.1-0.4
2	0.31	85.2	0.070	1.42	1.8	0.2-0.7
3	0.30	85.7	0.066	1.41	1.6	0.2-0.8
4	0.28	86.7	0.064	1.36	1.8	0.3-0.9

The thermal regimes adopted for the treatment of the four mixtures being relatively close in value led to quite low variations of the expanded samples features. Thus, the apparent density had values between 0.28-0.33 g/cm^3, considered small enough for use in construction as thermal insulation material. Also, the high porosity (84.3-86.7 %) and the low thermal conductivity (0.064-0.073 W/m·K) ensure adequate thermal insulation properties of the products. The level of compressive strength was more than acceptable (1.36-1.45 MPa) for this type of cellular glass and water absorption was determined at low values, below 1.8 vol. %.

The macrostructural aspect of the four foamed products in Fig. 2 showed a relatively fine and homogeneously organized porosity. The microstructural investigation of these products presented in Fig. 3 confirmed this appearance.

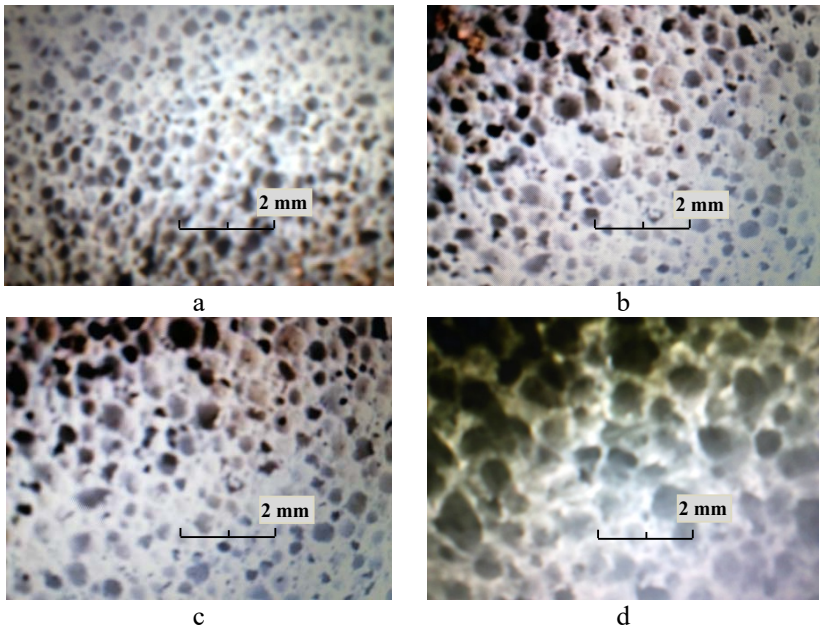

Fig. 3. Microstructural pictures of the cellular glass samples
a – variant 1; b – variant 2; c – variant 3; d – variant 4

Closed round pores formed the microstructure of the cellular glass samples. Their distribution was even according to Fig. 3. The size of cells was less than 1 mm, the dimensional ranges being shown in Table 4. The lowest dimensions characterized the sample obtained in variant 1, with the lowest proportions of SiC (2.8 %) and coal fly ash (9 %) and the highest dimensions belonged to the sample made with 3.1 % SiC and 11 % coal fly ash, corresponding to variant 4.

Comparing the features of products manufactured by microwave irradiation through SiC crucible coated with Y_2O_3 with that industrially made by conventional heating methods (without coal fly ash) [5] and especially with that experimentally obtained also by conventional methods using the same raw material types (glass waste and coal fly ash) and the same expanding agent type (SiC) (apparent density between 0.2-0.4 g/cm^3, optimal porosity of 75 %, and corresponded compressive strength of 1.5 MPa) [17] it can be observed that the differences in terms of qualyty are low. The main advantage of the method presented in the paper is the higher energy efficiency compared to conventional methods, the specific energy consumption being between 0.81-0.86 kWh/kg. In the industrial production of cellular glass and also in the numerous small-scale experiments presented in the literature, the energy consumption is not an important parameter, the predominant being the interest for the quality of the product. The literature provides few data on this. However, the few information shows that the average specific energy consumption of industrial processes is around 140 kWh/m^3, i.e. approximatelly between 0.80-1.16 kWh/kg [21]. It should be noted that the use of industrial-scale microwave equipment could increase the energy efficiency of the heating process by up to 25 % compared to a low power oven of the type used in this experiment [22].

4. Conclusions

The objective of the paper was to manufacture cellular glass with specific properties for use as thermal insulation material for buildings, from recycled post-consumer drinking bottle, coal fly ash and silicon carbide as an expanding agent, under the conditions of applying the unconventional method of microwave heating of the SiC crucible coated with Y_2O_3 film containing the pressed powder raw material. Knowing the property of Y_2O_3 as a remarkable microwave absorber as well as silicon carbide as a high microwave susceptible material, the original solution of using a SiC crucible coated with Y_2O_3 film was adopted for the process of indirect heating of raw material at temperatures of 960-970 ºC at which the sintering and expansion of the material takes place due to the formation of the porous structure. Also, the use of microwave heating in the cellular glass manufacturing process, unlike the conventional methods applied on an industrial scale, is one of the main originality elements of the work. As a consequence of the simultaneous use of microwave heating and the intensification of the process with Y_2O_3 film, the heating rate reached very high values (up to 29.5 ºC/min) and the specific energy consumption was reduced to 0.81-0.86 kWh/kg, i.e. at

the minimum limit of consumption in industrial processes. In terms of quality, the four variants of cellular glass had good thermal insulation properties (low apparent density, high porosity, and low thermal conductivity) required for use in building, adequate compressive strength and very homogeneous pore distribution in the material structure. The industrial application of the small-scale tested solution is feasible on a conveyor belt tunnel furnace by replacing the refractory vault with SiC plates coated with Y_2O_3 on the outer surface and mounting the microwave generators above the plates.

Referinţe

[1] M. Jacoby, „Why Glass Recycling in the US is Broken. Picking up the Pieces of US Glass Recycling", Inorganic Chemistry, vol. 97, no. 6, February 2019. https://cen.acs.org/materials/inorganic-chemistry/glass-recycling-US-broken/97/i6

[2] T.O. Ogundairo, D.D. Adegoke, I.I.Akinwumi, O.M. Olofinnade, „Sustainable Use of Recycled Waste Glass as an Alternative Material for Building Construction-A Review", 1st International Conference on Sustainable Infrastructural Development, IOP Cong. Series: Materials Science and Engineering, vol. 640, 2019. https://doi.org/10.1088/1757-899X/640/1/012073

[3] G. Scarinci, Giovanna Brusatin, E. Bernardo, „Glass Foams", in Cellular Ceramics: Structure, Manufacturing, Properties and Applications, M.Scheffler, P. Colombo (eds.) Wiley-VCH Verlag GmbH & KgaA, Weinheim, Germany, 2005, pp. 158-176.

[4] J. Hurley, „Glass-Research and Development", Final Report, A UK Market Survey for Foam Glass, The Waste and Resources Action Programme Publication, Banbury, Oxon, UK, 2003.

[5] *** „Environmental Product Declaration", Pittsburgh Corning Europe N.V., Tessenderlo, Belgium, 2021.

[6] *** „Environmental Product Declaration", Glasopor 10-60 (Cellular Glass Aggregate), Norsk Glassgjenvinning AS, Norway, 2014.

[7] *** „Environmental Product Declaration", Glapor Cellular Glass, Glapor Werk Mitterteich GmbH, Institut Bauen und Umwelt (publisher), Berlin, Germany, 2017.

[8] *** „Geocell Foam Glass Gravel-High Performance in Every Aspect", Geocell Schaumglas GmbH, Deutsches Institut für Bautechnik (publisher), Berlin, Germany, July 2017.

[9] M.F. Dragoescu, S.M. Axinte, L. Paunescu, A. Fiti, „Foam Glass with Low Apparent Density and Thermal Conductivity Produced by Microwave Heating", European Journal of Engineering and Technology, vol. 6, no. 2, pp. 1-9, 2018.

[10] S.M. Axinte, L. Paunescu, M.F. Dragoescu, Ana C. Sebe, „Manufacture of Glass Foam by Predominantly Direct Microwave Heating of Recycled Glass Waste", Transactions on Networks and Communications, vol. 7, no. 4, pp. 37-45, 2019. https://doi.org/10.14738/tnc.74.7214

[11] B.T. Grigoras, L. Paunescu, M.F. Dragoescu, „High Mechanical Strength Cellular Glass-Ceramic Manufactured in Microwave Field Using Blast Furnace Slag and Glass Waste", Nonconventional Technologies Review, vol. 24, no. 4, pp. 47-52, 2020.

[12] L. Paunescu, M.F. Dragoescu, Felicia Cosmulescu, „Microwave Heat Treatment of Wastes (Clay, Glass and Coal Ash) to Manufacture a High Mechanical Strength Cellular Aggregate", Nonconventional Technologies Review, vol. 24, no. 4, pp. 64-71, 2020.

[13] Felicia Cosmulescu, L. Paunescu, M.F. Dragoescu, S.M. Axinte, „Comparative Analysis of the Foam Glass Gravel Types Experimentally Produced by Microwave Irradiation", Journal of Engineering Studies and Research, vol. 26, no. 3, pp. 58-68, 2020.

[14] P. Lei, X. Chen, Y. Yan, J. Zhu, „The Tunable Dielectric Properties of Sputtered Yttrium Oxide Films", Applied Physics A, vol. 127, no. 99, 2021. https://link.springer.com/article/10.1007/s00339-021-04280-8
[15] *** „Yttrium Oxide (Y_2O_3) Nanoparticle-Properties, Applications", AzoNano Company, July 2013. https://www.azonano.com
[16] L. Paunescu, M.F. Dragoescu, S.M. Axinte, Ana C. Sebe, „Significant Enhance of the Indirect Microwave Heating Yield in the Foaming Process of Glass Waste", Nonconventional Technologies Review, vol. 23, no. 3, pp. 80-84, 2019.
[17] J.P. Wu, A.R. Boccaccini, P.D. Lee, M.J. Kershaw, R.D. Rawlings, „Glass-Ceramic Foams From Coal Ash and Waste Glass: Production and Characterization", Advances in Applied Ceramics, vol. 105, no. 1, pp. 32-39, 2006.
[18] Giovanna Brusatin, E. Bernardo, G. Scarinci, „Production of Foam Glass from Glass Waste", Proceedings of the International Conference Sustainable Waste Management and Recycling: Glass Waste, Kingston University of London, UK, pp. 68-82, Sept. 14-15, 2004.
[19]*** „Manual of Weighing Applications", Part 1, Density, 1999. http://www.docplayer.net/21731890-Manual-of-weighing-applications-part-1-density_html
[20] L.M. Anovitz, D.R. Cole, „Characterization and Analysis of Porosity and Pore Structures", Reviews in Mineralogy and Geochemistry, vol. 80, 2005, pp. 61-164.
[21] *** „Cellular Glass Manufacturing", Energocell, Daniella Ipari Park Kft., Debrecin Hungary, 2014. http://www.energocell.hu
[22] Oxana V. Kharissova, B.I. Kharissov, J.J. Ruiz Valdés, „Review: The use of microwave irradiation in the processing of glasses and their composites", Industrial & Engineering Chemistry Research, vol. 49, no. 4, pp. 1457-1466, 2010.

Aspecte privind calculul pereților structurali din zidărie

Aspects on the masonry structural walls computation

Robert Draghici[1], Ana Maria Pârvănuș[1], Daniel Stoica[1]

[1]Universitatea Tehnica de Constructii Bucuresti
B-dul Lacul Tei 122-124, Sector 2, Bucuresti
E-mail: daniel.stoica@utcb.ro

DOI: 10.37789/rjce.2022.13.3.4

Rezumat.
Codul romanesc CR6-2013, pornind de la EC6, propune 3 tipuri de pereți structurali din zidărie, care pot sa fie utilizați la clădirile cu structura de rezistenta din zidărie. Prezentul articol, își propune identificarea răspunsurilor acestor tipuri de pereți, pentru diferite niveluri de forte axiale N_{Ed} si dimensiuni ale pereților structurali.

Cuvinte cheie: structuri, zidarie, pereti, momente incovoietoare

Abstract.
The Romanian code CR6-2013, starting from EC6, proposes 3 types of structural masonry walls, which can be used for buildings with masonry resistance structure. This article aims to identify the answers of these types of walls, for different levels of axial forces N_{Ed} and dimensions of structural walls.

Key words: structures, masonry, walls, bending moment

1. Introduction

Traditional design is mainly based on increasing capacity in proportion to demand and increasing ductility. The structures are designed according to the principle "Strong columns and weak beams" so as to develop an optimal plasticity mechanism. An acceptable level of building performance during a seismic motion is the intrinsic ability of the structure strength to absorb and dissipate energy in the most stable manner and for as many cycles as possible. In the case of masonry buildings, although the oldest as a building material, this is quite little understood and calculated.

The three types of masonry presented in CR6 were considered, namely: URM, CM and WRM.

Taking into account all the CR6 recommendations, in all the case studies considered we have:

For Unreinforced Masonry (URM)

According to CR6-2013, for M_{Rd} the relations are:

- The compressed area is $A_{zc} = \frac{N_{Ed}}{0.85 f_d}$;
- The eccentricity of axial force is y_{zc};
- The compression design strength is $f_d = \frac{f_k}{\gamma_M} = \frac{K f_b^{0.7} f_m^{0.3}}{\gamma_M}$;
- The M_{Rd} become: $M_{Rd} = N_{Ed} y_{zc} = N_{Ed}\left[\frac{l_w}{2} - \frac{A_c}{2t * 0.85 f_d}\right] = \frac{N_{Ed}}{2}\left(l_w - \frac{N_{Ed}}{0.85 t f_d}\right)$

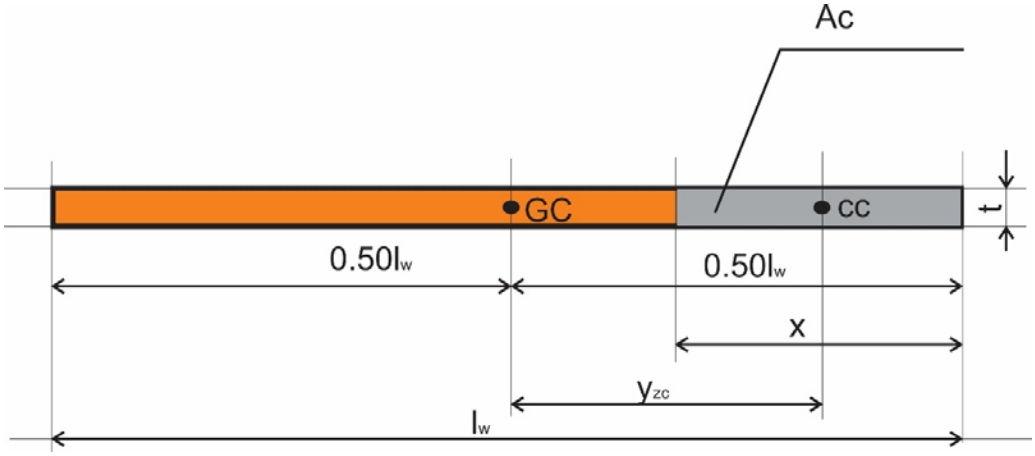

Figure 1 – URM masonry wall

For Confined Masonry (CM)

According to CR6-2013, for M_{Rd} the relations are:

- Equivalation of RC to masonry equivalent area into relation of the ratio $n = \frac{f_{cd}}{f_d}$;
- From n ratio we obtain $A_{em} = (n-1)A_{cc}$ so $b_e = \frac{A_{em}}{t} = \frac{(n-1)A_{cc}}{t}$
- The compressed area is $A_{zc} = \frac{N_{Ed}}{0.85 f_d}$;
- The eccentricity of axial force is y_{zc};
- The compression design strength is $f_d = \frac{f_k}{\gamma_M} = \frac{K f_b^{0.7} f_m^{0.3}}{\gamma_M}$;
- $M_{Rd} = M_{Rd}(URM) + M_{Rd}(As)$ where $M_{Rd}(URM) = N_{Ed} y_{zc}$ and $M_{Rd}(As) = A_s l_s f_{yd}$

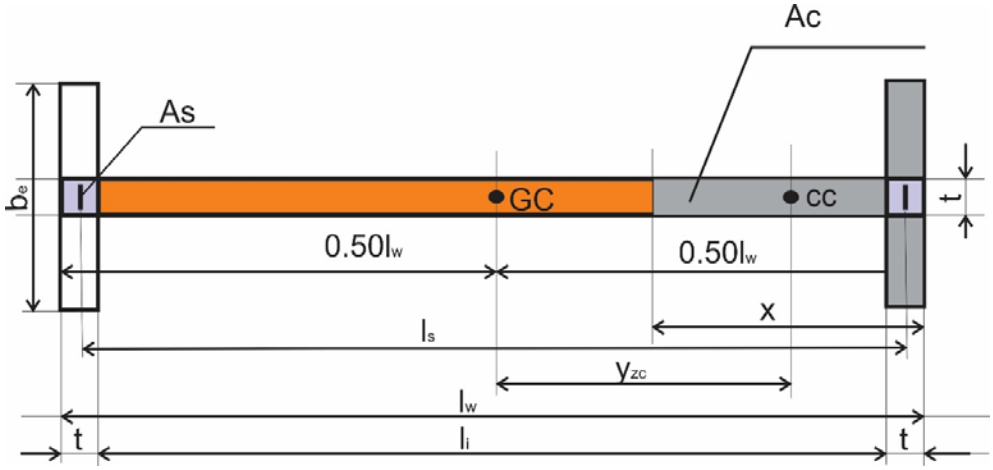

Figure 2 – CM masonry wall

For Web Reinforced Masonry (WRM)

According to CR6-2013, for M_{Rd} the relations are:

- Equivalation of RC to masonry equivalent area is proposed into relation of the ratio $n = \frac{f_{cd}}{f_d}$ so the dimensions of $t_{c,equivqlent}$ become $t_c n$
- The compressed area is $A_{zc} = \frac{N_{Ed}}{0.85 f_d}$;
- The eccentricity of axial force is y_{zc};
- The compression design strength is $f_d = \frac{f_k}{\gamma_M} = \frac{K f_b^{0.7} f_m^{0.3}}{\gamma_M}$;
- $M_{Rd} = M_{Rd}(URM) + M_{Rd}(As)$ where $M_{Rd}(URM) = N_{Ed} y_{zc}$ and $M_{Rd}(As) = 0.25 l_w^2 f_{yd}$

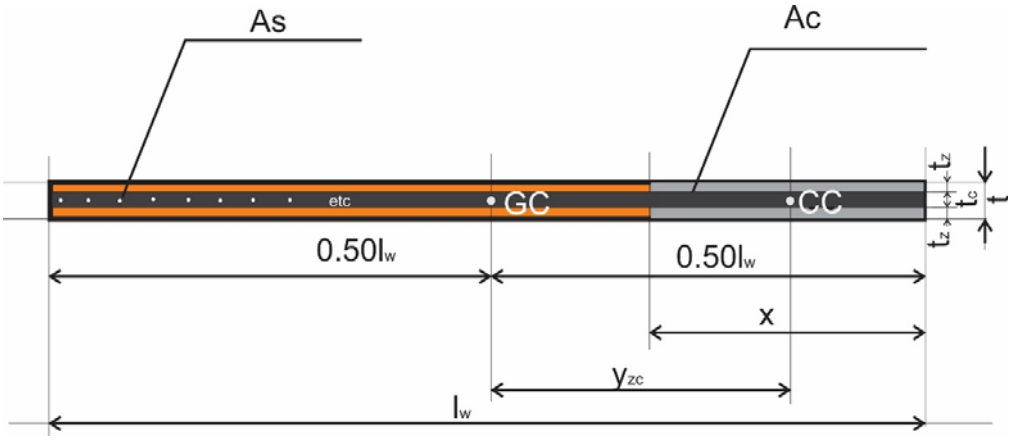

Figure 3 – WRM masonry wall

2. Proposed and completed case studies

The case studies (1365) we focused on consisted of:

- 455 studies for **URM**, wall lengths l_w between 1 and 10 m (every 10 cm), thickness t=0.25m, for 5 levels of axial force N_{Ed} (100, 200, 200, 400 and 500 kN), for a masonry with f_d=200 kN/m^2; The relations from CR6-2013 were considered using the MS Excel program.
- 455 studies for **CM**, wall lengths l_w between 1 and 10 m (every 10 cm), thickness t=0.25m, for 5 levels of axial force N_{Ed} (100, 200, 200, 400 and 500 kN), for a masonry with f_d=200kN/m^2, one reinforced concrete tie column (with f_{cd}=2000kN/m^2) at each end of the wall (with dimensions 25x25 cm) and with 4 reinforcements ϕ12 of a steel with f_{yd}=300000kN/m^2; The relations from CR6-2013 were considered using the MS Excel program;
- 455 studies for **WM**, wall lengths l_w between 1 and 10 m (every 10 cm), a total thickness t=0.25 m (of which 10 cm concrete web and on the outside two layers of masonry having 7.5 cm each), for 5 levels of axial force N_{Ed} (100, 200, 200, 400 and 500 kN), for a masonry with f_d=200kN/m^2, concrete in the web with f_{cd}=2000kN/m^2, with reinforcements ϕ8/100mm from a steel with f_{yd}=300000kN/m^2. Because the relationships in CR6-2013 were considered too simple, the Sekon® program was used for the calculations (developed at UTCB by Daniel Stoica) and which uses reinforced concrete theories. In this case, instead of equating concrete with masonry, masonry was equated with concrete. Three walls were selected (with 3, 6 and 9 m length for N_{Ed} = 100, 200, 300, 400 and 500 kN) for which other answers obtained with Sekon ® are presented.

All calculations were made only to determine the M_{Rd} capable bending moments (regardless of capable axial forces N_{Rd}).

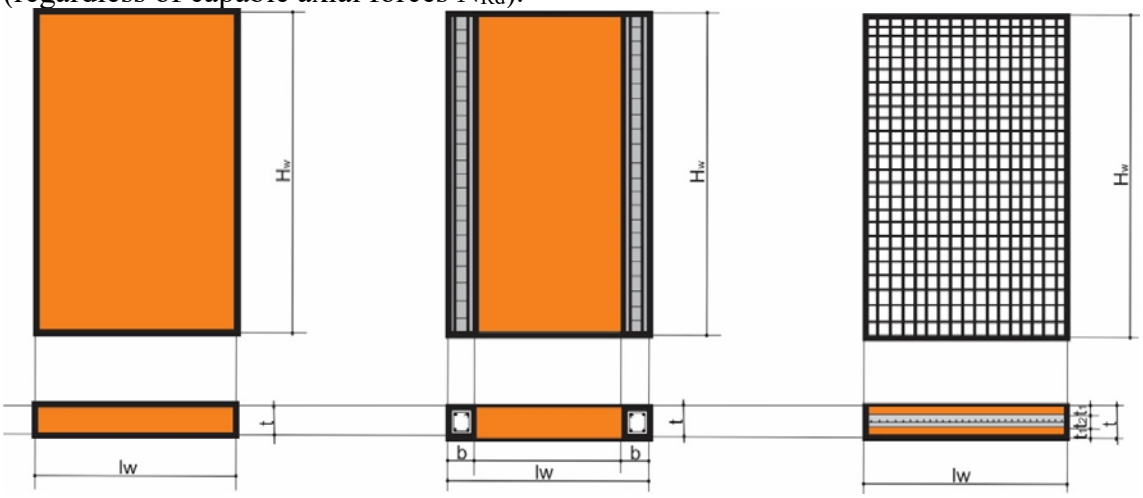

Figure 4 – URM, CM and WRM masonry walls for case studies

Strain | Stresses in concrete and reinforcement

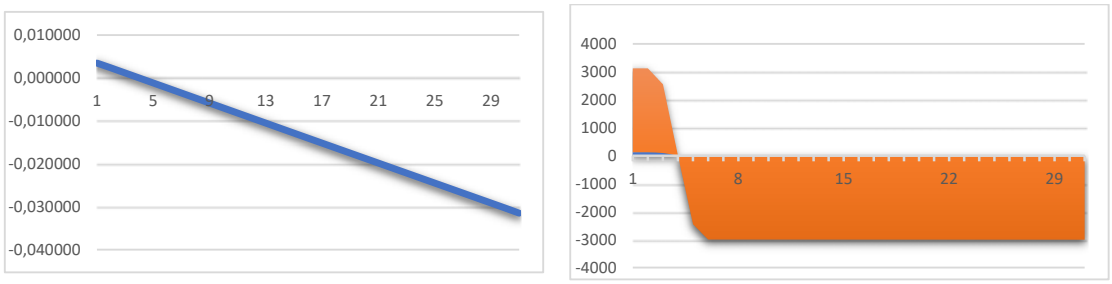

NEd=100 kN – l_w=3.00 m

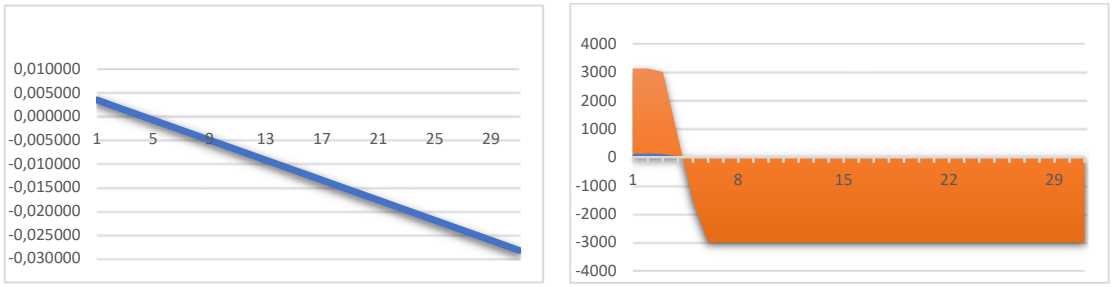

NEd=200 kN – l_w=3.00 m

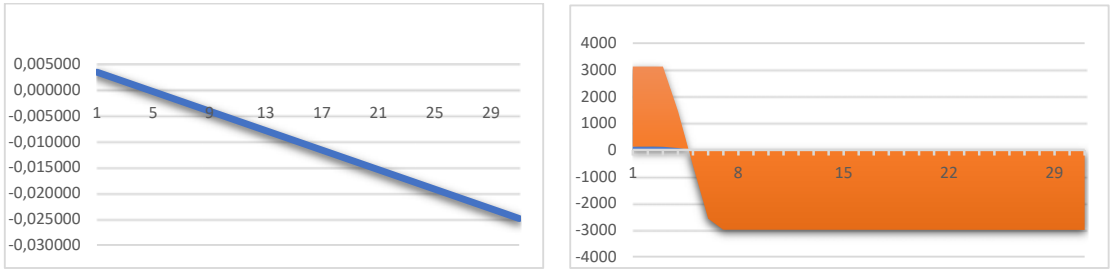

NEd=300 kN – l_w=3.00 m

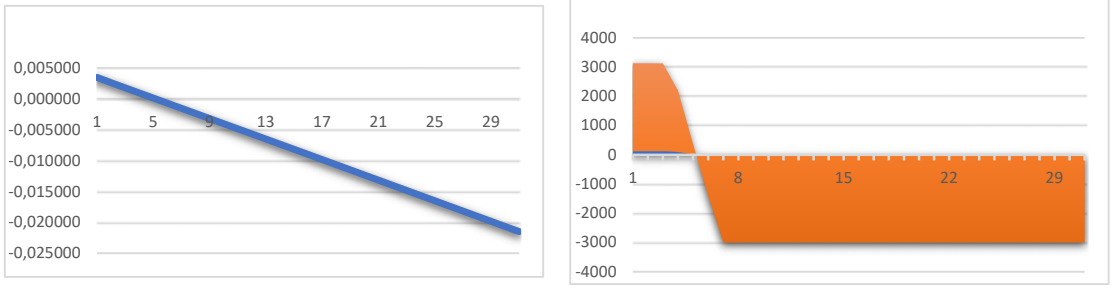

NEd=400 kN – l_w=3.00 m

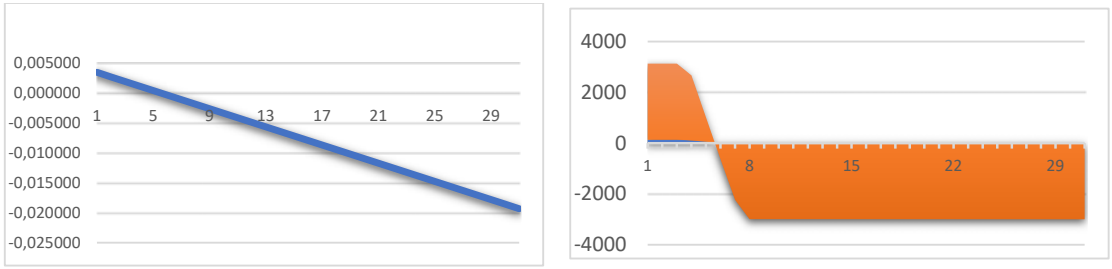

NEd=500 kN – l_w=3.00 m

Figure 5 – WRM – l_w=3.00 m

Strain | Stresses in concrete and reinforcement

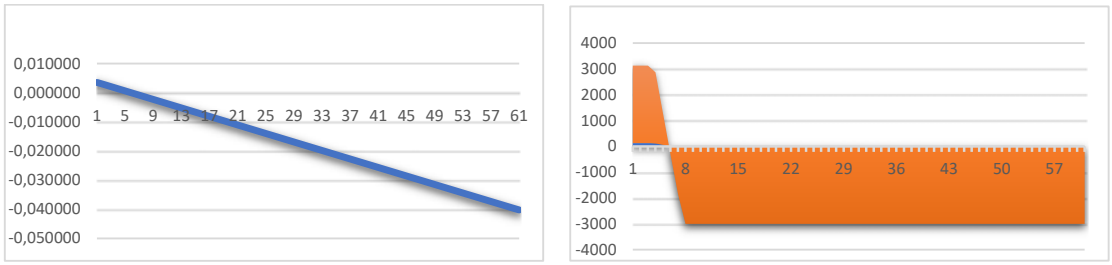

NEd=100 kN – l_w=6.00 m

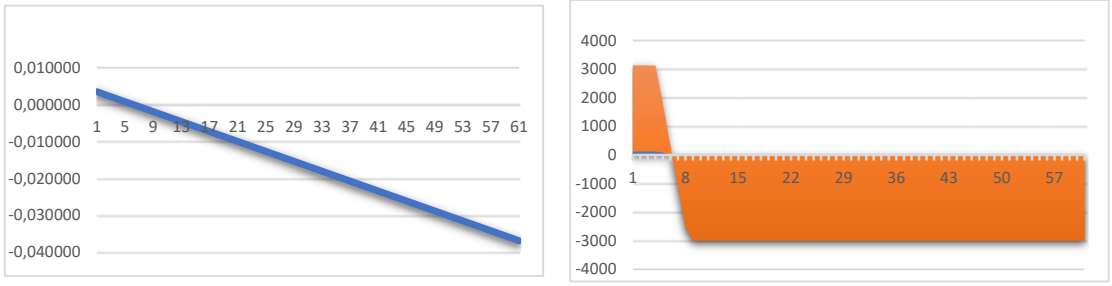

NEd=200 kN – l_w=6.00 m

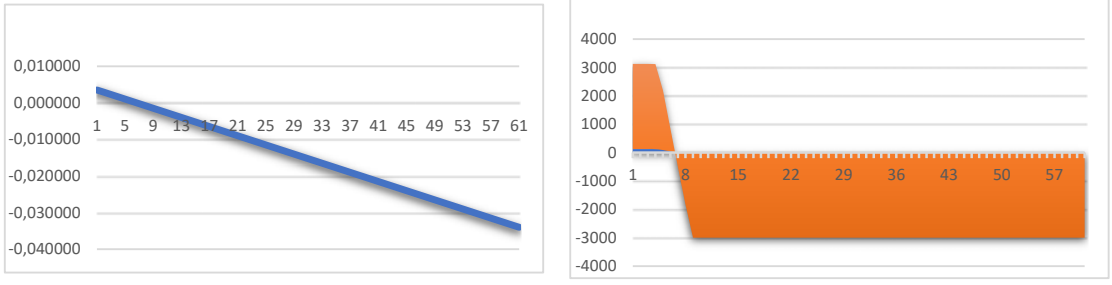

NEd=300 kN – l_w=6.00 m

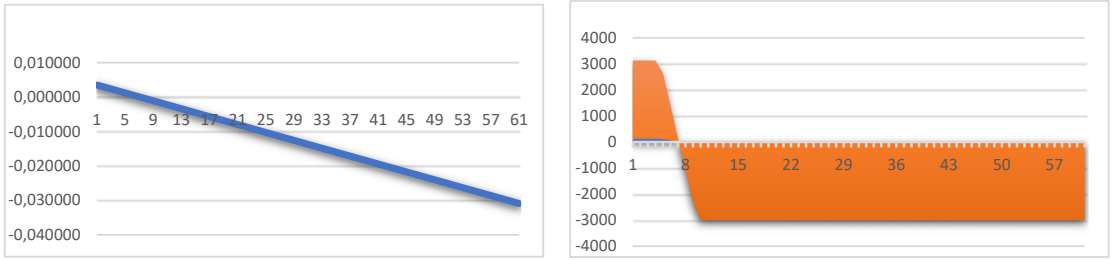

NEd=400 kN – l_w=6.00 m

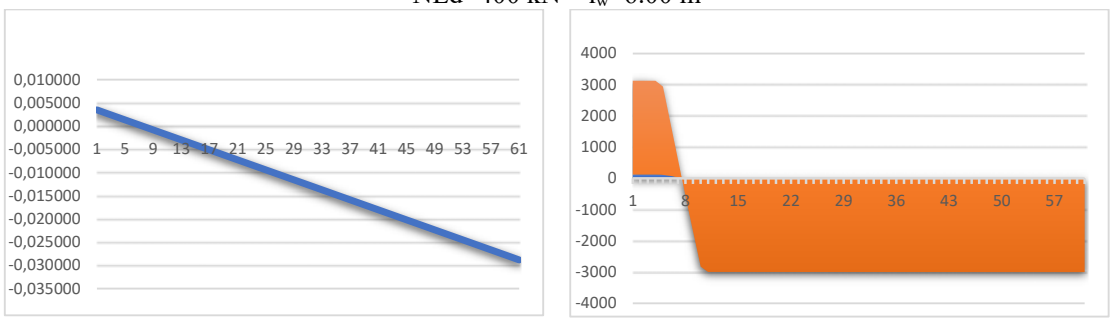

NEd=500 kN – l_w=6.00 m

Figure 6 – WRM – l_w=6.00 m

Strain | Stresses in concrete and reinforcement

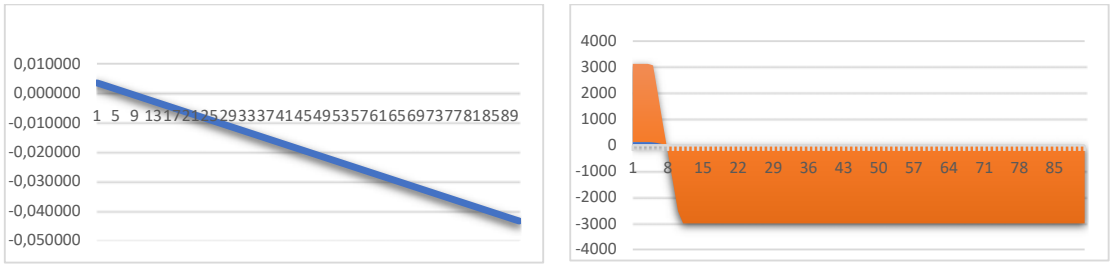

NEd=100 kN – l_w=9.00 m

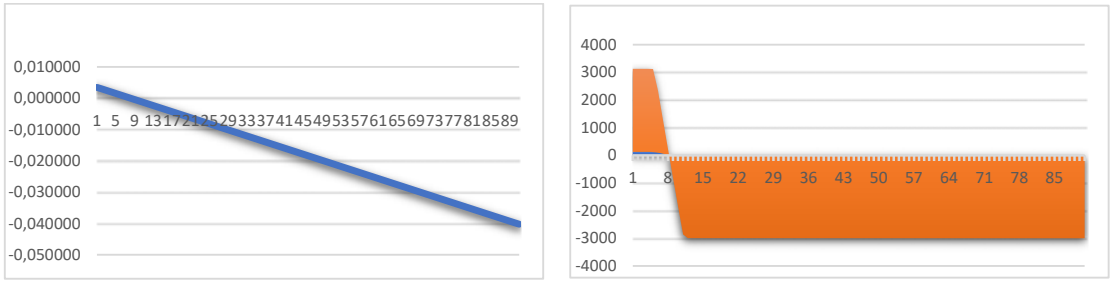

NEd=200 kN – l_w=9.00 m

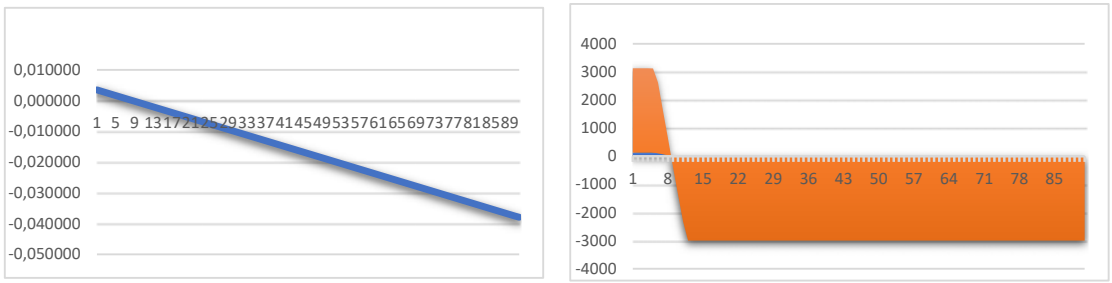

NEd=300 kN – l_w=9.00 m

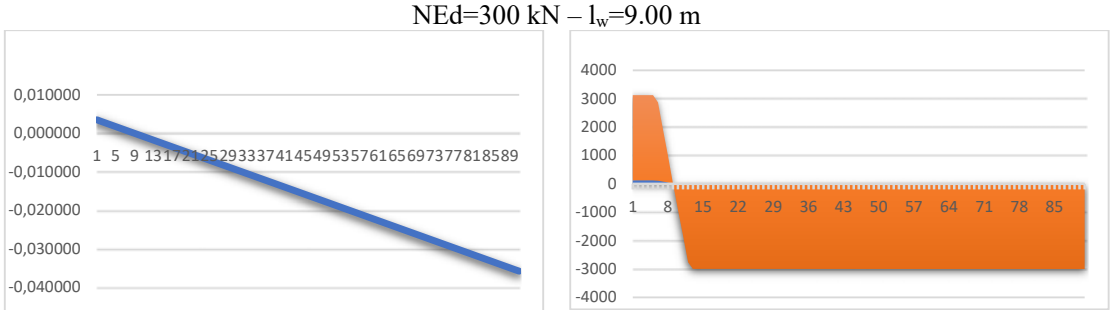

NEd=400 kN – l_w=9.00 m

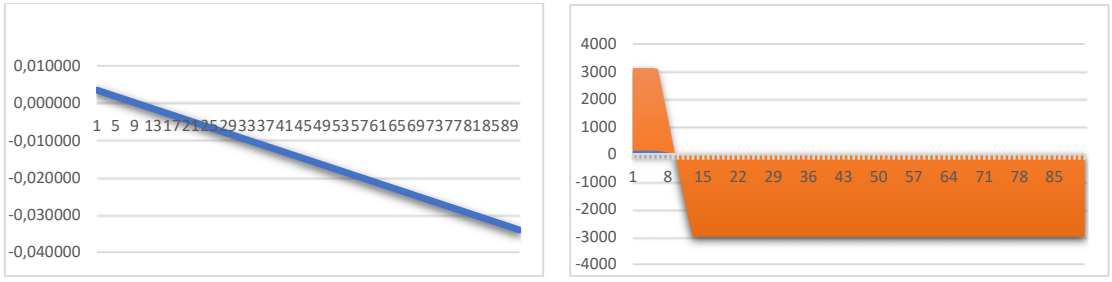

NEd=500 kN – l_w=9.00 m

Figure 7 – WRM – l_w=9.00 m

3. Comparisons between calculations performed for the three types of masonry, according to case studies

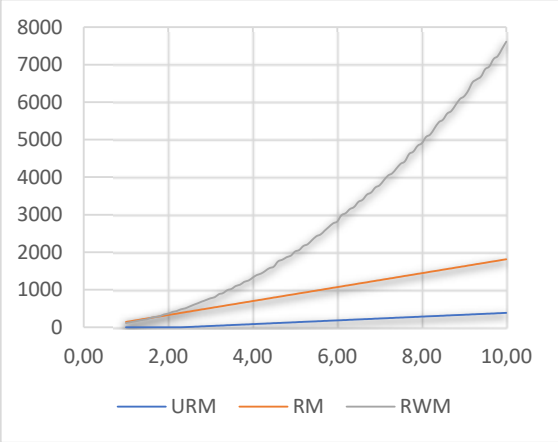

Figure 8 -M_{Rd} for N_{Ed}=100 kN

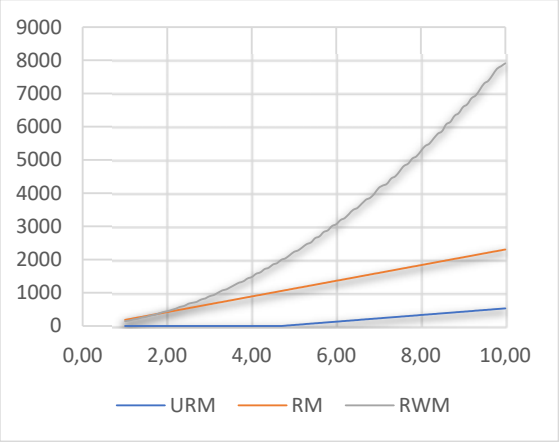

Figure 9 -M_{Rd} for N_{Ed}=200 kN

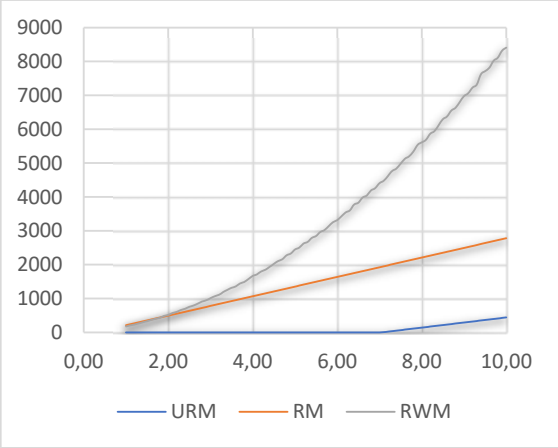

Figure 10 -M_{Rd} for N_{Ed}=300 kN

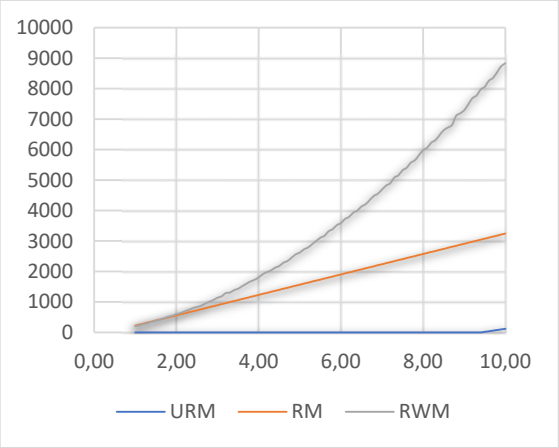

Figure 11 -M_{Rd} for N_{Ed}=400 kN

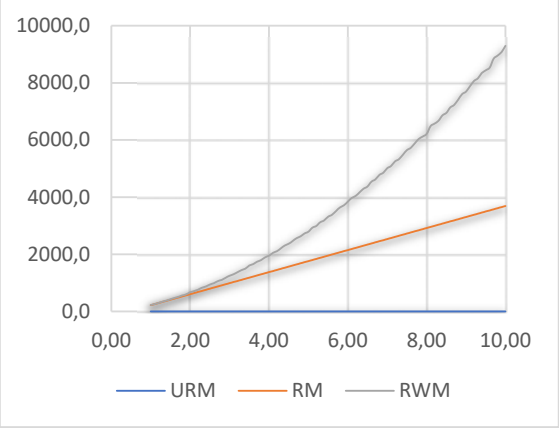

Figure 12 -M_{Rd} for N_{Ed}=500 kN

4. First attempt to obtain simple, empirical relationships to obtain M_{Rd} capable bending moments

Conclusions about the case studies comparisons:

- Looking at the diagrams of M_{Rd} capable bending moments, for the 3 types of masonry walls, it can be seen immediately that the lowest values are for URM and the highest values for WRM. A maximum possible for CM compared to URM and WRM being about half.
- It can also be seen that the formulas in CR6 are absolutely "linear" compared to the calculations made with the Sekon ® program.
- Also, although we do not take into account the N_{Rd}, it is observed that with the increase of the axial forces N_{Ed} on the walls, the M_{Rd} becomes zero at some point, for URM.
- Therefore, it is very clear that the walls of the URM respond poorly to seismic actions, even if out-of-plane actions are not taken into account.
- Considering the trendlines resulting for all the case studies performed, we tried to obtain some simpler relations for the M_{Rd} calculation, in the followings:

Considering all the numerical simulations performed for URM, CM and WRM, the following empirical relations of approximation of the capable bending moments (M_{Rd}) resulted:

For URM:

- If $l_w < 2.4P$ it turns out that $M_{Rd} = 0$;
- If $l_w \geq 2.4P$ it turns out that $M_{Rd} = 50P(l_w - 2.30P)$

For CM:

$$M_{Rd} = (0.1n + P^{0.90})l_w^2 + (2.50mA_S + P^{3.15})l_w$$

For WRM:

$$M_{Rd} = (0.93mA_{Sw} + P^{0.741})l_w^2 + 4nPl_w$$

Where:

$n = \frac{f_{cd}}{f_d}$ first transformation factor

$m = \frac{f_{yd}}{f_{cd}}$ second transformation factor

$P = 20\frac{N_{Ed}}{f_d}$

With:

- f_{cd} – design compressive strength of concrete in [kN/m^2]
- f_d – design compressive strength of masonry in [kN/m^2]
- f_{yd}- design tensile strength of the reinforcement in [kN/m^2]
- N_{Ed} – axial force on the masonry element in [kN]
- l_w – the length of the masonry wall in m

- A_S – the area of the reinforcements in the tensioned tie column in [cm^2]
- A_{Sw} – total vertical reinforcement area on the linear meter of WM concrete web in [cm^2]

5. Conclusion

Conclusions about the case studies comparisons:

- For the new generation of design codes, we believe that the relationships in CR6 should be improved and updated, trying to be homogeneous and not starting from things established in various other codes in the world.
- The objectives of this article were only about M_{RD} and we intend to continue this study, so as to obtain structural answers as close as possible to reality, possibly with simple but consistent calculation relationships.
- Here I used as a correct comparison the Sekon® program, made by one of the authors of the article, but also other calculation programs, postprocessors such as CSICol, Graitec, etc. can be easily used.

6. References

- CR6-2013 - DESIGN CODE FOR MASONRY STRUCTURES (COD DE PROIECTARE PENTRU STRUCTURI DIN ZIDĂRIE CR6-2013)
- P100/1-2013 - SEISMIC DESIGN CODE - PART I - DESIGN PROVISIONS FOR BUILDINGS (COD DE PROIECTARE SEISMICĂ – PARTEA I – PREVEDERI DE PROIECTARE PENTRU CLĂDIRI)
- Daniel Stoica - User guide for calculating the strength capacity of reinforced concrete elements – Sekon®
- MS – Excel

Non-linear numerical study of the dynamic response of elevated steel conical tank under seismic excitation

Studiu numeric neliniar al răspunsului dinamic al rezervorului conic de oțel ridicat sub excitație seismică

Nasser Dine Hadj Djelloul[1]*, Mohamed Djermane[1], Noor Sharari[2]

[1]FIMAS Laboratory, University of Tahri Mohammed, Bechar B.P 417, Bechar 08000, Algeria
[2]Department of Civil Engineering, University of Technology Sydney, Sydney, NSW 2007, Australia

DOI: 10.37789/rjce.2022.13.3.5

ABSTRACT
Elevated cylindrical and conical steel tanks are widely used to conserve water or chemical liquids. These important structures are required to stay protected and operative at any time. The wall angle inclination of conical tank part,as well as the presence of the vertical earthquake component, can cause damage to this structure and even lead to its failure. The purpose of this study is to examine the effect of the wall angle inclination of the tank and the vertical earthquake acceleration component on the nonlinear dynamic stability of the elevated steel conical tanks under seismic excitation. The elevated steel conical tank is simulated utilizing the finite element analysis method using ANSYS software. The fluid-structure interaction is considered using a suitable interface that allows the fluid to apply hydrodynamic pressures on the structure. Three different models, namely Model –A-30°, Model –B-45°and Model –C-60°were investigated; it has been concluded that the impact of inclination of the tank wall significantly affects the nonlinear stability of the elevated steel conical tank. While considering the vertical ground acceleration, inclination plays a significant role in the design of this type of structures. Therefore, it should be appropriately included in the seismic analysis of elevated steel conical tanks to satisfy the safety of the elevated steel conical tank response under seismic loading.

Keywords: Non-linear dynamic analysis, Fluid–structure interaction, Steel conical tanks, Stability,Vertical acceleration

1. Introduction

Elevated storage tanks are strategic structures in daily industrial activities. These structures are used in water storage facilities and in the industry for the storage of chemical products. There are different types of tanks having different shapes, for example:cylindrical,conical,and spherical. However, the elevated conical tanks are the most constructed ones. Under seismic excitation, the walls of the upper tank and the elevated tank support tower experience additional stresses. These forces can lead to several phenomena, such as buckling of the walls [1].

In terms of seismic analysis, many researchers have studied the dynamic behaviour of elevated tanks. Chandrasekaran and Krishna (1965) [2] were the first to use the single degree of freedom model to study the dynamic response of elevated tanks. They found that during an earthquake, the parameter of energy absorption is very important and needs to be taken into consideration when designing the tank's structure. They also observed that the critical case is that of a full tank. Ramiah and Gupta (1966) [3] also used a model with one degree of freedom to analyse the dynamic response of elevated tanks on different types of soil.

However,in the late 1950s and early 1960s, Housner [4] enabled practising engineers to perform seismic response analysis of elevated tanks using the two-mass method. This simplified model is considered for the movement of the liquid relative to the tank and also the movement of the tank relative to the base,whereas, another application of this simplified model in the seismic analysis of elevated tanks has been reported by Sonobe (1969) [5].

Furthermore, one of the first analytical methods considering the flexibility of the tank walls was proposed by Veletsos (1974)[6]. This method is an extension of the Chopra (1970) [7] method which is used in the seismic calculation of gravity dams. Authors concluded that the flexibility of the walls has a great effect on the impulsive component.

Particularly after the damage caused by the earthquake on elevated conical tanks in Belgium in the 1970s, research work was carried out on conical tanks under hydrostatic loading by Vandepitte et al. (1982)[8]. Indeed, El Damatty.A.A. et al. (1997) [9] studied the static buckling of conical tanks with geometric imperfections under hydrostatic pressures. A non-linear finite element analysis based on a shell member was used in his work. The numerical results show that the presence of such geometric imperfections led to a 35-40% reduction in the critical load.

Moreover, Leonard et al. (1990) [10] evaluated the buckling capacity of an elevated steel tank using the finite element technique. In this work, the analysis of the buckling modes is made by means of the ABAQUS software to estimate the effects of the stiffener arrangements on the buckling modes.

Eventually, Shenton and Hampton (1999) [11] studied the effects of seismic supports on the dynamic response of elevated tanks under seismic excitation without taking into account the sloshing component. The supports are considered asparts of one linear elastic system. The results show that the supports reduced the stress at the base of the elevated tanks. The effect of seismic supports on the dynamic response of elevated tanks was also discussed by MK Shrimali, RS Jangid (2003) [12]. They studied the response of elevated steel tanks under different earthquakes with fixed bases and isolators at the base, and reached to the conclusion that the shear force due to the impulsive component decreases due to the isolation effect, but the sloshing displacement is increased due to the isolation effect.

In addition to this, Sweedan and El Damatt (2005) [13] studied numerically the influence of the vertical component of the earthquake on an elevated conical tank using the equivalent mechanical model. Results show that the seismic force due to the vertical component of earthquakes accounts for about 35% of the forces due to hydrostatic pressure.

Apart from this, Sekhar Chandra Dutta et al. (2009) [14] examined the dynamic characteristics of the elevated tanks under the effect of soil-structure interaction. They concluded that consideration of soil-structure interaction in the design of these categories of tanks is very important. In the same subject, Pallavi S. Dhamak et al. (2014) [15] analysed the dynamic response of elevated tanks, taking into account soil-structure interaction. In this study, a 3D finite element model was produced using ABAQUS software. The results obtained show that soil-structure interaction analysis must be included in the elevated tanks seismic design.

The present work is motivated by the lack of information on the nonlinear dynamic behaviour of elevated conical steel tanks. In the first part of this work-study, the dynamic nonlinear response of elevated steel tanks is studied with three different angles of inclination of the tank wall namely Model –A-30°, Model –B-45°, and Model –C-60°, under seismic excitation using the finite element method. The second part of this work is to evaluate the effect of vertical component of the earthquake on the dynamic behaviour of elevated steel conical tanks. This work represents the first study on the response of elevated conical steel tanks with different angles of inclination of the tank wall and under the vertical seismic excitation by modelling the fluid in three dimensions considering the fluid-structure-interaction, flexibility of the walls, the non-linearity of materials, the geometric non-linearity, the non-linearity of the excitation and the sloshing effect.

2. Failure modes of steel tanks

Steel liquid storage tanks involve different modes of damage mechanisms. A wide variety of mechanisms damage are possible, depending on the geometric configuration of the tank, as well as a large number of other factors such as tank material, type of structure, etc. Nevertheless, the characteristics of earthquakes also have a significant influence on tanks seismic response. Assessment of the behaviour of cylindrical steel tanks demonstrates that they are susceptible to buckling under a seismic load; this is due to the hydrodynamic pressures which tend to make them uplift from their functions. This in turn initiates the development of very high compressive stresses which can cause buckling, tilting of the tank or the complete destruction of this sort of structure (Figure 1). As evidenced by the report on the fragility of metal tanks established by The American Lifelines Alliance claims that the damage to these structures is manifested by buckling [16].

Rotation of tank **Buckling** **Collapse**

Figure 1: Examples of the damage done on the steel elevated tank [17] [18]

3. Code provision

After reviewing the available literature, it is shown that the two American codes: API 650 (American Petroleum Institute) [19] for the design of tanks used in the petroleum industry, and the AWWA (American Water Works Association) [20] for the design of water storage tanks, were the most generally utilized codes for the seismic analysis and computation of steel storage tanks [25].

However, over the last twenty years, other recent codes have seen the day as the European Euro code [21] is on a few focuses considerably more developed than the past two code.

According to the European code, hydrodynamic pressure can be given by the following expressions:

Impulsive rigid pressure:

$p_i(\xi, \varsigma, \theta, t) = C_c(\xi, \varsigma)\, \rho_w H \cos(\theta)\, A_g(t)$ 1)

$$C_c(\xi,\varsigma) = \sum_{n=0}^{\infty}\left(\frac{(-1)^n}{\acute{I}_1\left(\frac{v_n}{\gamma}\right) v_n^2}\cos(v_n,\varsigma)\, I_1\left(\frac{v_n\,\xi}{\gamma}\right)\right) \quad 2)$$

In which

$v_n = \frac{2n+1}{2}\,\pi$, $\gamma = H/R$

Impulsive flexible pressure:

$P_f(\theta, \varsigma, t) = \rho_w H\, \Psi \sum_{n=1}^{\infty}\left(d_n \cos(v_n,\varsigma)\cos(\theta)\, A_f(t)\right)$ 3)

$$\Psi = \frac{\int_0^1 f(\varsigma)\left[\frac{\rho_S\, S}{\rho_W\, H} + \sum_{n=0}^{\infty}(b_n \cos(v_n,\varsigma))\right] d_\varsigma}{\int_0^1 f(\varsigma)\left[\frac{\rho_S\, S}{\rho_W\, H} f(\varsigma) + \sum_{n=0}^{\infty}(b_n \cos(v_n,\varsigma))\right] d_\varsigma} \quad 4)$$

$$b_n = 2\frac{(-1)^n I_1\left(\frac{v_n}{\gamma}\right)}{v_n^2 \grave{I}_1\left(\frac{v_n}{\gamma}\right)} \quad 5)$$

$$d_n = 2\,\frac{\int_0^1 f(\varsigma)\cos(v_n,\varsigma)\, d_\varsigma I_1\left(\frac{v_n}{\gamma}\right)}{v_n \grave{I}_1\left(\frac{v_n}{\gamma}\right)} \quad 6)$$

Convective pressure:

$Pc = \sum_{n=1}^{\infty}(\Psi n\, cosh(\lambda n\, \gamma\, \varsigma)\, J_1(\lambda n\, \xi)\cos(\theta)\, A_n(t))$ 7)

$$\Psi n = \frac{2R}{(\lambda_n^2 - 1)\, J_1(\lambda n)\, cos\, h(\lambda n\, \gamma)} \quad 8)$$

λ_1=1,8112, λ_2=5,3314, and λ_3=8,5363

$$H_{eq} = \frac{H}{\cos\theta} \quad 9)$$

$$R_{eq} = \frac{(2R + H\ \tan\theta)}{2\ \cos\theta} \quad 10)$$

$$t_{eq} = t$$

The conical shape is the most popular one used for elevated tanks in the world. Unfortunately, the current standards code of training do not provide any data for the designs of the conical tanks for the practising engineers. The codes are limited to cylindrical and rectangular tanks with the exception of the AWWA code, which gives a methodology based on the calculation of the dimensions of an equivalent cylinder from a conical shape (Figure 2) [20],

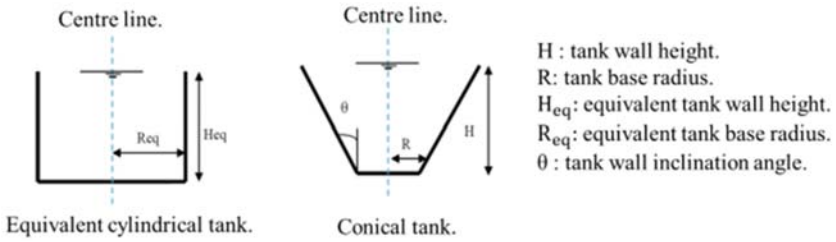

Figure 2: Conical tank and cylindrical equivalent tank [26]

4. Case study

The example of this study is an elevated real conical steel tank of 1000 m^3 capacity, which is located in Kalimna near the entrance to the lakes in Victoria, Australia. The simplified geometry of the model is shown in Figure 3 [10].

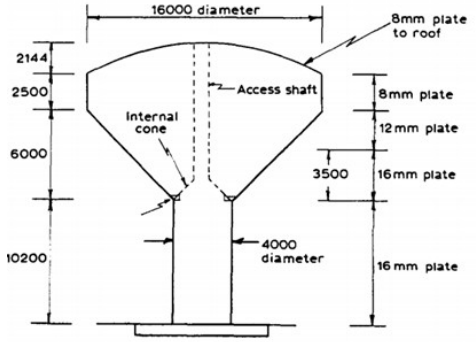

Figure 3: Elevated steel water storage tank used in this study(Leonard R. Allen, et al) [10]

The materials used for the wall and the roof of the elevated tank are elastoplastic, while the material characteristic of the tank as well as of the liquid are presented in Table 1:

Table 1:
Mechanical characteristics of the tank as well as of the liquid (Leonard R. Allen, et al)

Steel	
Density	7850 kg/m^3
Poisson ratio	0.3
Elasticitymodulus	2.06 ×10^5 MPa
Yield stress	2.5 ×10^{3}Pa MPa
Tangent modulus	1.45×10^{4}MPa
Water	
Density	1000 kg/m^3
Bulkmodulus	2.0684 ×10^4 MPa
Viscosity	1.123×10^{-3}N.S/M²

4.1 Numerical model

In this study, the modelling of the elevated steel tank is performed by means of the ANSYS software using finite element analysis. The tower, tank and roof are modelled using Shell 63 element for modal analysis and Shell 181 element "plastic capacity" for transient analysis. The two elements have six degrees of freedom at each node; translations in the nodal directions x, y and z and rotations around the nodal x, y and z-axes [22] [27].

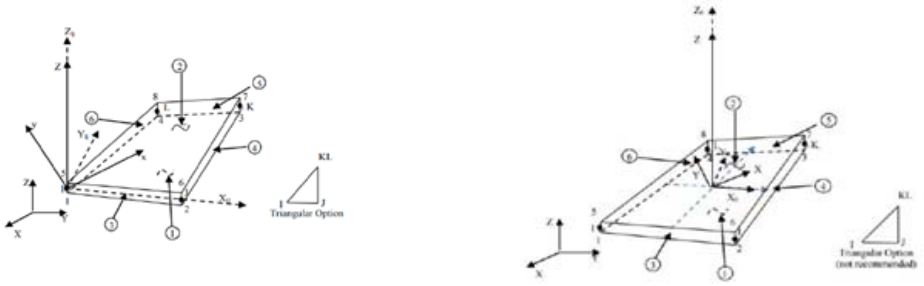

Shell 63 Shell 181

Figure 4: (a) shell 63, (b) shell 181, (The ANSYS Structural Software*)* [22]

4.1.1 Fluid

To model the liquid element FLUID80 is used; this element type is used by other researchers as Mehdi Moslemiet et al[23],Hadj Djelloul N.D.et al[24]. This elementis particularly well suited to the calculations of hydrostatic pressures and fluid-structure interactions, acceleration effects, such as sloshing problems. The element is defined by eight nodes having three degrees of freedom at each node: translation in the nodal directions x, y and z.

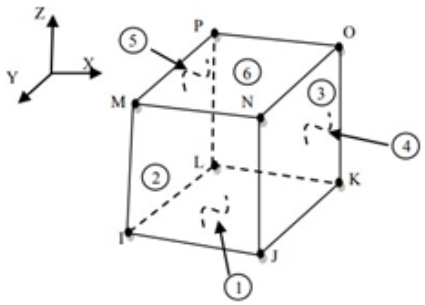

Figure 5: Fluid 80 element and the nodes degree of freedom (The ANSYS Structural Software [22]).

4.1.2 Fluid structure interaction

The effect of the fluid-structure interaction is considered by coupling the nodes located in the common faces of these two fields. For that, the mesh of each field must ensure that the external nodes of the fluid elements will be located at the same geometrical points as the nodes of the shell elements. This implies that the fluid cannot separate from the wall surface but can apply pressure to the walls [28].

4.2 Validation of the conical tank model with the fluid structure interaction

To validate the numerical model with the fluid-structure interaction;a conical aluminium tank was studied using the finite element method. The results are compared with the experimental values obtained by El Damatty et al. (2005)[24], and the numerical values obtained by Moslemi et al.(2011)[23]; the geometric and material properties are presented in Table 2 figure 6:

Table 2:
Material properties (of the reference model used in validation (El Damatty et al. (2005).

	Young's modulus	**Mass density**	**Poisson's ratio**
Aluminum shell	69 GPa	2700 kg/m3	0.33
	Mass density	Bulkmodulus	Viscosity
Fluid	1000 kg/m^3	2.0684 ×10^4 MPa	1.123×10^{-3}N.S/M^2

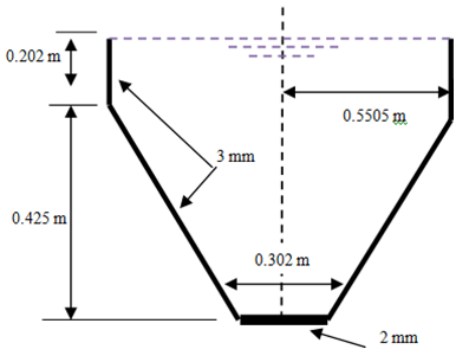

Figure 6:Geometry of a conical tank (El Damatty et al. (2005).

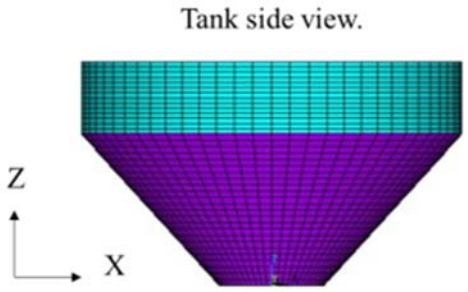

Figure 7: Finite element model used in the current study

4.3 Results and discussion

4.3.1 Modal analysis results

Table 3 presents the results obtained by the finite element analysis model with those obtained from the experimental work done by El Damatty (2005)[25] and another finite element analysis model done by Moslemi (2011)[23].

Table 3:

Free vibration analysis results for the conical tank model [Hz]

	El Damatty	Moslemi	Present work
Convective fundamental mode frequency	0.82	0.84	0.818
implusive fundamental mode frequency	43.5	42.36	41.25

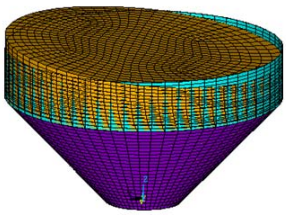

Fundamental convective mode

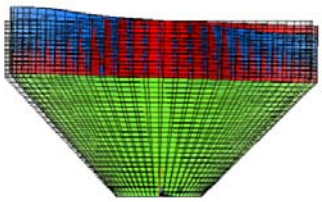

Side view

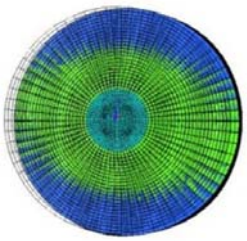

Top view

Fundamental Impulsive mode

Figure 8: Deformation of fundamental modes for the conical elevated tank

Examination of the results shows that:

• The finite element model frequencies are in very good agreement with those obtained from the experimental results of El Damatty.et.all (2005) [25] and the

numerical results of Moslemi.et.all (2011)[23].

• A significant free surface sloshing motion is observed, and no shell vibration is observed during the fundamental convective mode. For the fundamental impulsive mode, the deformation is cos (θ) mode and the section of the shell remains circular.Similar results are also reported by El Damatty et al. (2005)[25], and Moslemi et al. (2011)[23].

Hence, the numerical model can be used with good precision for this case study.

4.3.2 Elevated tank model

The models of the 1000 m3 real elevated steel conical tank considered in this study are the original model (model B-45) plus two other different models with different cone angles. Models A, C, are created by increasing and decreasing the angle (α) of inclination of the original model (Model A-angle = 30 degrees and model C-60 angle = 60 degrees). The main objective of the first part of the study is to evaluate the effect of the angle of the inclined wall tank on the nonlinear dynamic behaviour of the elevated steel conical tanks.

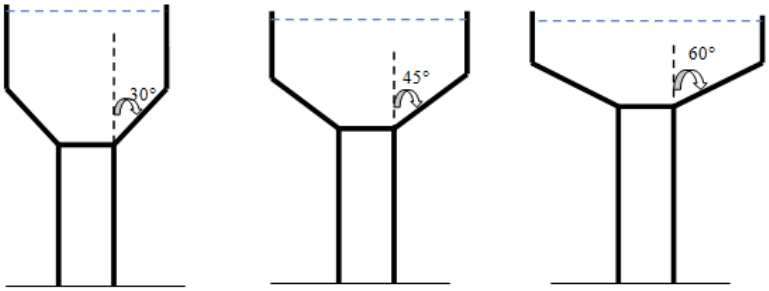

Figure 9. Elevated tank geometry

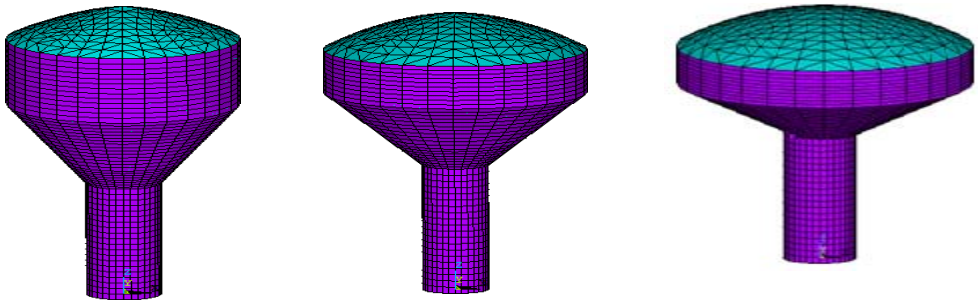

Figure 10: FE idealization for the elevated steel tanks models

4.3.2.1 Modal analysis results of the three models

The values of the fundamental frequencies of the three models numerically are grouped in Table 4. The results show that the fundamental convective modes of the

liquid for all three cases involve sloshing of the liquid without any involvement of the shell walls deformation. The fundamental impulsive mode for the three cases is the column type, (Meslmi 2011) [23] [30].

Table 4:

Free vibration analysis results for the elevated conical tank model [Hz]

	Model –A-30		Model –B-45		Model –C-60	
	Frequency	The participating mass percentage	Frequency	The participating mass percentage	Frequency	The participating mass percentage
Convective	0.258	0.375	0.204	0.572	0.163	0.709
Impulsive	1.07	0.579	1.24	0.379	1.19	0.229

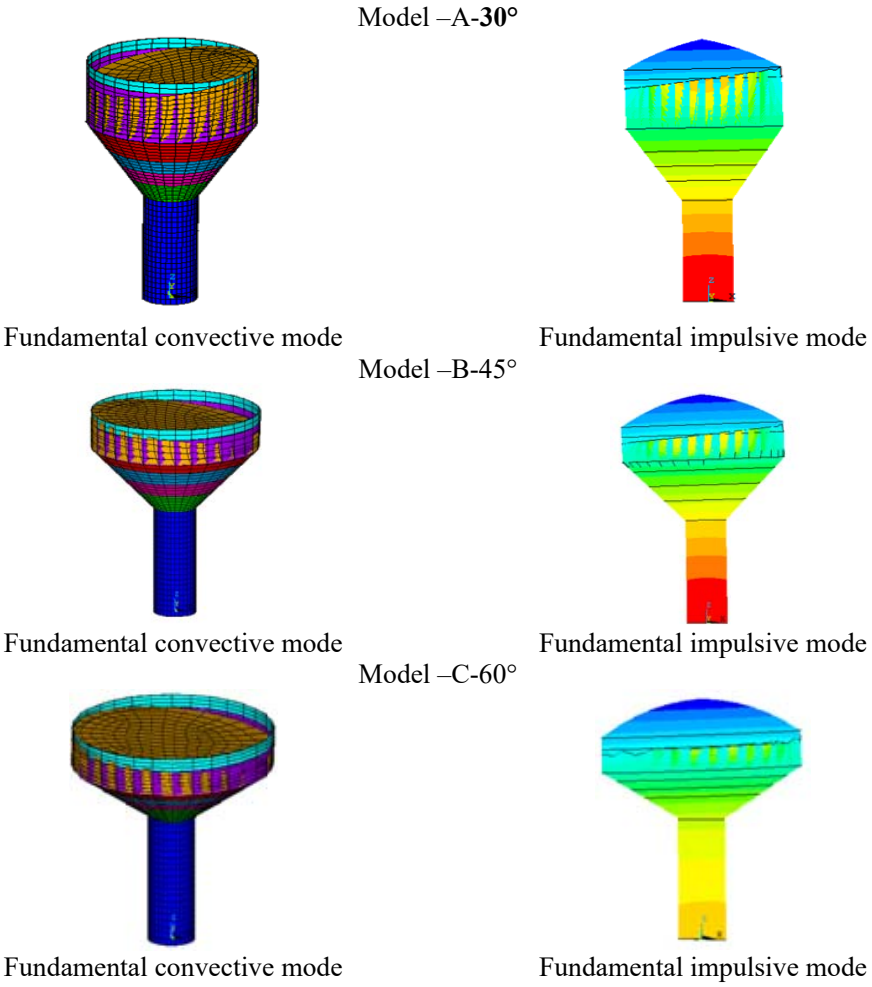

Figure 11 Modal deformation of the elevated tanks used in this study

By comparing the results of the mass ratios for the three cases, we can notice that, by increasing the angle of inclination of the wall tank relative to the vertical axis the participating mass ratio of the convective mode is increased unlike the impulsive mass ratio. We can also notice that for the cone with a large radius, the convective

component is dominant. However, this is not the case for the impulsive component that dominates by decreasing the radius of the tank. This relation is compatible with Housner's theory (1963) [4] for the cylinder case [29].

4.3.2.2 Transient analysis:

The dynamic transient analysis of the three models considering the effect of the fluid-structure interaction, the flexibility of the walls and the fluid sloshing was carried out. The applied seismic excitation of the San Fernando earthquake was used including material plasticity in order to study the stability of the three models, and to perceive the buckling zones of the elevated steel conical tank.

Figures 14 and 15 show the horizontal displacements, phase plane and the deformation corresponding to each model.

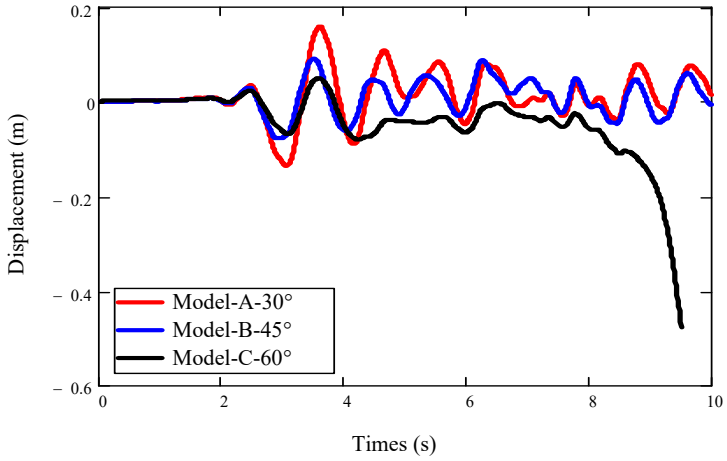

Figure 12:Time history of horizontal displacement

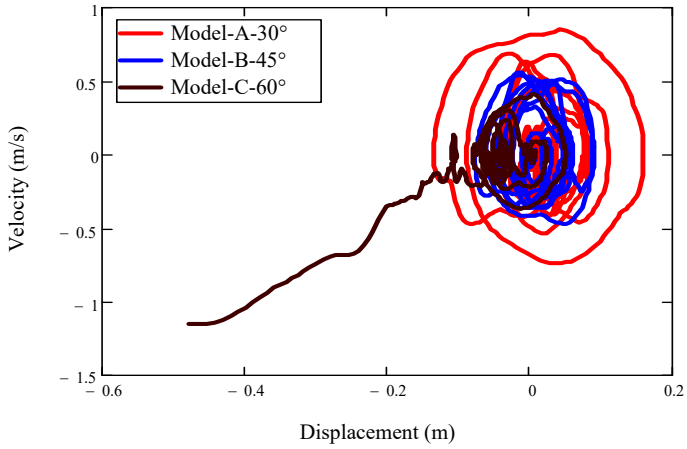

Figure 13: Phase plane

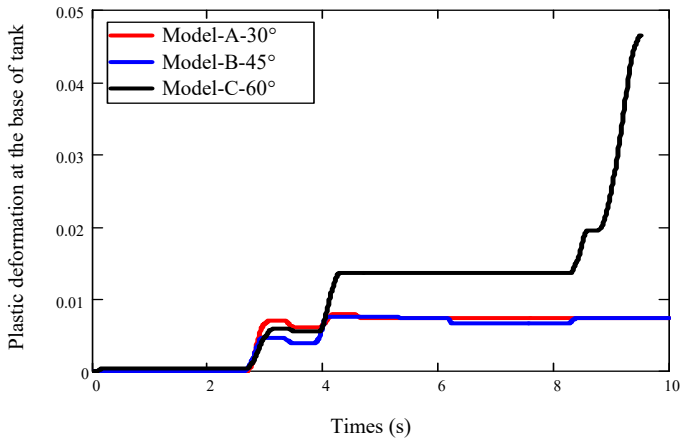

Figure 14: Plastic strain at the base of tank

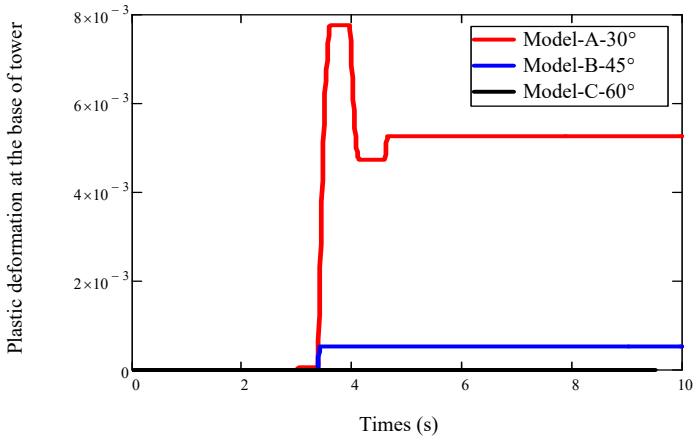

Figure 15: Plastic strain at the base of the tower

Figure 12 clearly shows the influence of the inclination of the wall tank angle on the stability of the structure. Note that the displacement values of Model A with an inclination angle of 30 degrees are greater than the values obtained by Model B with an inclination angle of 45 degrees (44.9% difference). A clear jump in displacement is observed in the chronological curves of Model C (inclination angle of the tank 60 degrees), which corresponds to the total instability of this Model under horizontal seismic excitation.

Figures 13 show the phase plane of each model. Comparing model, A and B, the curve (u, v) relating to the model C presents a significantly different curve (outside the initial oscillations pole); this confirms that the structure with an inclination angle of 60 degrees is unstable.

Figure 14 illustrates the deformation for the three cases. The three tanks deform and keep their deformation even after the end of the seismic excitation. The lower part of the tank shell is subjected to a biaxial stress state combining two vertical and

horizontal forces tending to generate the buckling failure (elastoplastic deformation). Regarding the comparison between deformations at the base of the tower of the three models, Figure 15 shows a remarkable difference. It is noticed that Model A – 30° undergoes large deformations compared to the other models.

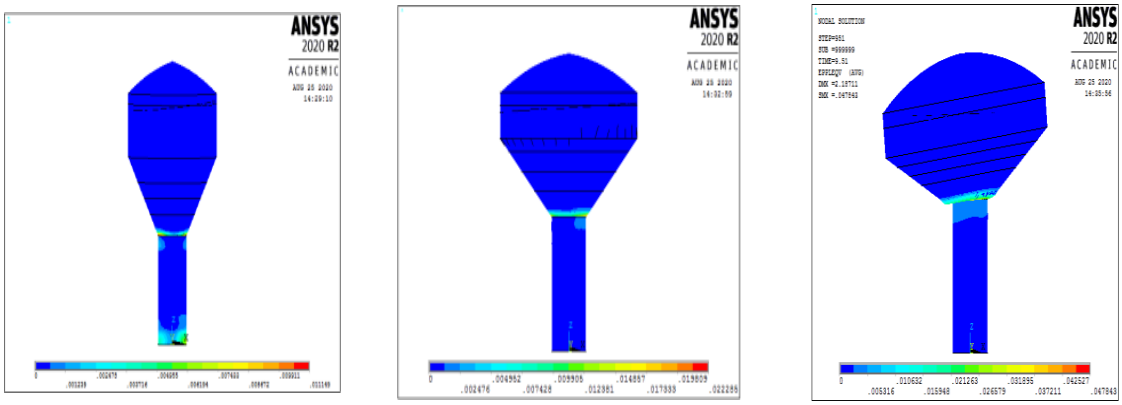

Model –A- 30 ° Model –B- 45 ° Model –C- 60 °

Figure 16: Plastic strain of shell wall of elevated model tanks

Figure 15 shows that the maximum deformations are located along the support-tank interface, and this is due to the sudden change in the geometry at this interface for the three case studies. In addition, it is observed that the total destruction happened in the support-tank interface for the Model C - 60°, which is due to the large rotation of the tank. In addition, it is shown that a maximum deformation in Model A-30° is observed in two different points the support-tank interface and at the foot of the tower; on the other hand, in the other cases, the maximum strain is observed at the upper part.

4.3.3 The effect of vertical earthquake excitation

One of the important factors influencing the dynamic behaviour of elevated steel conical tanks, and which has not been considered in previous analyses, is the effect of the vertical excitation of the earthquake. In most codes, the effect of the vertical excitation is considered. In this part, the accelerations are combined using the 30% rules. (Eurocode 8 Part 1 2004) to evaluate the effect of vertical ground acceleration on the dynamic behaviour of model A.

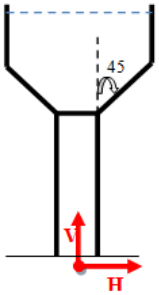

Figure 17: Two seismic component

The results obtained clearly show the values of the horizontal displacements, of the combinations H and H +0.3 V are significantly higher than the values obtained by the cases 0.3 H + V. It is also noted that the effect of the vertical component of the earthquake on the horizontal displacement of the Model-A is insignificant. Indeed, the sloshing results have a slight difference between the sloshing values for the two combinations of H+V and H +0.3 V (an increase of 2.83%), unlike the third case 0.3 H+ 1.0 V under which the values are reduced by 46%. Considering the 30%, vertical excitation does not have too much influence on the shear force at the base. The 0.3H + V combination produced an underestimation of the shear force.

The 0.3 H + V combination has a great influence on the vertical reaction of the Model-A. The vertical reaction values increase by 18.93% compared to the H combination. However, the vertical reaction values remain almost the same for the H + 0.3V combination compared to the H combination.

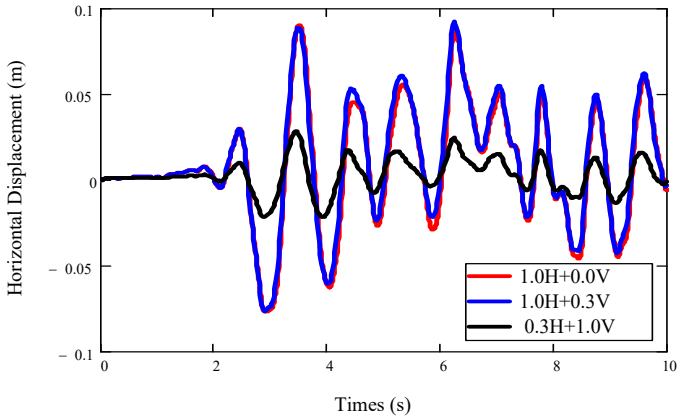

Figure 18: Time history of horizontal displacement

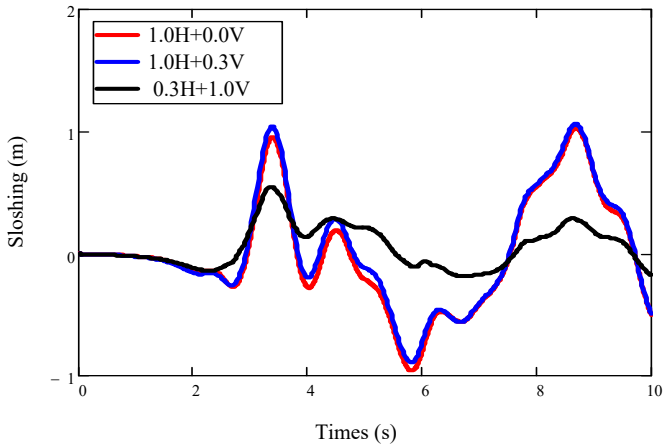

Figure 19: Time history of Sloshing displacement

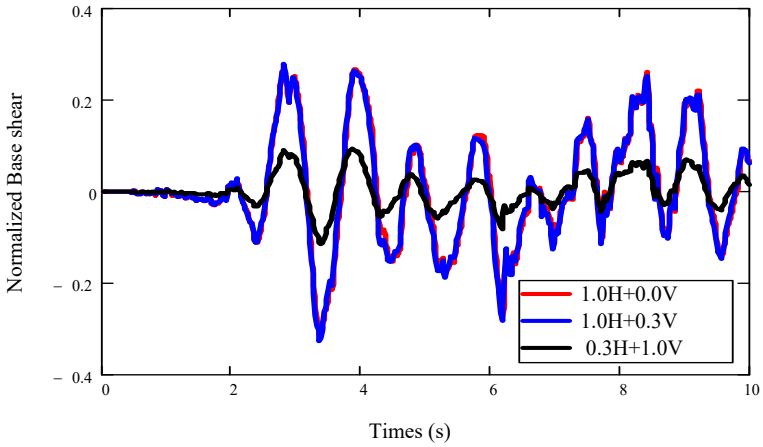

Figure 20: Time history of base shear

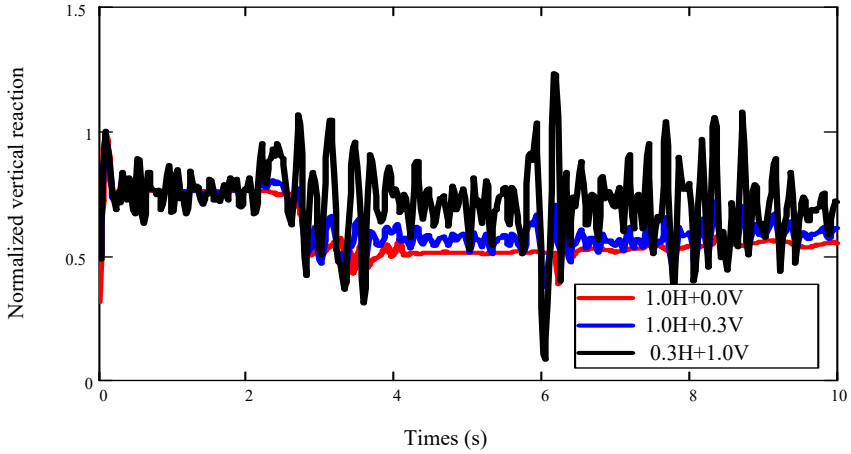

Figure 21: Time history of normalized vertical reaction

5. Conclusions

This study investigated the dynamic behaviour of elevated steel conical tanks under the seismic effect using the finite element analysis technique. Considering several factors as fluid-structure interaction, the large amplitude sloshing, the non-linearities of material and geometry, three models having a tilt angle of 30°, 45° and 60° of inclination of the tank wall have been studied. Firstly, the numerical models proposed were validated by comparing the results of the modal analysis obtained with the results obtained by other researchers. In the second part, the effect of the inclination of the tank on the seismic behaviour of elevated conical steel tanks was studied. The following conclusions are found:

1. The percentage of the mass participation of the convective part increases with the increase in the angle of inclination of the tank relative to the vertical axis, in contrast to the percentage of the mass participation for the impulsive part.
2. The reinforcement of the support-tank part has great importance on the buckling resistance of the wall, which can increase the tank stiffness.

3. The angle of inclination of the tank is a key parameter for the seismic design of elevated conical tanks. It was concluded that the design of the tank with an angle of inclination of 45° had better seismic performance under the horizontal seismic component compared to 30- and 60-degrees.

A study of the seismic behaviour of elevated steel conical tanks was then carried out to investigate the effect of the vertical component of the earthquake on their dynamic behaviour. As the elevated conical steel tank with an angle of inclination of 45 degrees is used,it has been found that the vertical component of the earthquake had no effect on the horizontal displacement and shear force at the base. However, vertical fluid displacement increased by 2.83%. It was also observed that the vertical excitation of earthquakes had a greater effect on the vertical reaction of the elevated tank (an increase of 18.93%). The results obtained also show that the combination of 0.3H + V gives an underestimation of stresses. Therefore, the long-ignored effect of the vertical excitation of the earthquake should be considered appropriately in the seismic analysis of elevated conical steel tanks.

Acknowledgements:

This work was supported by FIMAS Laboratory, University of Tahri Mohammed Bechar, Algeria.

The authors would like to thank Dr Ghomri Tedj for the invaluable help he provided in writing this paper

1. Joshi SP. Equivalent mechanical model for horizontal vibration of rigid Intze tanks. ISET J Earthq Technol 2000;37:39–47.
2. Chandrasekaran, A.R., and Krishna J. (1965), “Water Towers in Seismic Zones”, Proc. of 3rd World Conference on Earthquake Engineering, New Zealand, 3(4), pp.161-171.
3. Ramiah, B.K., and Rajata Mohana Gupta, D.S. (1966), “Factors Effecting Seismic Design of Water Towers”, Proc. of the American Society of Civil Engineers, ST4, pp.13-30.
4. Housner GW. The dynamic behavior of water tanks. Bull Seismol Soc Amer 1963: 53(2):381–9.
5. Sonobe, Y., and Nishikawa, T., (1969), “Study on the Earthquake Proof Design of Elevated Water Tanks”, Proc. of the 4th World Conference on Earthquake Engineering, 3 (B-4), Santiago, pp. 11- 24
6. Veletsos.A.S : Seismic Response and Design of Liquid Storage Tanks, Guidelines for seismic Design of Oil and Gas Pipelines System ZSCE, New York, 1984, 255-370.
7. Chopra, A.K., 1970 : Earthquake Response of Concrete Gravity Dams. Journal of the Eng. Mech. Div., ASCE 96, 443–454.
8. Vandepitte, D., Rathe, J., Verhegghe, B., Paridaens, R., and Verschaeve, C. 1982. Experimental investigation of hydrostatically loaded conical shells and practical evaluation of the buckling load. Proceedings of State of the Art Colloquium. Universitat Stuttgart, Germany. pp. 375–399.
9. El Damatty A.A, Korol R.M, and Mirza F.A, “Stability of Imperfect Steel Conical Tanks under Hydrostatic Loading”, Journal of Structural Engineering, ASCE, and Volume: 123, Issue: 06, pp. 703-712, 1997.
10. Allen, L.R., Hutchinson, G.L., Stevens, L.K. (1990). Buckling considerations in the design of elevated steel water tanks. Thin-Walled Structures, 9(1-4): 389-406.
11. Shenton III, H.W., and Hampton, F.P. (1999), “Seismic Response of Isolated Elevated Water Tanks”, Journal of Structural Engineering, 125(9), pp. 965-976.

12. Shrimali, M.K., Jangid, R.S. (2003). Earthquake response of isolated elevated liquid storage steel tanks. Journal of Constructional Steel Research, 59(10): 1267- 1288.

13. Sweedan A.M.I and El Damatty A.A, "Equivalent Models of Pure Conical Tanks under Vertical Ground Excitation", Journal of Structure Engineering. ASCE, Volume: 131, Issue: 05, pp. 725-733, 2005.

14. Sekhar Chandra Dutta, Somnath Dutta and Rana Roy,"Dynamic behavior of R/C elevated tanks with soil-structure interaction", Engineering Structures, Volume: 31, pp. 2617-2629, 2009

15. Pallavi S.Dhamak, Prof. V. R. Rathi and Prof. Dr. K. B. Ladhane, "Dynamic Response of an Elevated Water Tank," International Journal of Engineering Research & Technology, (IJERT) Vol. 3 Issue 8, pp. 1198-1204, 2014.

16. American Lifelines Alliance. Seismic fragility formulations for water systems. ASCE; 2001. [Mal 06] Malhotra, P. K : Seismic Design Of Liquid Storage Tanks, Rapport Technique, American Society Of Civil Engineers (Asce), 2006

17. Soheil Soroushnia, Sh. Tavousi Tafreshi, F. Omidinasab, N. Beheshtian, Sajad Soroushnia : Seismic Performance of RC Elevated Water Tanks with Frame Staging and Exhibition Damage Pattern, Procedia Engineering, Volume 14, 2011, Pages 3076-3087, ISSN 1877-7058,

18. Standard 650 : Welded Tanks for Oil Storage, ELEVENTH EDITION, 2008.

19. American Water Works Association (AWWA), 1984 and 2005, Welded steel tanks for water storage. AWWA D100, CO.

20. European Committee for Standardization (CEN). (2006). Eurocode 8: Design of structures for earthquake resistance—Part 4: Silos, tanks and pipelines.

21. The ANSYS Structural Software System

22. Moslemi, M., Ghaemmaghami, A.R., Kianoush, M.R. (2016). Parametric based study for design of liquid-filled elevated tanks. Canadian Journal of Civil Engineering, 43(7): 619-630.

23. Hadj Djelloul, N.D., Djermane, M., Sharari, N. (2020). Effect of supporting system on dynamic buckling of elevated water tanks: A case study. International Journal of Safety and Security Engineering, Vol. 10, No. 3, pp. 333-342.

24. A.A. El Damatty, M.S. Saafan, A.M.I. Sweedan, Experimental study conducted on a liquid-filled combined conical tank model, Thin-Walled Structures, Volume 43, Issue 9, 2005, Pages 1398-1417, ISSN 0263-8231,

25. Djermane, M., Zaoui, D., Labbaci, B., Hammadi, F. (2014). Dynamic buckling of steel tanks under seismic excitation: Numerical evaluation of code provisions. Engineering Structures, 70: 181-196.

26. Ahmed Musa, Ashraf El Damatty, Effect of vessel base rotation on the seismic behaviour of conical shaped steel liquid storage tanks, Engineering Structures,Volume 166, 2018, Pages 454-471, ISSN 0141-0296,

27. Zhang R, Chu S, Sun K, Zhang Z, Wang H. Effect of the Directional Components of Earthquakes on the Seismic Behavior of an Unanchored Steel Tank. *Applied Sciences*. 2020

28. Hadj-Djelloul, N.D., Djermane, M. (2020). Effect of geometric imperfection on the dynamic of elevated water tanks. Civil Engineering Journal, 6(1): 85-97.

29. Stefano Caprinozzi, Matjaž Dolšek, Seismic performance assessment of non-code-conforming and code-conforming supporting structures of elevated tanks using conventional and risk based decision models, Engineering Structures, Volume 227, 2021, 111469, ISSN 0141-0296,

30. J.C. Drosos, S.V. Tsinopoulos, D.L. Karabalis, Seismic retrofit of spherical liquid storage tanks with energy dissipative devices, Soil Dynamics and Earthquake Engineering, Volume 119, 2019, Pages 158-169, ISSN 0267-7261.

Considerarea riglele de cuplare la pereții din zidărie

Regarding the coupling beams in the calculation of the masonry walls

Robert Draghici[1], Ana Maria Pârvănuș[1], Daniel Stoica[1]

[1]Universitatea Tehnica de Constructii Bucuresti
B-dul Lacul Tei 122-124, Sector 2, Bucuresti
E-mail: daniel.stoica@utcb.ro

DOI: 10.37789/rjce.2022.13.3.6

Rezumat.
Pereții de zidărie funcționează în mod normal legați fie prin plăci, prin grinzi de cuplare din zidărie, beton armat sau prin secțiuni compozite (zidărie și beton armat etc.). Comportamentul grinzilor de cuplare, inclusiv în codurile de proiectare actuale, este insuficient abordat, cunoscut și tratat. Din acest motiv, efectul indirect al pereților adus de grinzile de cuplare este insuficient cunoscut - majoritatea proiectanților (din lipsă de informații) preferă să nu-i ia în considerare în calculul general. După testele efectuate pe mese seismice pe modele 3D, dar și după cutremurele majore, reale, se poate observa cu ușurință influența deosebită a grinzilor de cuplare asupra comportării de ansamblu a pereților structurali de zidărie (de tip montanți sau spalete). Toate acestea atât pentru pereți structurali sau despărțitori, cât și pentru pereți normali sau de calcan. Deoarece aceste date nu sunt suficient de bine cunoscute în practica de proiectare, acest studiu încearcă să arate cum prin utilizarea programului ETABS, fie pentru energia disipată, fie pentru energia de distorsiune, putem obține indicații suficient de sugestive despre comportarea riglelor de cuplare, precum și a pereților de zidărie.

Cuvinte cheie: structuri, zidărie, rigla de cuplare, energie disipata

Abstract.
Masonry walls normally work connected either by floor slabs, by coupling beams made from masonry, reinforced concrete or by composite sections (masonry and reinforced concrete, etc.). The behavior of the coupling beams, including in the current design codes, is insufficiently approached, known and treated. For this reason, the indirect effect of the walls from the coupling beams is insufficiently known - most designers (due to lack of information) prefer not to consider them in the overall calculation. After the tests performed on seismic masses on 3D models, but also after the major, real earthquakes, one can easily see the special influence of the coupling beams on the overall behavior of the structural masonry walls (cantilevers or piers type). All bout these both for structural or partition or for normal and blind walls. Because these data are insufficiently well known in design practice, this study attempts to show how by using the ETABS program, for either dissipated energy or distortion energy, we can get sufficiently suggestive indications about the behavior of coupling beams as well as masonry walls.

Key words: structures, masonry, coupling beam, dissipated energy

1. Introduction

Considering the current state on a national and international level, regarding the behavior of the masonry coupled walls (and for masonry there is the behavior of the pier type and cantilever type, different from the similar elements of reinforced concrete) was considered as it is necessary to carry out a complex study, for a similar number of cases, so that the conclusions we will obtain can become general and thus help the designers.

2. Study on the identification of the behavior of hollow masonry walls

In this large study two types of walls (solid walls and hollow walls) and also two heights rise where considered (2 and 4 levels).
For all cases it is considered a 2.80m level height (h_l) in correlation with the seismic zone with ag = 0.30g (table 1 and figure 1).
For hollow walls we keep the level and vary:

- h_p (parapet height) 0-150cm (every 30 cm);
- h_h (hollow height) 60-210 cm (every 30 cm);
- h_{cb} (coupling beam height) from 70 cm to which 220 cm (made from masonry and 25 cm reinforced concrete belt);

We keep the total length l_w and vary:

- l_{w1} and l_{w2} (from 80 cm to 200 cm);
- h_p (parapet height) 0-150cm (every 30 cm);
- h_{cb} (coupling beam height) from 70 cm to which 220 cm (made from masonry and 25 cm reinforced concrete belt);
- We want to identify several aspects: the correlated dimensions h_{cb}, h_l, respectively l_{w1}, l_{cb} and l_{w2} for which we have cantilever behavior and pier behavior.
- Initially we try to have left / right walls with equal lengths ($l_{w1}=l_{w2}$). Later we try to have $l_{w1}\neq l_{w2}$, so that we obtain different types of walls behavior.

Table 1 – Study cases

Masonry walls with equal spans								
l_w	**l_{w1}**	**l_{w2}**	**l_{cb}**	**h_{cb}**	**h_{cb}/l_{cb}**	**$\rho=h_l*h_{cb}/l_{cb}$**	**$1/\rho$**	**Wall type**
2	0.80	0.80	0.60	0.70	1.17	3.27	0.31	**Pier**
	0.80	0.80	0.60	1.00	1.67	4.67	0.21	**Pier**
	0.80	0.80	0.60	1.30	2.17	6.07	0.16	**Pier**
	0.80	0.80	0.60	1.60	2.67	7.47	0.13	**Pier**
	0.80	0.80	0.60	1.90	3.17	8.87	0.11	**Pier**
	0.80	0.80	0.60	2.20	3.67	10.27	0.10	**Pier**
3	1.20	1.20	1.00	0.70	0.70	1.96	0.51	**Cantilever**
	1.20	1.20	1.00	1.00	1.00	2.80	0.36	**Pier**
	1.20	1.20	1.00	1.30	1.30	3.64	0.27	**Pier**

	1.20	1.20	1.00	1.60	1.60	4.48	0.22	**Pier**
	1.20	1.20	1.00	1.90	1.90	5.32	0.19	**Pier**
	1.20	1.20	1.00	2.20	2.20	6.16	0.16	**Pier**
5	1.60	1.60	1.40	0.70	0.50	1.40	0.71	**Cantilever**
	1.60	1.60	1.40	1.00	0.71	2.00	0.50	**Cantilever**
	1.60	1.60	1.40	1.30	0.93	2.60	0.38	**Pier**
	1.60	1.60	1.40	1.60	1.14	3.20	0.31	**Pier**
	1.60	1.60	1.40	1.90	1.36	3.80	0.26	**Pier**
	1.60	1.60	1.40	2.20	1.57	4.40	0.23	**Pier**
6	2.00	2.00	2.00	0.70	0.35	0.98	1.02	**Cantilever**
	2.00	2.00	2.00	1.00	0.50	1.40	0.71	**Cantilever**
	2.00	2.00	2.00	1.30	0.65	1.82	0.55	**Cantilever**
	2.00	2.00	2.00	1.60	0.80	2.24	0.45	**Pier**
	2.00	2.00	2.00	1.90	0.95	2.66	0.38	**Pier**
	2.00	2.00	2.00	2.20	1.10	3.08	0.32	**Pier**
Masonry walls with different spans								
l_w	**l_{w1}**	**l_{w2}**	**l_{cb}**	**h_{cb}**	**h_{cb}/l_{cb}**	**$\rho=h_l*h_{cb}/l_{cb}$**	**$1/\rho$**	**Wall type**
5	1.50	1.20	1.80	0.70	0.39	1.09	0.92	**Cantilever**
	1.70	2.00	0.80	1.60	2.00	5.60	0.18	**Pier**
	2.00	1.00	1.50	0.70	0.47	1.31	0.77	**Cantilever+Pier**
5	1.60	2.00	1.40	0.70	0.50	1.40	0.71	**Cantilever**
	1.60	2.00	1.40	1.60	1.14	3.20	0.31	**Pier**
	2.00	1.00	2.00	1.00	0.50	1.40	0.71	**Cantilever+Pier**

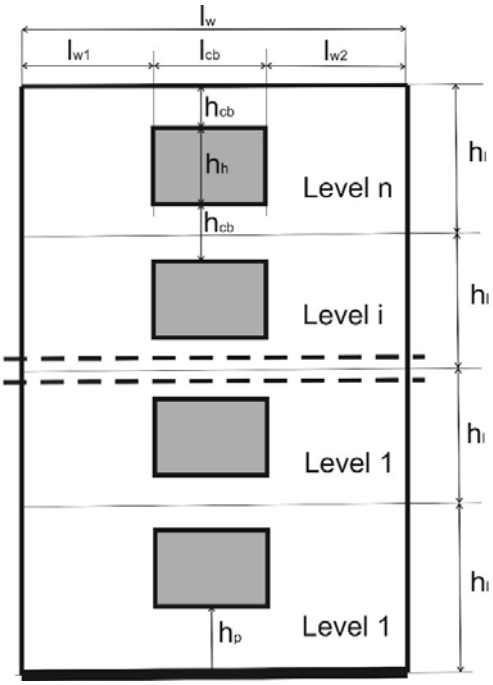

Figure 1 Coupling masonry walls models and notations

3. Dissipated and distortion energies

In the following figures, for each study case (72 in total) the dissipated and distortion energy are presented:

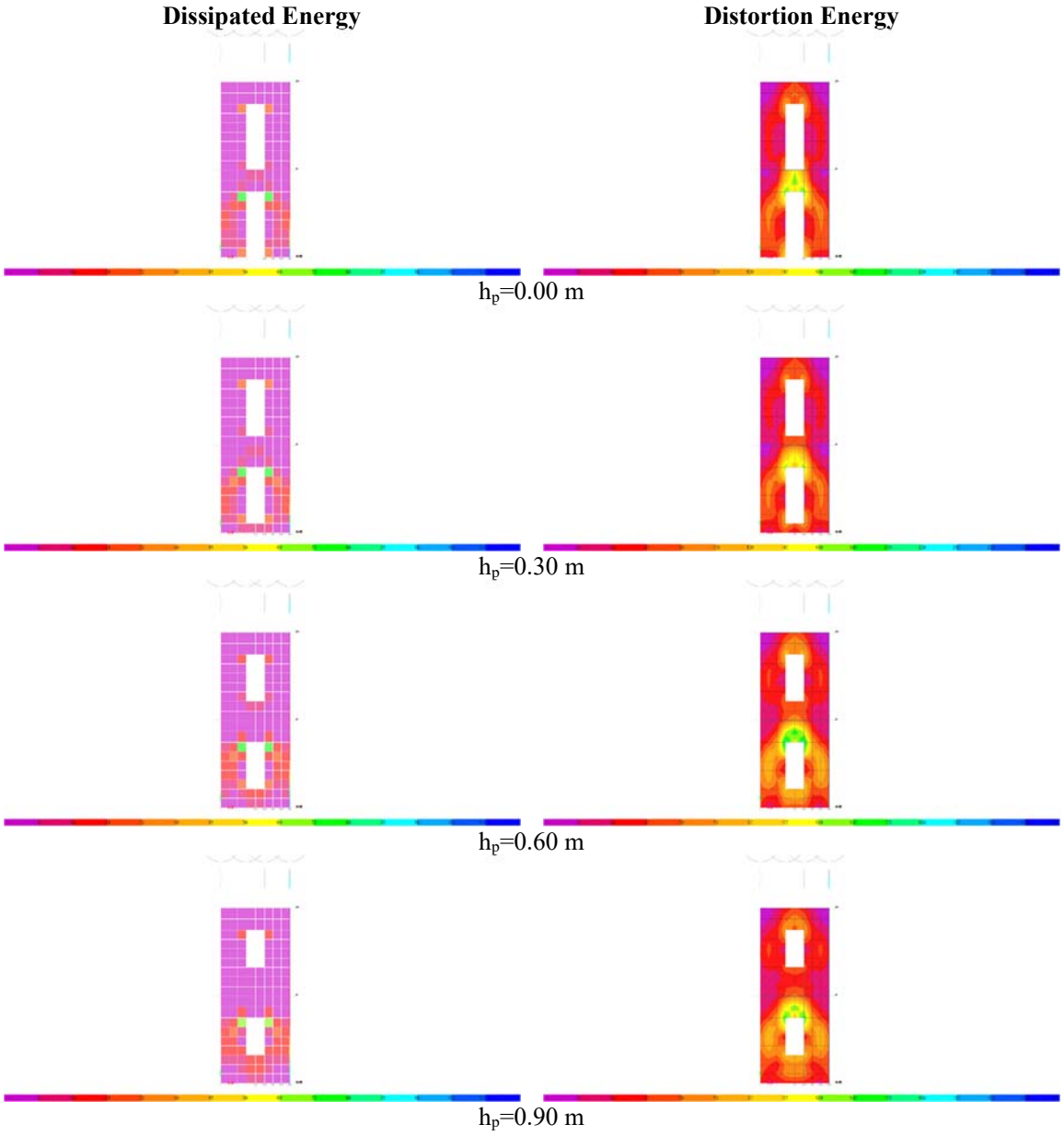

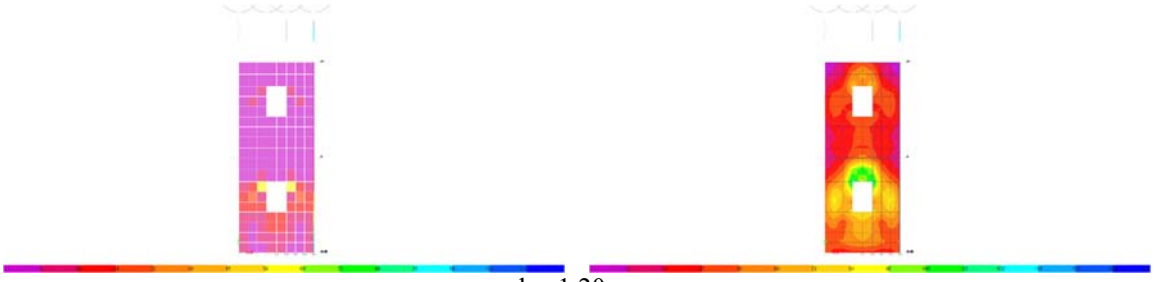

h_p=1.20 m

h_p=1.50 m

h_p=without hollows

Figures 2-15 l_w=0.80 m; l_{cb}=0.60 m – 2 levels building

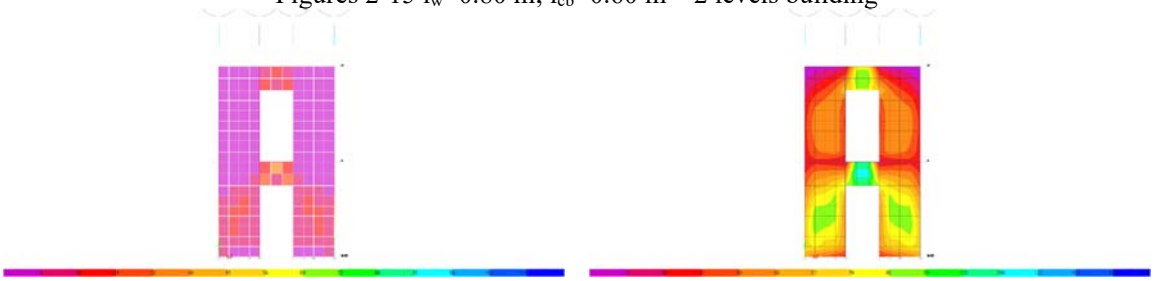

h_p=0.00 m

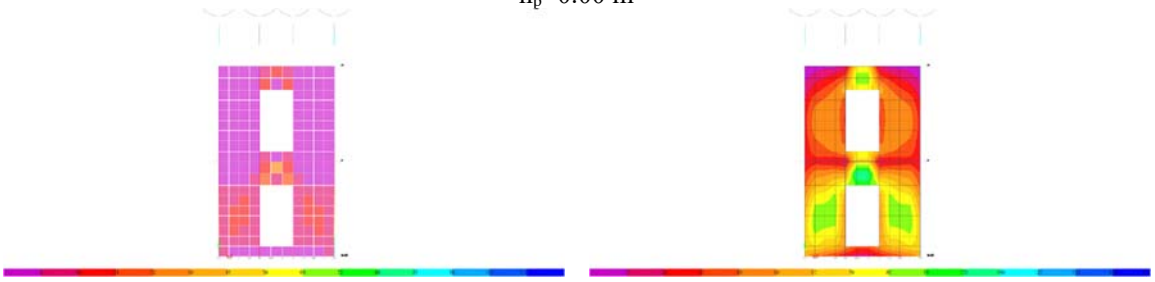

h_p=0.30 m

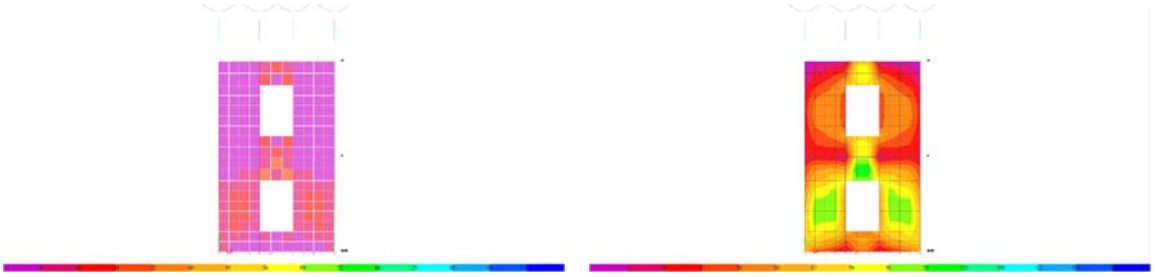

h_p=0.60 m

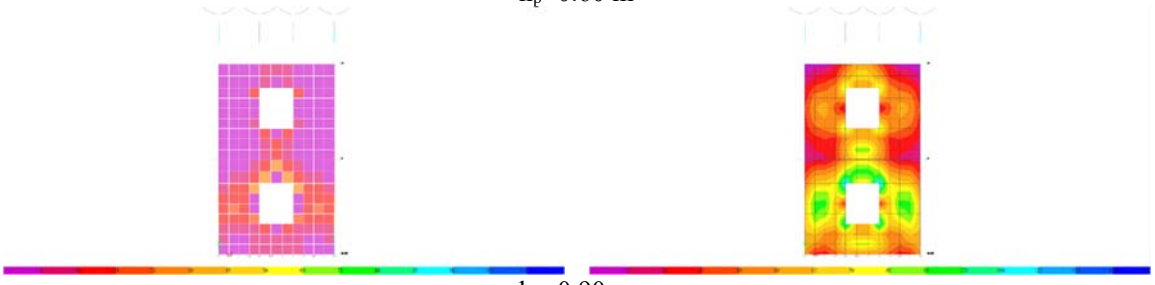

h_p=0.90 m

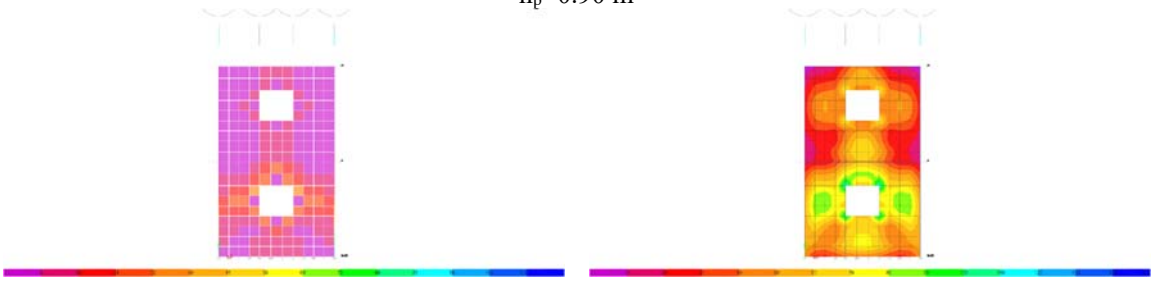

h_p=1.20 m

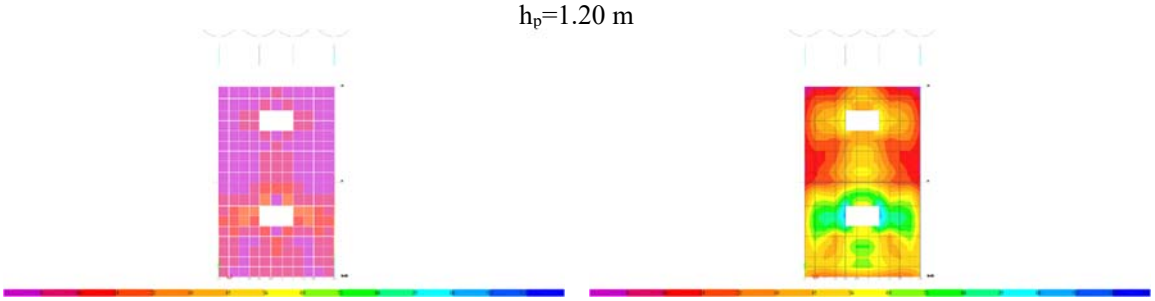

h_p=1.50 m

h_p=without hollows

Figures 16-29 l_w=1.20 m; l_{cb}=1.00 m – 2 levels building

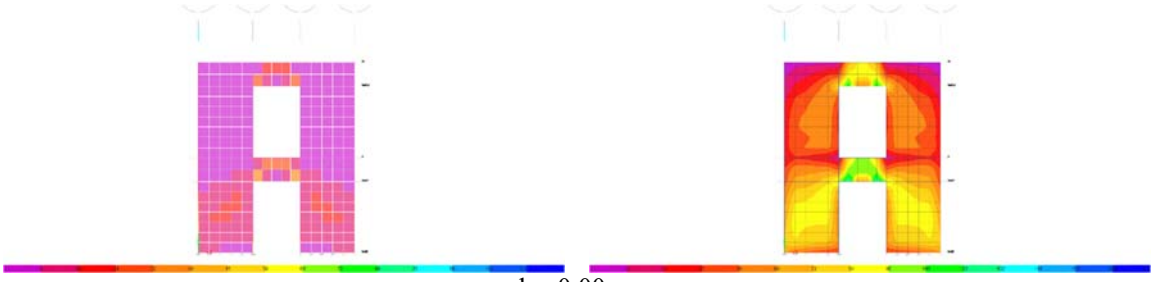

h_p=0.00 m

h_p=0.30 m

h_p=0.60 m

h_p=0.90 m

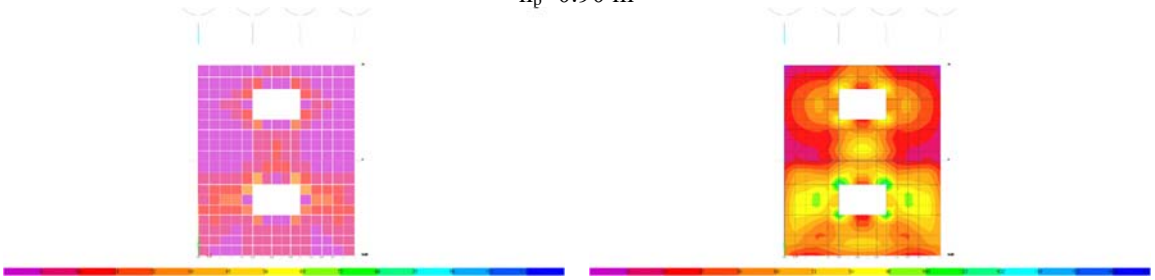

h_p=1.20 m

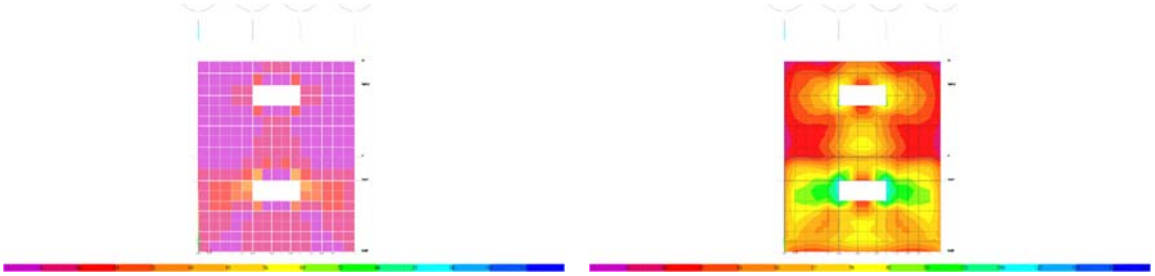

h_p=1.50 m

h_p=without hollows

Figures 30-43 l_w=1.60 m; l_{cb}=1.40 m – 2 levels building

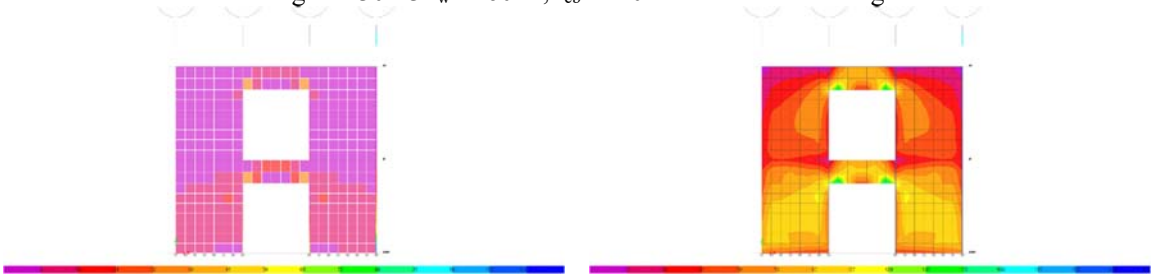

h_p=0.00 m

h_p=0.30 m

h_p=0.60 m

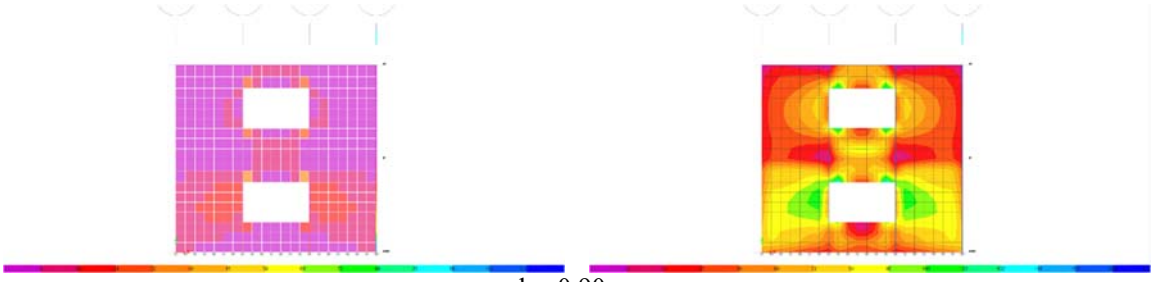

h_p=0.90 m

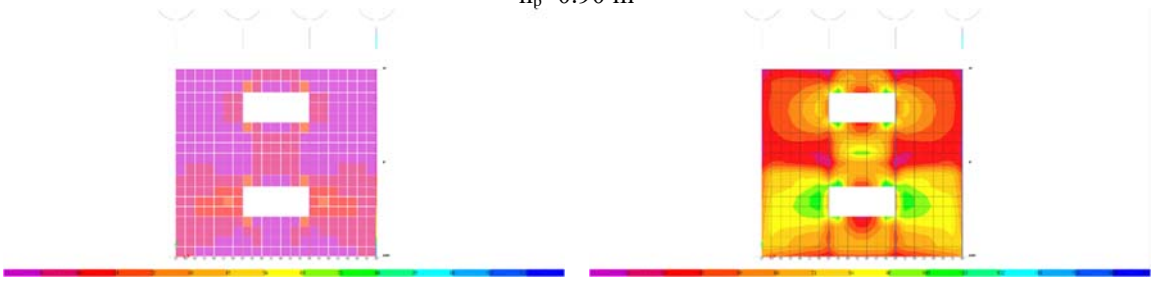

h_p=1.20 m

h_p=1.50 m

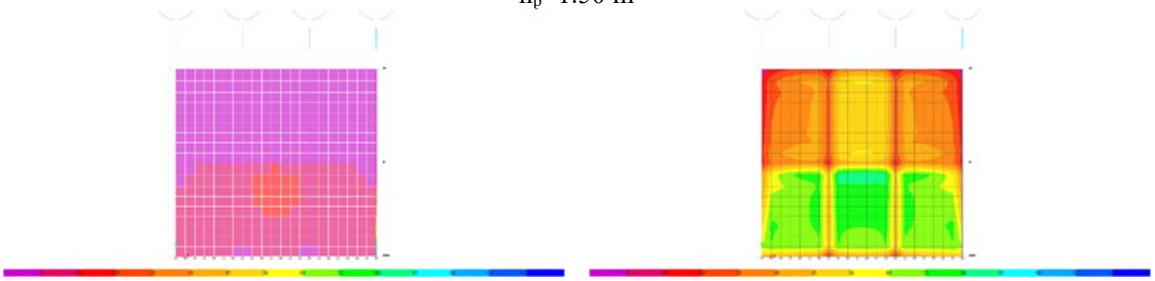

h_p=without hollows

Figures 44-57 l_w=2.00 m; l_{cb}=2.00 m – 2 levels building

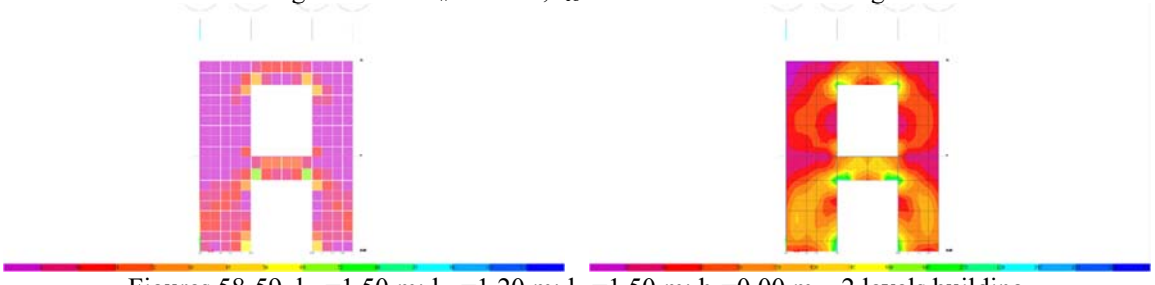

Figures 58-59 l_{w1}=1.50 m; l_{w2}=1.20 m; l_{cb}=1.50 m; h_p=0.00 m – 2 levels building

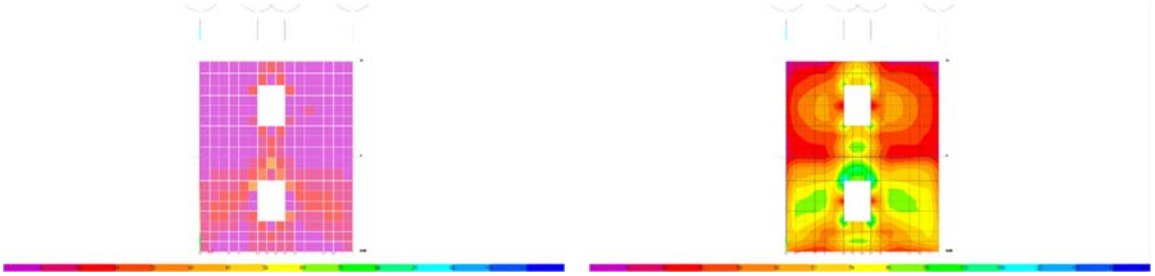

Figures 60-61 l_{w1}=1.70 m; l_{w2}=2.00 m; l_{cb}=0.80 m; h_p=0.90 m – 2 levels building

Figures 62-63 l_{w1}=2.00 m; l_{w2}=1.00 m; l_{cb}=1.50 m; h_p=0.00 m – 2 levels building

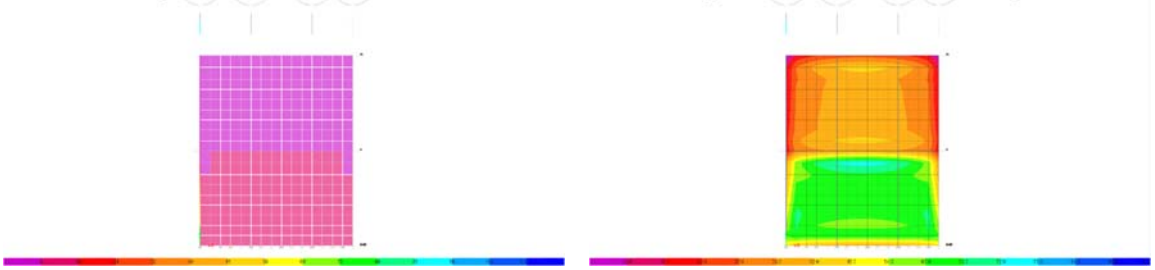

Figures 64-65 l_w=4.50 m – 2 levels building

Figures 66-67 l_{w1}=1.60 m; l_{w2}=2.00 m; l_{cb}=1.40 m; h_p=0.00 m – 2 levels building

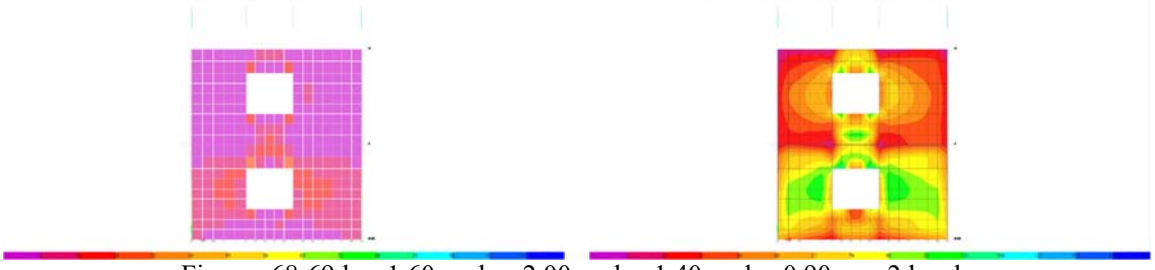

Figures 68-69 l_{w1}=1.60 m; l_{w2}=2.00 m; l_{cb}=1.40 m; h_p=0.90 m – 2 levels

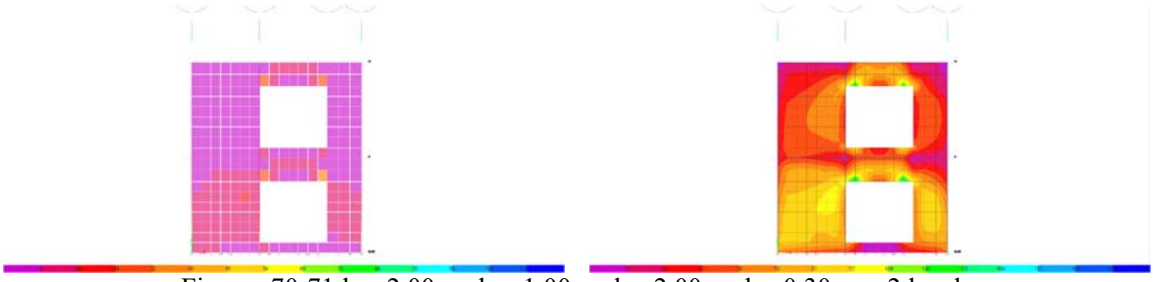

Figures 70-71 l_{w1}=2.00 m; l_{w2}=1.00 m; l_{cb}=2.00 m; h_p=0.30 m – 2 levels

Figures 72-73 l_w=5.00 m – 2 levels building

h_p=0.00 m

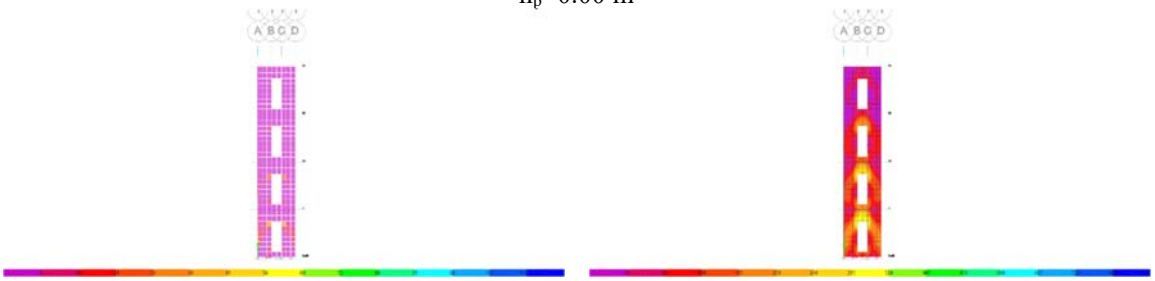

h_p=0.30 m

h_p=0.60 m

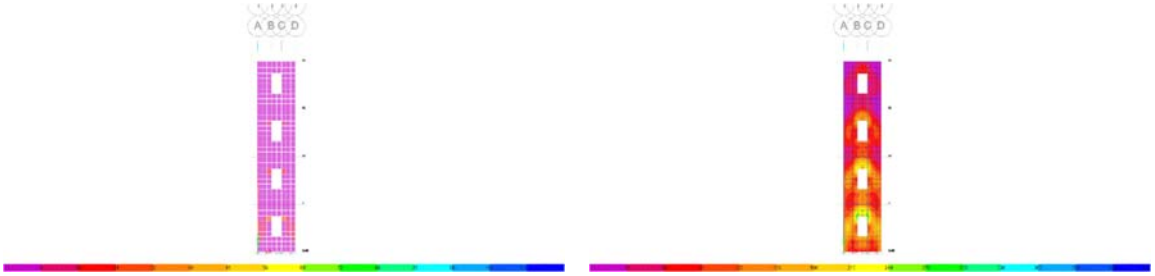

h_p=0.90 m

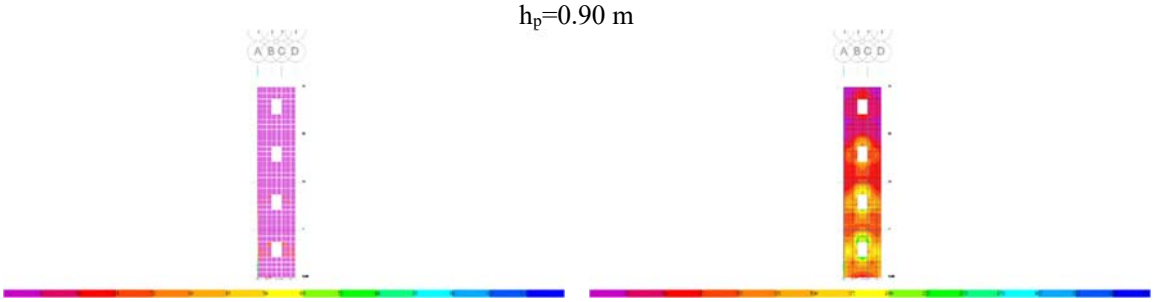

h_p=1.20 m

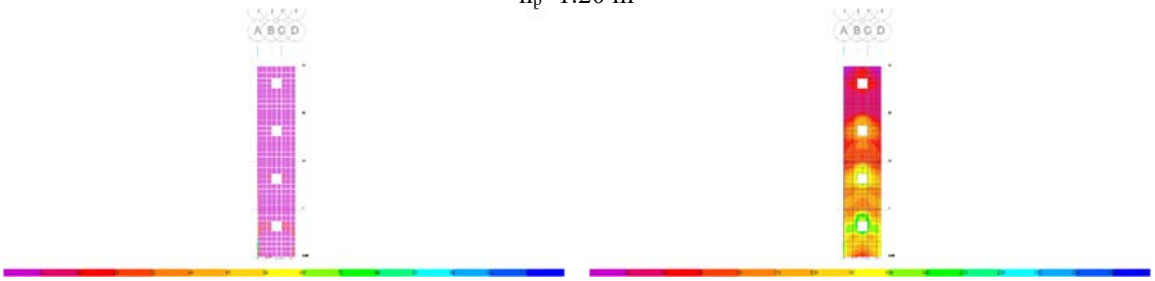

h_p=1.50 m

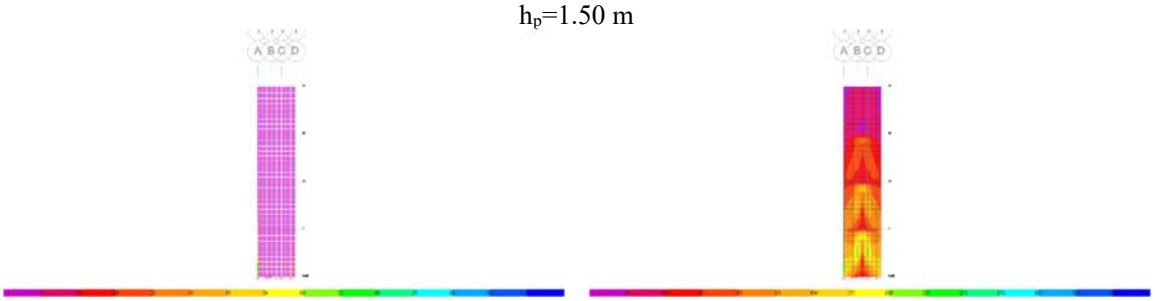

h_p=without hollows

Figures 74-87 l_w=0.80 m; l_{cb}=0.60 m – 4 levels building

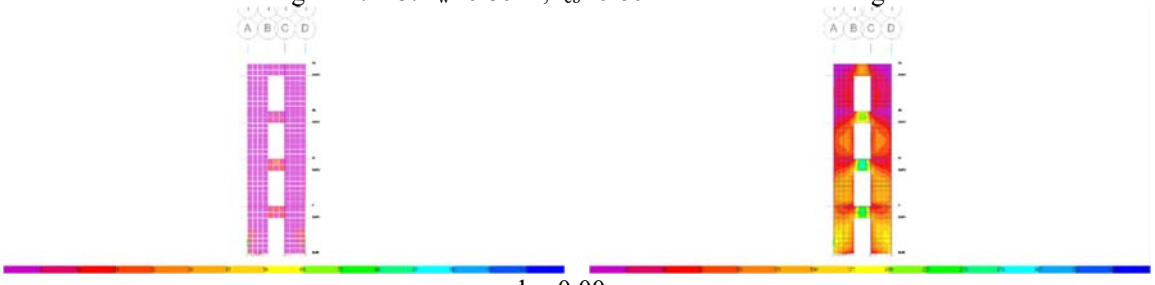

h_p=0.00 m

h_p=0.30 m

h_p=0.60 m

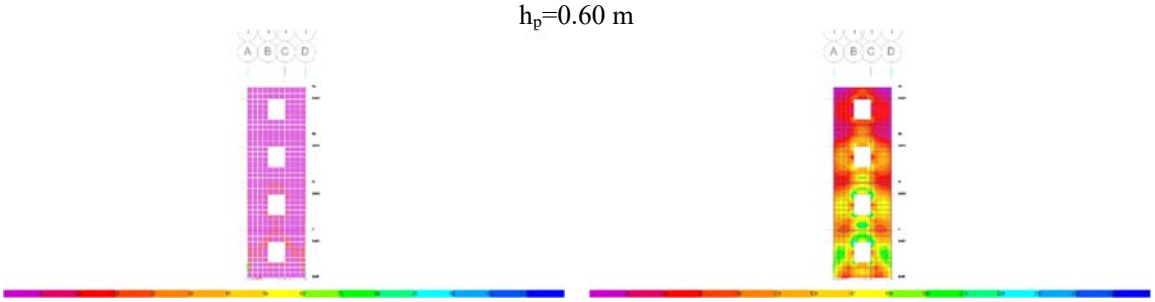

h_p=0.90 m

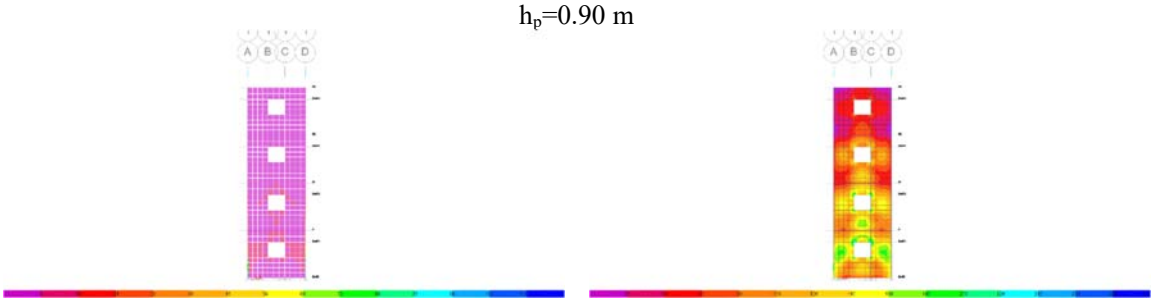

h_p=1.20 m

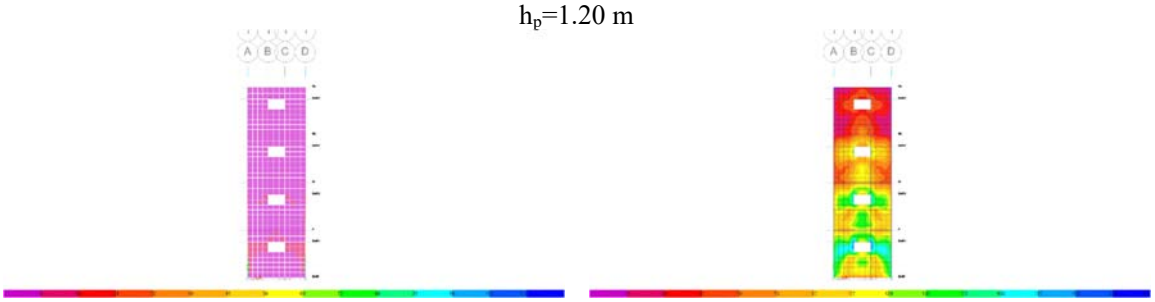

h_p=1.50 m

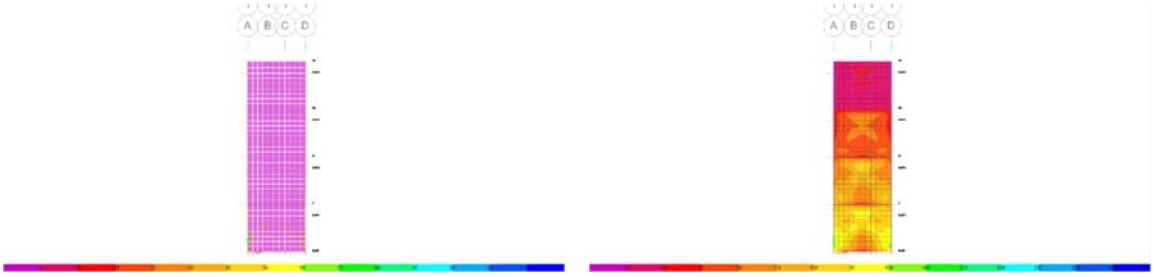

h_p=without hollows

Figures 88-101 l_w=1.20 m; l_{cb}=1.00 m – 4 levels building

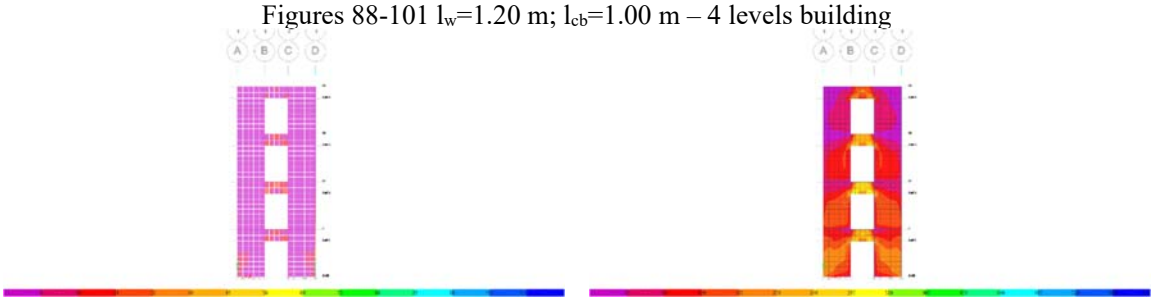

h_p=0.00 m

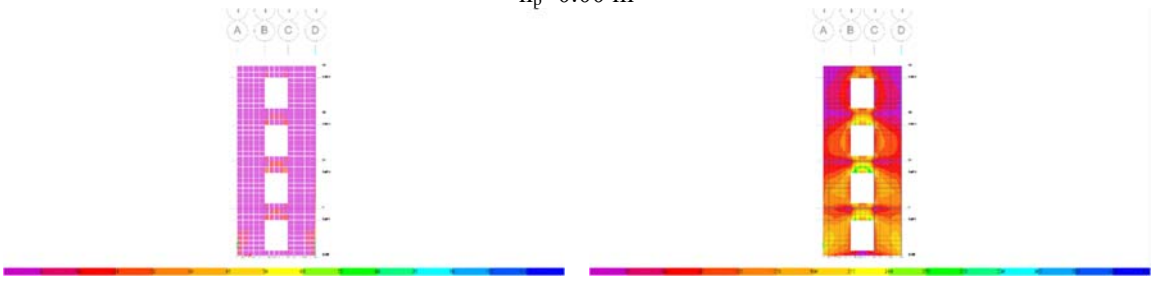

h_p=0.30 m

h_p=0.60 m

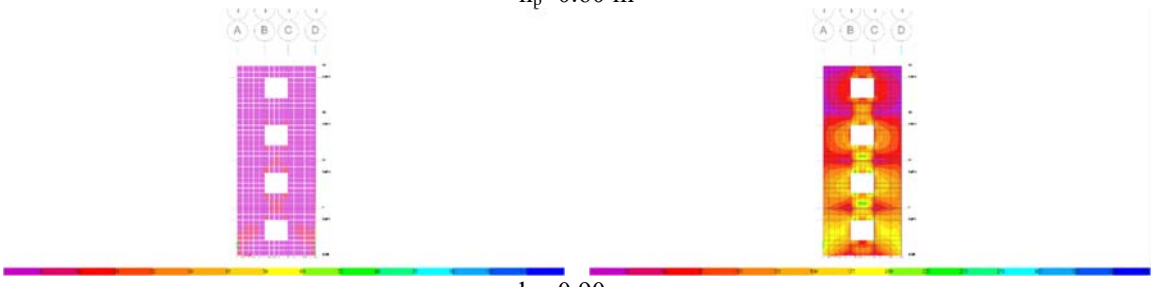

h_p=0.90 m

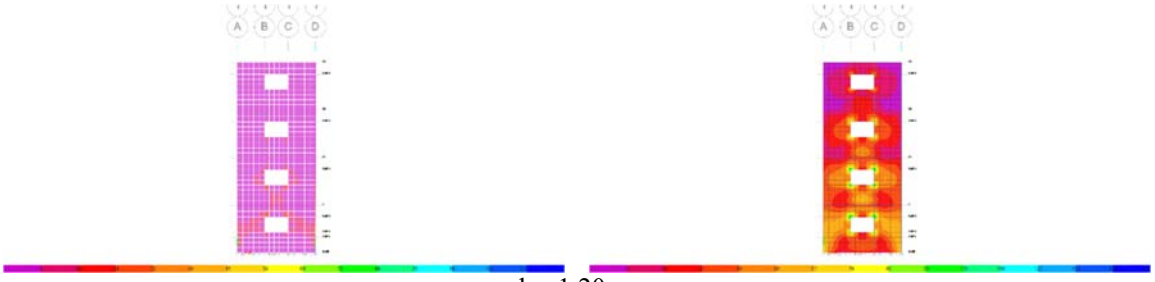

h_p=1.20 m

h_p=1.50 m

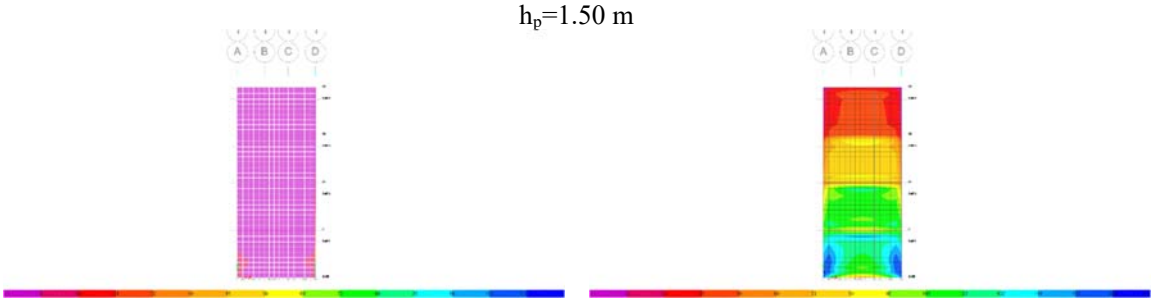

h_p=without hollows

Figures 102-115 l_w=1.60 m; l_{cb}=1.40 m – 4 levels building

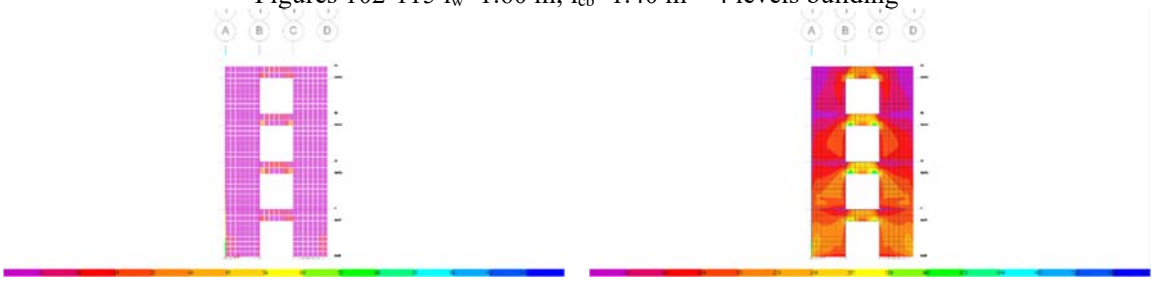

h_p=0.00 m

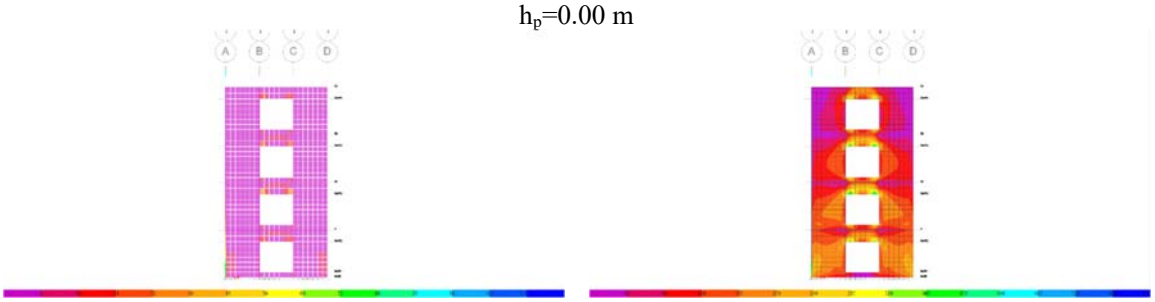

h_p=0.30 m

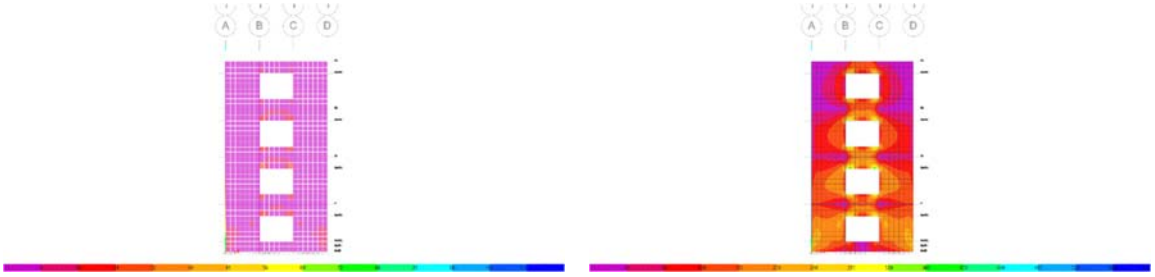

h_p=0.60 m

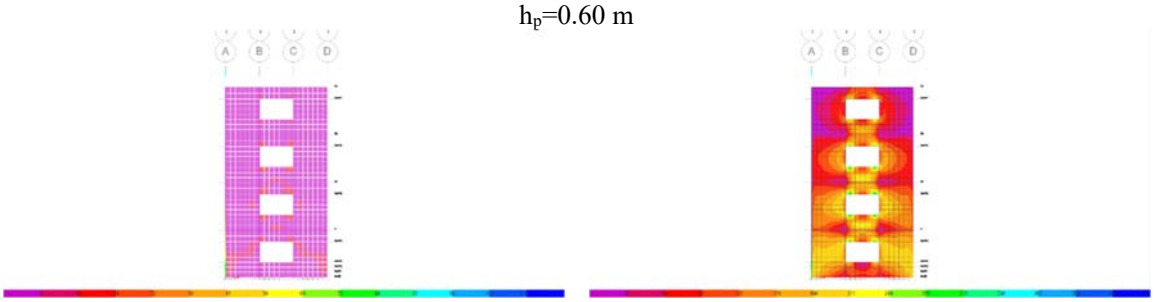

h_p=0.90 m

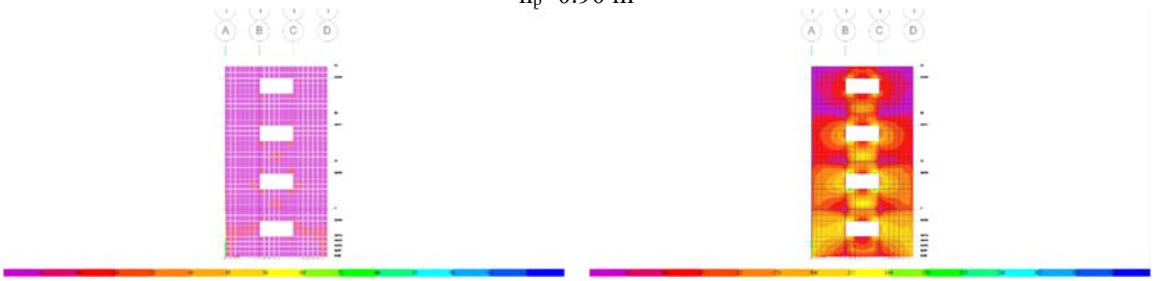

h_p=1.20 m

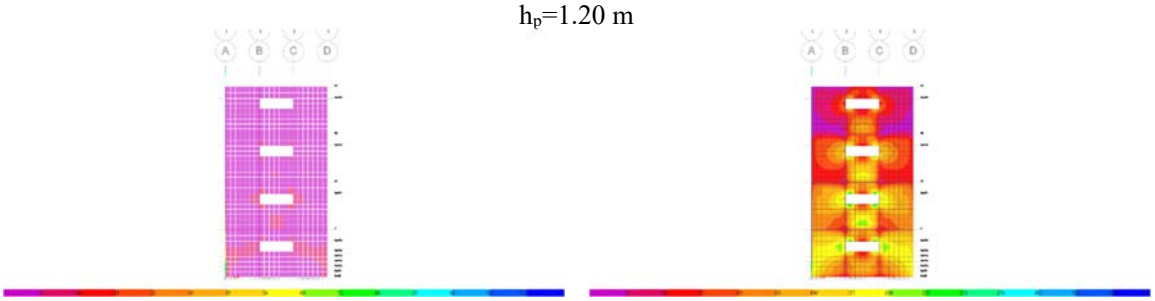

h_p=1.50 m

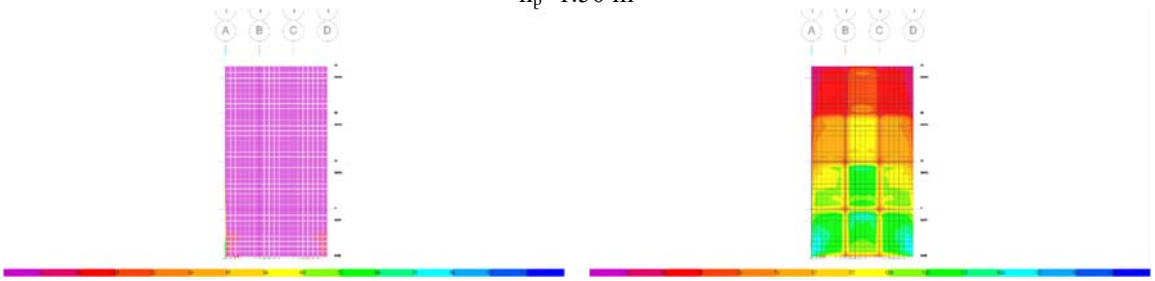

h_p=without hollows

Figures 116-129 l_w=2.00 m; l_{cb}=2.00 m – 4 levels building

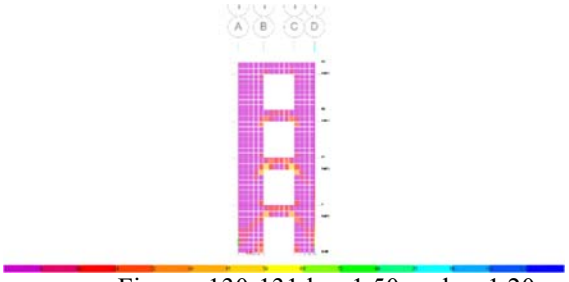
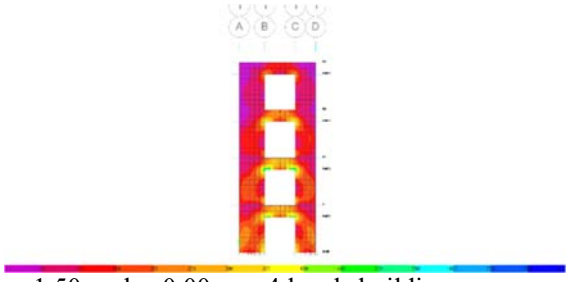

Figures 130-131 l_{w1}=1.50 m; l_{w2}=1.20 m; l_{cb}=1.50 m; h_p=0.00 m – 4 levels building

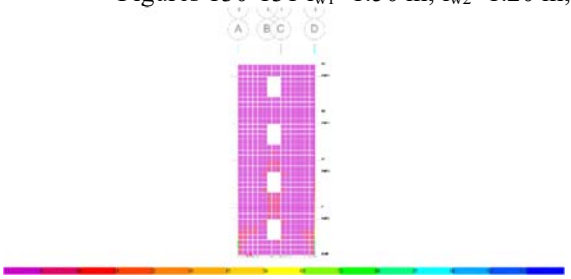
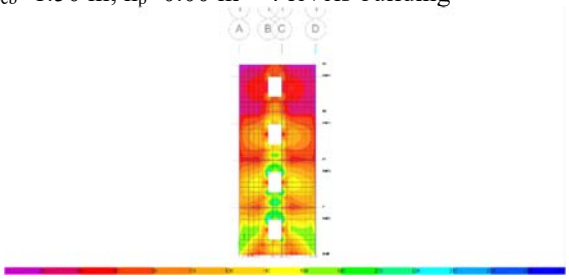

Figures 132-133 l_{w1}=1.70 m; l_{w2}=2.00 m; l_{cb}=0.80 m; h_p=0.90 m – 4 levels building

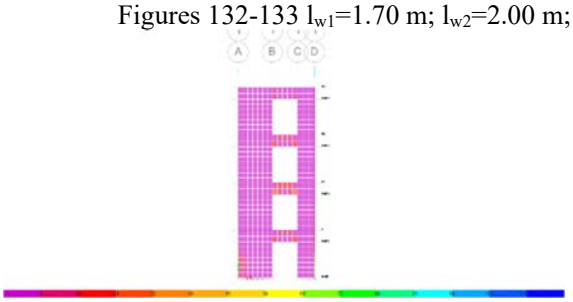
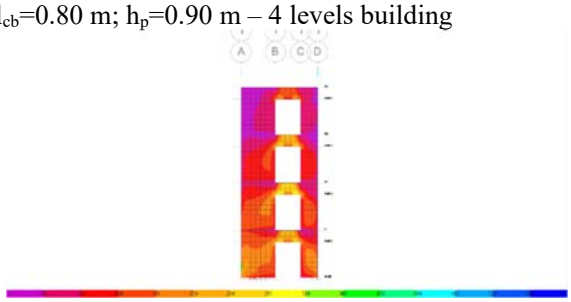

Figure 134-135 l_{w1}=2.00 m; l_{w2}=1.00 m; l_{cb}=1.50 m; h_p=0.00 m – 4 levels building

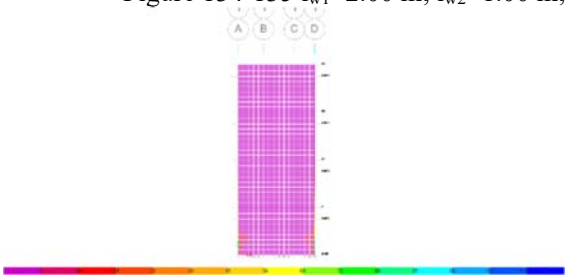
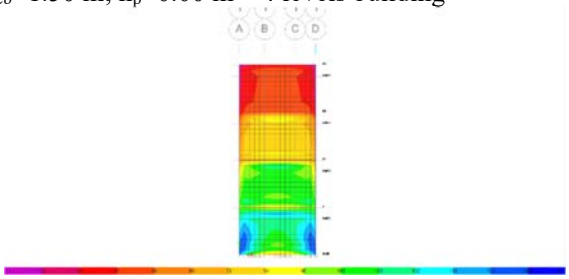

Figures 136-137 l_w=4.50 m – 4 levels building

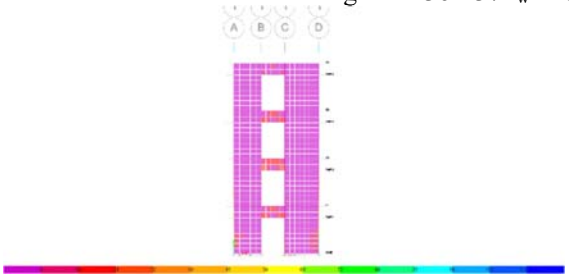
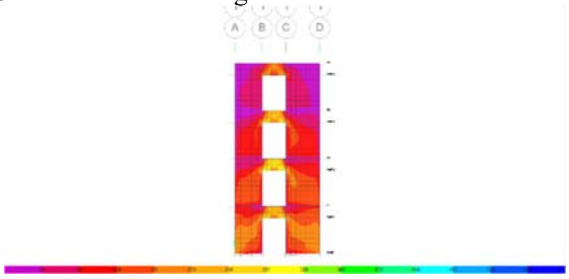

Figures 138-139 l_{w1}=1.60 m; l_{w2}=2.00 m; l_{cb}=1.40 m; h_p=0.00 m – 4 levels building

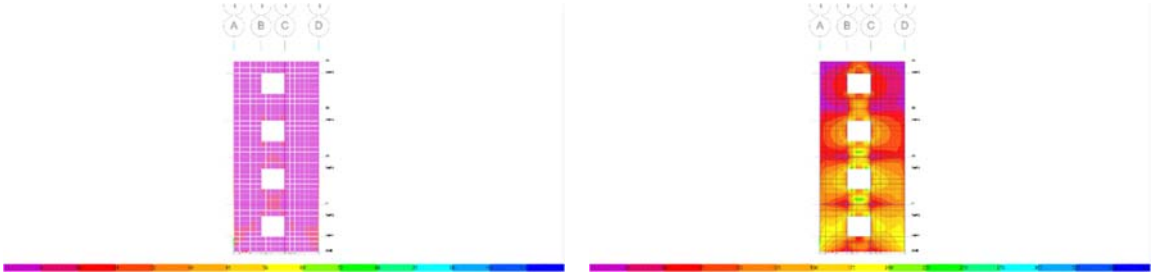

Figures 140-141 l_{w1}=1.60 m; l_{w2}=2.00 m; l_{cb}=1.40 m; h_p=0.90 m – 4 levels

Figures 141-142 l_{w1}=2.00 m; l_{w2}=1.00 m; l_{cb}=2.00 m; h_p=0.30 m – 4 levels

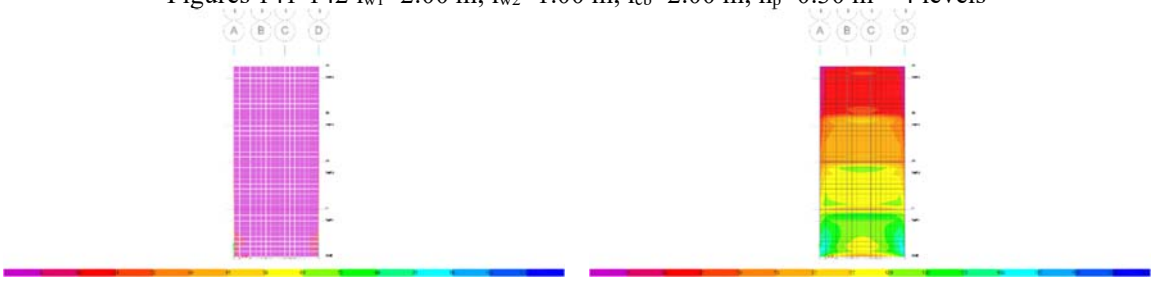

Figures 143-144 l_w=5.00 m – 4 levels building

5. Conclusion

Conclusions about the case studies comparisons:

- One can easily observe, from the 72 case studies carried out (half for two-level models and the other half for 4-level buildings) a close correlation between dissipated and distortion energies highlighted in the ETABS program, for the corresponding seismic action.
- The models were planar (for simplicity and eloquence in interpreting structural responses) but the same is true for 3D models.
- Figures 2-144 show all these diagrams, which intuitively suggest how the component structural elements (coupling rulers / walls) will degrade. In principle, from previous personal studies, if step-by-step models are made in which finite elements are removed (preferably as fine as possible) with energy dissipation over 66% at each of the steps, the degradation mode clearly corresponds tests performed in laboratories, on real models, or post-earthquake observations.
- Figures 145-146 suggestively collected some of the data presented above.
- Following all the case studies carried out, the following can be stated with certainty:

- **A wall has a pier behavior when: $l_w < h_l \frac{h_{cb}}{l_{cb}}$**
- **A wall has a cantilever behavior when: $l_w \geq h_l \frac{h_{cb}}{l_{cb}}$**

- The method can be used easily, including modeling buildings with linear elements (columns, beams) and not only surface elements such as walls. This modeling (regardless of the type of element) must be done with surface elements. Also, for different material types.

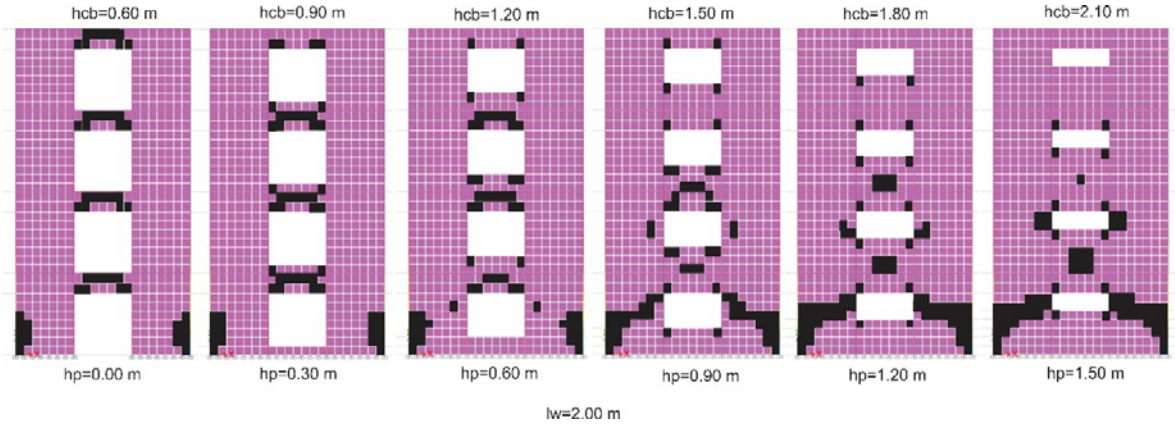

Figure 145 ETABS - dissipated energy in coupling walls (l_{w1}=l_{w2})– parallel comparisons

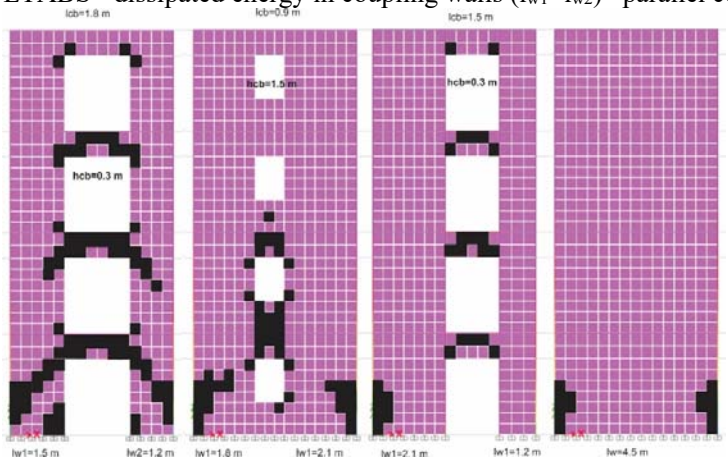

Figure 146 ETABS dissipated energy in coupling walls (l_{w1}≠l_{w2})– parallel comparisons

6. References

- CR6-2013 - DESIGN CODE FOR MASONRY STRUCTURES (COD DE PROIECTARE PENTRU STRUCTURI DIN ZIDĂRIE CR6-2013)
- P100/1-2013 - SEISMIC DESIGN CODE - PART I - DESIGN PROVISIONS FOR BUILDINGS (COD DE PROIECTARE SEISMICĂ – PARTEA I – PREVEDERI DE PROIECTARE PENTRU CLĂDIRI)
- ETABS program user guide
- MS – Excel